DEVELOPMENT AND CHARACTERIZATION OF PEPTIDE NANOFIBERS FOR CARTILAGE REGENERATION

A DISSERTATION SUBMITTED TO

THE GRADUATE SCHOOL OF ENGINEERING AND SCIENCE

OF BILKENT UNIVERSITY

IN PARTIAL FULFILLMENT OF THE REQUIREMENTS

FOR THE DEGREE OF

DOCTOR OF PHILOSOPHY

IN

MATERIALS SCIENCE AND NANOTECHNOLOGY

By

SEHER YAYLACI

September, 2015

DEVELOPMENT AND CHARACTERIZATION OF PEPTIDE NANOFIBERS FOR CARTILAGE REGENERATION

By Seher Yaylacı

September, 2015

We certify that we have read this thesis and that in our opinion it is fully adequate, in scope and in quality, as a thesis of the degree of Doctor of Philosophy.

…….

Asst. Prof. Dr. Ayşe Begüm Tekinay (Advisor)

…….

Assoc. Prof. Dr. Mustafa Özgür Güler (Co-Advisor)

…….

Assoc. Prof. Dr. Aykutlu Dana

…….

Assoc. Prof. Dr. Hüseyin Özkan

…….

Assoc. Prof. Dr. Çağdaş Son

…….

Assoc. Prof. Dr. Hatice Duran

Approved for the Graduate School of Engineering and Science:

…….

Prof. Dr. Levent Onural

Director of the Graduate School of Engineering and Science

ABSTRACT

DEVELOPMENT AND CHARACTERIZATION OF PEPTIDE NANOFIBERS FOR CARTILAGE REGENERATION

Seher Yaylacı

PhD in Materials Science and Nanotechnology

Supervisor: Asst. Prof. Dr. Ayşe Begüm Tekinay

Co-Supervisor: Assoc. Prof. Dr. Mustafa Özgür Güler

September, 2015

Articular cartilage is a tissue that is continuously exposed to cyclical compressive stresses, but exhibits no capacity for self-healing following trauma. Cartilage has a dense extracellular matrix that is sparsely populated with cells, and the whole tissue lacks blood and lymphatic vessels, which complicates the cell infiltration response that ordinarily occurs during inflammation. In addition, the only cell type capable of synthesizing new cartilage matrix lies deeper in the tissue, near the bone boundary, and due to the dense extracellular matrix, chondrocytes cannot migrate to the defect site following injury. Consequently, cartilage tissue cannot effectively respond to treatment options. Treatment options exist for the short-term reduction of pain in smaller defects, but larger injuries necessitate tissue donation, and there is a severe shortage of articular cartilage that can be donated for autografting.

Microfracture and autologous chondrocyte implantation are the current treatment options that use cellular therapy for the repair of cartilage. However, the cartilage

tissue that forms in the course of these treatments is not the functional hyaline cartilage, but rather fibrous cartilage, which is mechanically weaker and degenerates over time. Tissue engineering studies using biodegradable scaffolds and autologous cells are gaining importance as effective long-term treatment options for the post-injury production of hyaline cartilage. Such scaffold systems are designed to be biodegradable and bioactive, which allows them to induce new tissue formation in shorter periods of time.

In this dissertation, peptide nanofibers mimicking glycosaminoglycan molecules, which are important constituents of cartilage extracellular matrix, are designed and the effectiveness of these materials in terms of chondrocyte differentation are tested under *in vitro* conditions. As a follow-up study to *in vitro* experiments, the capacity of bioactive peptide nanofibers to support cartilage regeneration is evaluated in the rabbit osteochondral defect model. Structural and mechanical properties of newly deposited cartilage are highly dependent on the quality and quantity of its extracellular matrix, which also has a major impact on the integration of replacement cartilage into the surrounding healthy tissue. Signals provided by bioactive peptide nanofibers to cells at the defect site can strongly alter the quality of the newly synthesized extracellular matrix. Consequently, we designed glycosaminoglycan-mimetic peptide nanofibers that closely imitate the structure of the native cartilage extracellular matrix and demonstrated that these nanofiber networks are able to induce the synthesis of collagen II and aggrecan molecules, which are the main constituents of cartilage tissue, during chondrogenic differentiation.

Keywords: *Cartilage Regeneration, Mesenchymal Stem Cells, Biomaterials, Peptide Amphiphile Nanofibers, Glycosaminoglycans*

ÖZET

KIKIRDAK REJENERASYONU İÇİN PEPTİT NANOFİBERLERİN GELİŞTİRİLMESİ VE KARAKTERİZASYONU

Seher Yaylacı

Malzeme Bilimi ve Nanoteknoloji, Doktora

Tez Danışmanı: Yrd.Doç.Dr. Ayşe Begüm Tekinay

Eş Danışman: Doç.Dr. Mustafa Özgür Güler

Eylül, 2015

Artiküler kıkırdak dokusu sürekli olarak tekrarlayan kompresif strese maruz kalan fakat küçük boyutlu yaralanmalarda dahi kendini yenileyemeyen bir dokudur. Kıkırdak dokusu yoğun hücrelerarası matrise ve sınırlı sayıda kondrosit hücresine sahip bir dokudur. Doku genelinde kan ya da lenf damarları bulunmamakta ve herhangi bir enflamasyon durumunda dokuya projenitör hücre girişi olmamaktadır. Bunun yanında, yeni dokunun oluşmasını sağlayacak tek hücre tipi olan kondrosit hücreleri kıkırdak dokusunun daha derinlerinde kıkırdak kemik sınırına yakın olarak bulunmakta ve yoğun hücrelerarası matristen dolayı hasar bölgesine göç edememektedir. Bundan dolayı günümüzde uygulanan ve küçük boyutlu hasarlarda acıyı ortadan kaldıran ancak kısa süreli çözüm olabilen tedavi yöntemlerine rejenerasyonla cevap verememektedir. Ağır kıkırdak hasarları ise doku transferini

gerektirmekte fakat otograft olarak bağışlanacak kıkırdak dokusu azlığı nedeniyle herkese uygulanamamaktadır.

Mikrokırık ve otolog kondrosit implantasyonu günümüzde uygulanan rejenerasyon amaçlı hücre terapisinin kullanıldığı yöntemlerdir. Fakat bu yöntemler sonucu oluşan kıkırdak dokusu fonksiyonel doku olan hiyalin kıkırdak değil zamanla dejenere olan fibröz kıkırdak dokudur. Bu sebeplerle uzun vadeli etkili çözüm üretebilecek biyobozunur iskele ve otolog hücrelerin kullanıldığı çalışmalar önem kazanmaktadır.

Bu tezde, kıkırdak hücrelerarası matrisinin önemli bileşenlerinden olan glikozaminoglikan moleküllerin taklit eden malzemeler geliştirilmiş ve bu malzemelerin *in vitro* ortamda kıkırdak farklılaşmasını desteklediği gösterilmiştir.

İn vitro deneyleri takip eden *in vivo* deneylerde, biyoaktif peptit nanofiber sistemler kıkırdak doku hasarı tamiri yetisi bakımından tavşan osteokondral hasar modelinde test edilmiştir. Yeni oluşan dokunun yapısal ve mekanik özellikleri ve çevresindeki doku ile entegrasyonu içerdiği hücrelerarası matrisin niteliğine ve miktarına bağlıdır. Hasar bölgesinde biyoaktif peptit nanofiberlerle sağlanan sinyaller, hücrelerin üreteceği ektraselüler matrisin niteliğini belirlemiştir. *İn vitro* çalışmada gözlendiği üzere glikozaminoglikan benzeri peptitler hücrelerin farklılaşmasını ve bunu takiben kıkırdak dokusunun temel bileşenleri olan kollajen II ve agrekan moleküllerinin sentezini tetiklemiştir. *İn vivo* çalışmamızda da hasarlı kıkırdak bölgesinde peptit nanofiberler yardımıyla kollajen II ve agrekan molekülleri bakımından zengin hiyalin kıkırdak dokusu üretimi gözlenmiştir.

Anahtar Kelimeler: Kıkırdak Rejenerasyonu, Mezenkimal Kök Hücre, Biyomalzemeler, Peptit Amfifil Nanofiberleri, Glikozaminoglikanlar

ACKNOWLEDGEMENTS

The completion of this doctoral dissertation was possible with the mental and emotional support of several people. I would like to express my sincere gratitude to all of them.

Firstly, I would like to sincerely thank my advisors Prof. Tekinay and Prof. Guler for their guidance, motivation, care, understanding and immense knowledge I received through my Ph.D research. They provided me with an excellent atmosphere for doing research. Besides my advisors, I would like to thank the rest of my thesis committee for their insightful comments.

I would like to acknowledge the financial supports of The Scientific and Technological Research Council of Turkey (TÜBİTAK); BİDEB 2214/A for PhD scholarship and projects 111M710 and 113T045 for experimental works.

A very special thanks goes out to my husband Ali Kemal Yaylacı, without whose motivation, encouragement and hearty support I would not have completed this thesis. I am also grateful to Lütfiye Yaylacı, Musa Yaylacı and Furkan Yaylacı for their hearty support.

I would like to express my most sincere thanks to Hakan Ceylan, Hilal Gülsüner and Zeynep Ülger for their friendship, moral support and motivation, which made my lab hours more enjoyable.

Special thanks to Merve Sen, Özlem Bulut, Melis Sardan and Aysegul Tombuloglu for their excellent collaboration in projects we took part together. I am especially grateful Alper Özkan for his willingness for editing papers, reviews and even this thesis. I would also like to thank all labmates of the Nanobiotechnology Lab and Biomimetics Lab for providing a warm and peaceful research environment.

Finally, I would like to express my heartfelt thanks to my parents, Habibe Üstün, Hasan Üstün, to my brother Gökhan Üstün, to my brother's wife Özlem Üstün, and to my nephews Hakan Kerem Üstün and Enes Üstün for supporting me spiritually throughout of my life and encouraging me with their best wishes.

CONTENTS

LIST OF FIGURES

LIST OF TABLES

ABBREVIATIONS

ACI	:	Autologous chondrocyte implantation
AEMA	:	2-aminoethyl methacrylate
ATDC5	:	Mouse 129 teratocarcinoma AT805 derived cell line
Boc	:	Tert-butoxycarbonyl
BSA	:	Bovine serum albumin
CD	:	Circular dichroism
CH	:	Chondrogenic medium
DCM	:	Dichloromethane
DIEA	:	N-ethyl-diisopropylamine
DMF	:	N, N-Dimethylformamide
DMEM	:	Dulbecco's modified Eagle's medium
DMMB	:	Dimethyl methylene blue
ECM	:	Extracellular matrix
EdU	:	5-ethynyl-2'-deoxyuridine
EDTA	:	Ethylenediaminetetraacetic acid
E-PA	:	Lauryl-VVAGE
FBS	:	Fetal bovine serum
FDA	:	Food and Drug Administration
Fmoc	:	9-Fluorenylmethoxycarbonyl
GAG	:	Glycosaminoglycan
GAG-PA	:	Lauryl-VVAGEGD-K(p-sulfobenzoyl)-S-Am
Glc-PA	:	Lauryl-VVAGKS(β-Glc)-Am
HA	:	Hyaluronic acid
HBTU	:	O-Benzotriazole-N,N,N',N'-tetramethyl-uronium-hexafluoro-
HPLC	:	High performance liquid chromatography

K-PA	:	Lauryl-VVAGK-Am
LC-MS	:	Liquid chromatography-mass spectrometry
MACI	:	Matrix-induced autologous chondrocyte implantation
mMSC	:	Mouse mesenchymal stem cell
MT	:	Maintenance medium
MTT	:	3-(4,5-dimethylthiazol-2-yl)-2,5-diphenyltetrazolium bromide
OA	:	Osteoarthritis
PA	:	Peptide amphiphile
PLA	:	Polylactic acid
PGA	:	Polyglycolic acid
PBS	:	Phosphate-buffered saline
PCM	:	Pericellular matrix
PG	:	Proteoglycan
rMSC	:	Rat mesenchymal stem cell
SEM (Microscopy)	:	Scanning electron microscope
SEM (Statistics)	:	Standard error of the mean
TIS	:	Triisopropylsilane
TCP	:	TCP
TEM	:	Transmission electron microscope
TFA	:	Trifluoroacetic acid
TRITC	:	Tetramethylrhodamine

CHAPTER 1

1 Introduction: Cartilage Tissue Engineering

1.1 Cartilage Tissue

1.1.1 Basic Properties of Cartilage Tissue

Cartilage is a type of connective tissue found in both vertebrates and invertebrates. Connective tissues form the majority of the body mass, in terms of both cellular and extracellular components. They are responsible for a variety of functions, such as mechanical support, cell migration and differentiation and wound healing, which strongly depend on mostly cellular elements for nerve, epithelial or muscle tissues. However, the properties and functions of cartilage tissue are primarily determined by the arrangement, type and amount of its extracellular matrix (ECM) components. Vertebrate cartilage is consequently classified on the basis of its predominant ECM elements. Accordingly, hyaline cartilage is primarily composed of glycosaminoglycans and found in joints between bones, sternum and ribs; elastic cartilage is composed of elastic fibers and present in ear pinna, eustachian tubes and the epiglottis; and fibrous cartilage is composed mainly of type I collagen and found in intervertebral discs and the pubic symphysis. Lastly, articular hyaline cartilage is mostly known for its function in joints, where it permits the movement of one bone against another while absorbing impact forces by imparting the joint with low friction coefficients and high load resistance[1].

Cartilage can function as a transitional tissue during human bone development or as a permanent tissue to provide mechanical rigidity while retaining a degree of

flexibility. It is also capable of defining the external morphology of some organs, such as the ear and the nose.

During embryogenesis, cartilage arises from the mesodermal germ layer. Cartilage development involves a series of dynamic and strictly regulated processes involving mesenchymal cell recruitment, progenitor cell condensation and chondrogenic differentiation, which ultimately leads to the formation of various types of cartilage [2]. Cellular condensation is the pivotal stage during chondrogenesis and results in production of specialized chondroblast cells that secrete the characteristic cartilage ECM. Further deposition of ECM elements increases the distance between individual chondroblasts, leading to their encapsulation within the tough, dense ECM and stimulating their differentiation into mature chondrocytes [3].

1.1.2 Cartilage Structure and Composition

The composition of cartilage tissue changes as the tissue develops, with mature articular cartilage ECM being composed mainly of water, collagen fibers and PGs (though noncollagenous proteins and glycoproteins also exist in smaller amounts). Water is the most abundant component of articular cartilage, accounting for approximately 70-80% of its wet weight. Most of the water is associated with the interfibrillar space of collagens, while the remainder is contained in small pores within the intracellular space. Adult cartilage is characteristically aneural, alymphatic and avascular, and nourishment and waste transport is primarily performed through long-range diffusion in synovial fluid.

Chondrocytes are the only metabolically active units of cartilage, and facilitate the turnover and synthesis of the tissue despite occupying only around 5% of the tissue. Chondrocytes have different morphologies and expression patterns depending on the

zone in which they reside. Cells near the tissue edge display a flattened morphology, while those in the middle and deep zones are more spherical [4].

Cartilage tissue shows two distinct levels of organization, being stratified in a depth-dependent manner and exhibiting a second layer of matrix compartmentalization within each strata (Figure 1.1). Consequently, features such as chondrocyte morphology, biochemical composition and collagen fiber orientation differ between the surface and deeper regions of the tissue. The superficial zone represents the first 10-20% of articular cartilage by depth, and is a region in which collagen fibers are aligned in parallel to the cartilage surface. This zone is responsible for most of the tensile properties of cartilage and protects deeper regions from forces imposed by articulation. The middle zone makes up the middle 40-60% of cartilage; collagen fibers are oriented obliquely in this region. Chondrocytes are found in lower amounts in the middle zone, and display a spherical morphology. The deep zone is responsible for resisting the bulk of the compressive forces exerted on cartilage, and performs this duty through the assistance of its radially oriented collagen fibers and high PG content. Chondrocytes are arranged in columnar structures in this zone. The second layer of organization is observed in the ECM surrounding chondrocytes, which is divided into zones depending on its distance from cells [5]. The pericellular matrix (PCM) is the closest to chondrocytes, possesses a distinct collagen fiber type and bears a rich aggrecan content. Signaling molecules such as growth factors are also concentrated in this region [6–8]. The territorial matrix, which surrounds the PCM, is thicker than the PCM and has been suggested to play a role in protecting chondrocytes from mechanical stress. The interterritorial region is the most distal from the cells and the largest of 3 matrices. It is responsible for most of the biomechanical properties of cartilage.

As previously mentioned, the dry weight of cartilage tissue is mainly composed of collagen and PGs, and these two molecules form the networks that imbue cartilage tissue with its mechanical properties.

Cartilage tissue is known to contain collagen types II, VI, IX, X, and XI, although type II collagen comprises the 90-95% of total collagen in the tissue [9]. Different from other collagen types, type II collagen has a greater amount of bound carbohydrate groups, which allows it to establish stronger interactions with water molecules. Collagen fiber orientation also differs in each zone: Tangential fibers are found in superficial zones, while the deep zone contains radially oriented fibers [10].

The predominant PG found in articular cartilage is aggrecan, which exists in aggregates of hyaluronan and chondroitin sulfate through connections formed by link proteins [11]. Aggrecan is responsible for providing the osmotic pressure cartilage requires resisting compressive loads. Other than aggrecan, small PGs such as decorin, perlecan and biglycan are also present in cartilage. Similar to aggrecan, these PGs are also comprised of a core protein that is associated with various glycosaminoglycan species attached as side chains [12].

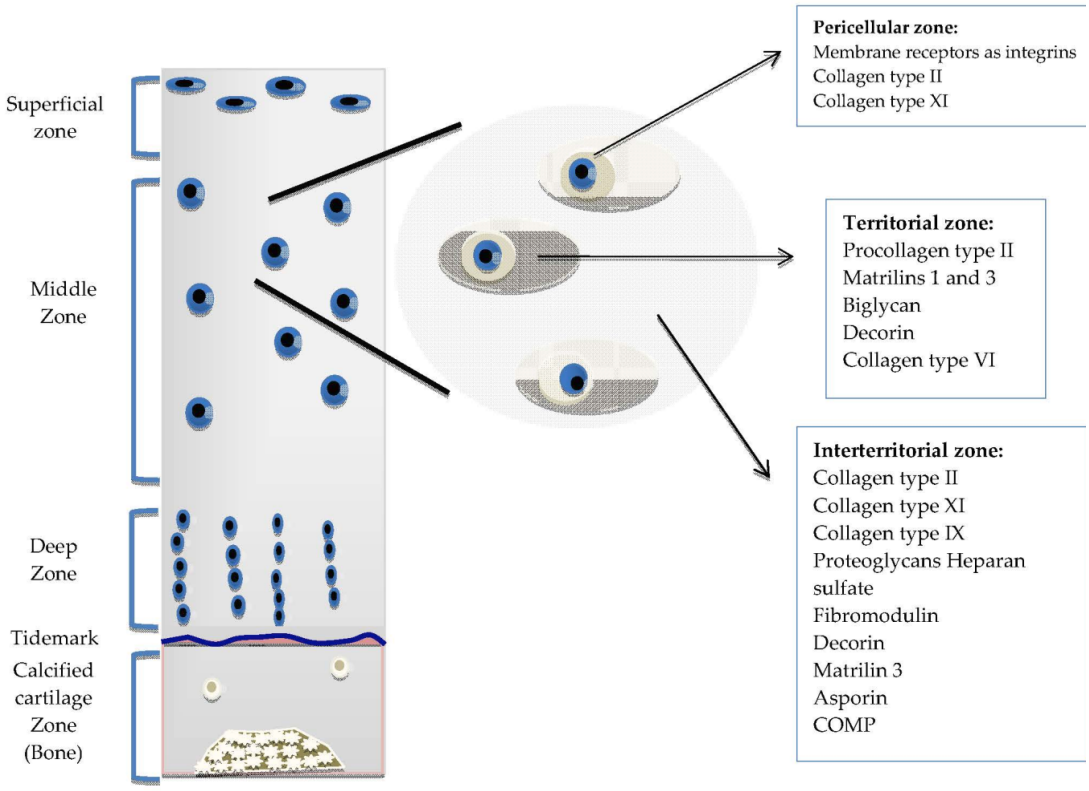

Figure 1.1 The Organization of Normal Articular Cartilage.

The organization of cartilage tissue is divided depthwise into superficial, middle and deep zones, while the cartilage ECM is classified depending on its distance from the chondrocytes. Each zone has specific ECM components and a characteristic chondrocyte morphology. (© 2013 García-Carvajal ZY, Garciadiego-Cázares D, Parra-Cid C, Aguilar-Gaytán R, Velasquillo C, Ibarra C, Castro Carmona JS. Published in [179] under CC BY 3.0 license.).

1.1.3 Chondrocyte-ECM Interactions

Chondrocytes have cell long processes that allow their interaction with ECM molecules; however, they have no direct contact with other cells within the tissue. Thus, the regulation of tissue homeostasis depends heavily on cell-matrix interactions.

ECM serves not only as structural support for cells, but also acts as a bioregulatory niche that modulates tissue formation, organization and maintenance. ECM is therefore an extraordinarily dynamic and versatile environment; as cells embedded in the matrix actively remodel its components through enzymatic or non-enzymatic pathways. The physical and chemical diversity of ECM components determine tissue characteristics and can vary from one tissue to another, or even between two different physiological states of the same tissue. The reciprocal and dynamic signaling between cell and ECM compartments has attracted special attention in cartilage, where cell-matrix interactions predominate and cell-cell interaction are minimal due to the sparsity of cells in this tissue. Most cell-matrix interactions are mediated by transmembrane receptors, and this interaction helps the cells to sense changes in the ECM [13–15].

Articular chondrocytes have been shown to express transmembrane extracellular receptors such as CD44 and integrins [16–18]. Both of these receptors interact with adjacent extracellular macromolecules and detect changes in matrix composition and state. It is known that disruption of either CD44- or integrin-mediated interactions may have drastic effects on the cartilage metabolism.

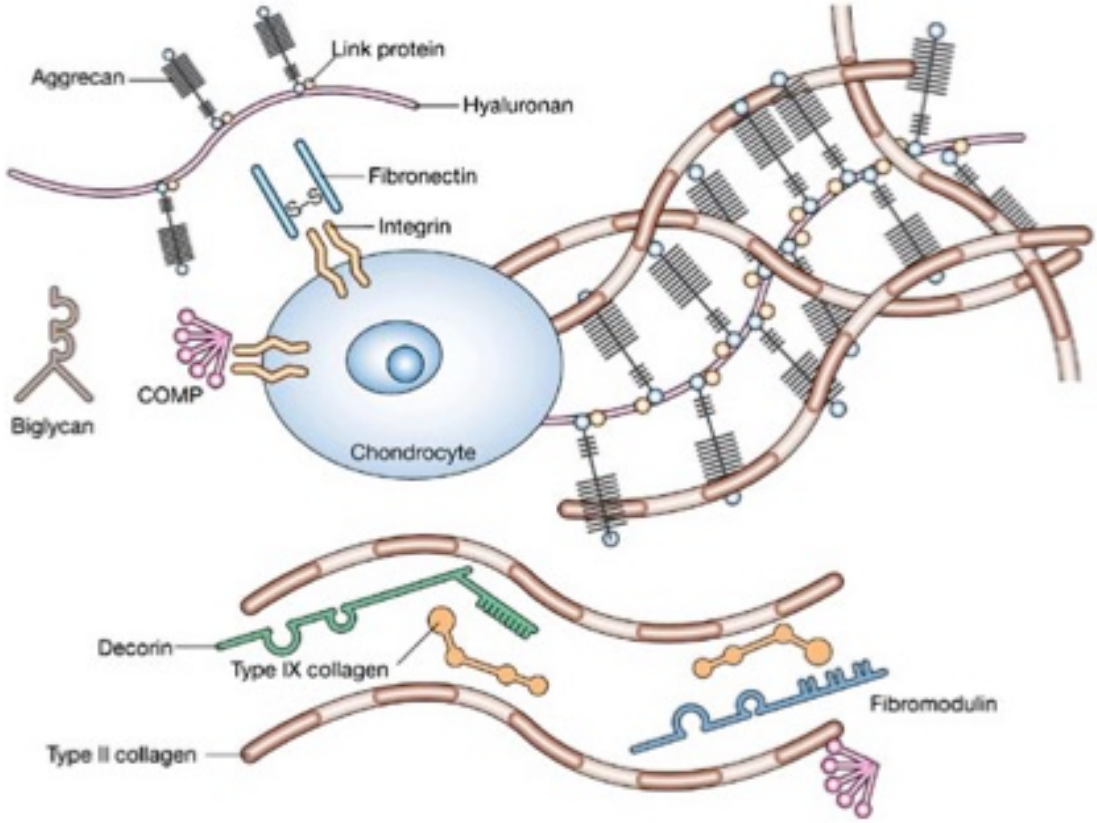

Figure 1.2 Cartilage Tissue ECM

Cartilage ECM is composed of three major components; collagens, proteoglycans and water. The predominant collagen type is type II, and the most abundant proteoglycan is aggrecan. (Reproduced from Ref. 180 with permission from Nature Publishing Group).

CD44 is the primary receptor for hyaluronic acid (HA) molecules in many cells [19]. In cartilage tissue ECM, HA molecules are found interacting with aggrecan at a ratio of about 50 HA to one core protein, with link proteins serving to connect the two [20]. Thus, the binding of HA to CD44 in cartilage mediates the retention of large HA/PG/link protein aggregates at the surface of chondrocytes [21]. Several experiments with anti-CD44 antibodies and CD44 antisense oligonucleotides support the idea that CD44 is an important mediator of chondrocyte cell-matrix interactions that involve proteoglycan (PG)/HA/link protein aggregates [22].

The unique organization of CD44 at the cell surface may function to establish and also to regulate the structure of the PCM in conjunction with a hyaluronan scaffold. The interaction of the cytoplasmic domain of CD44 with components of the cytosolic proteins, and the interaction of the extracellular domain of CD44 with the matrix, are indicative of both inside-out and outside-in communication patterns. It was shown that the inhibition of CD44-matrix interactions through the use of antisense oligonucleotides or HA oligosaccharides results in a chondrocytic chondrolysis cascade [23].

Adult articular chondrocytes also express members of integrin subfamilies. These integrins mediate adhesion to several different ECM proteins found in cartilage. Chondrocytes were found to use integrins to attach to fibronectin, collagen types II and VI, vitronectin, osteopontin, and bone sialoprotein II [24]. The functional role of integrins in cartilage has not been determined in full. Chondrocyte integrins might be expected to help regulate processes involved in cell survival, growth, and differentiation, as well as matrix remodeling. Chondrogenesis was inhibited in mouse limb bud cells by blocking integrin with integrin antibodies [25]. In one study, RGD

peptides were used to inhibit integrin-ECM interactions and it was shown that differentiation of epiphyseal chondrocyte was ceased [26].

1.2 Issues Related to Cartilage Repair and Their Clinical Significance

Defects in articular cartilage can result from traumatic injury or pathological degeneration. The capacity of cartilage to repair injury is limited, and when not treated, such defects can progress to degenerative arthritis. The increasing prevalence of osteoarthritis (OA) is correlated with an aging population and the growing problem of obesity. 9% of the United States population aged 30 and older suffer from OA of the hip or knee, and more than 250,000 knee and hip replacements are performed each year for end stage disease joint failure [27]. In addition, cartilage damage resulting from sports injuries can also result in premature cartilage degeneration in the younger or more active individuals.

1.2.1 Cartilage Repair Strategies

Various repair strategies are currently used in the treatment of cartilage defects. Arthroscopic techniques, such as lavages and debridements, aim to clean out the defect site and alleviate pain associated with the inflammation of the cartilage tissue [28]. These procedures are considered to be palliative, as they only provide short-term relief by removing unstable cartilage flaps and preventing inflammation; they do not restore the function of the damaged site [29]. An arthroscopic lavage involves the washing of the joint space for the removal of blood or loose debris, while debridement is the removal of unstable cartilage flaps. The main targets of these procedures are patients with very small cartilage defects [30].

Other arthroscopic techniques aim to utilize the intrinsic repair capacity of cartilage, and include drilling and microfractures. Both of these techniques consist of the penetration and subsequent bleeding of subchondral bone to induce fibrocartilage formation. They rely on the formation of a blood clot at the defect site by stimulating bone marrow, which triggers the deposition of mechanically weak fibrocartilage tissue at the defect site. The microfracture technique is used for defects smaller than 2.5 cm^2, and involves the removal of the unstable cartilage for the creation of a well-defined defect environment that is surrounded by healthy cartilage [31]. In this procedure, a microscopic awl is used to penetrate subchondral bone without damaging its integrity. The defect is then filled with clot material from the subchondral bone, which contains mesenchymal stem cells (MSCs) that will oversee the subsequent repair of cartilage tissue. The outcome of the treatment depends mainly on how well the patient can avoid overexerting the cartilage tissue with excessive weight loads. Clinical data suggest that 75% of patients display short-term clinical improvements; however, functional deterioration of the defect site begins within 24 months in 48-80% of cases [32]. Low numbers of MSCs, or their dilution by synovial fluid, can result in low regeneration capacity and early deterioration following the procedure. Adequate regeneration therefore depends on the optimization of the number of cells extracted from subchondral bone, which is performed by controlling the depth and numbers of the holes produced on the cartilage surface.

Grafting is the preferred way of treating larger cartilage defects and consists of the removal of healthy cartilage tissue from non-weight bearing areas of the knee, followed by the transplantation of the removed tissue into the defect site [33]. Multiple plugs may be required depending on the depth and scale of the defect site. Grafts are

self-secured to the defect site without using any adhesives; their success depends heavily on whether draft plugs from non-load bearing regions are able to withstand the stresses applied to the weight-bearing parts of the tissue. Another concern about the treatment of cartilage injuries through osteochondral grafting is the negative effect the procedure has on the viability of cells at the margins of the grafts. Cells in these regions are more prone to be affected by stress, and the resulting cell death may lead to the degeneration of the tissue over time [34]. In addition, the dead space between the graft and native tissue affects the integrity of repaired cartilage.

A new generation of tissue repair strategies involving the external administration of autologous or donor cells into the defect site have been developed to replace damaged cartilage with biomechanically stronger and functional hyaline cartilage. Autologous chondrocyte implantation is one such strategy and utilizes the patient's own chondrocytes. It is conducted in three stages: Chondrocytes are first arthroscopically extracted from non-load bearing parts of cartilage, subsequently expanded in an *in vitro* environment until sufficient numbers of cells are obtained, and finally reimplanted back into the defect site and secured with a periosteal graft taken from the tibia [35]. The use of the patient's own chondrocytes prevents immune responses and the isolation of chondrocytes can be performed through a minor biopsy operation, which reduces potential complications at the donor site. However, the operations involved are complex and the procedure necessitates a longer recovery time to allow the maturation of new cartilage tissue [36]. Graft hyperthrophy is one of the most pronounced post-surgery complications of this technique.

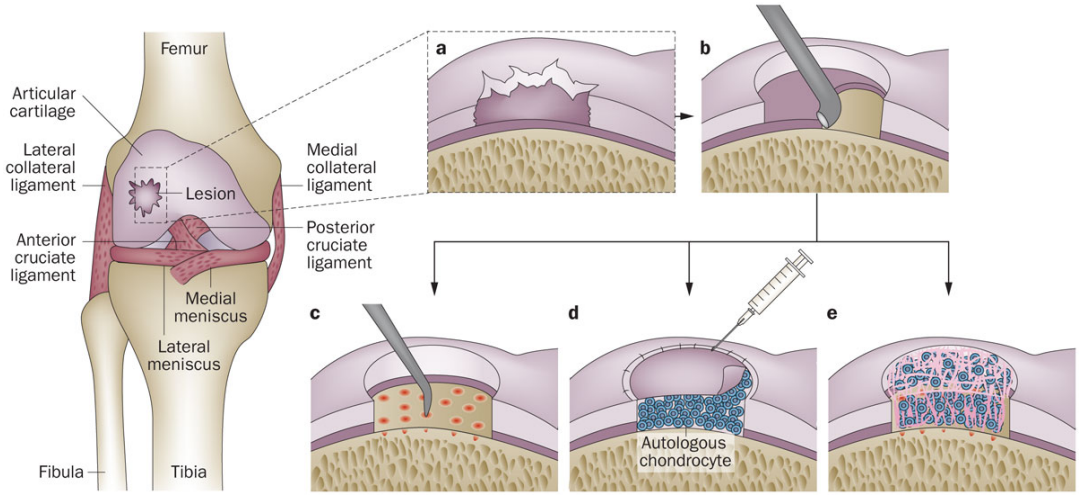

Figure 1.3 Cartilage Regeneration Techniques.

a) A full-thickness chondral lesion. b) The lesion is cleaned to have stable margins for integration of the host tissue. c) Microfracture is used to bleed subchondral bone and subsequent flow of blood and progenitor cells start to repair processes. d) ACI utilizes the patient's own chondrocytes to fill defect site and it is covered with periosteal flap e) In MACI restorable collagen matrices are used instead of periosteal flaps different from ACI. (ACI, autologous chondrocyte implantation; MACI, matrix-assisted autologous chondrocyte implantation). (Reproduced from Ref. 50 with permission from Nature Publishing Group)

Second-generation autologous chondrocyte implants (ACI) use restorable collagen matrices instead of periosteal flaps. A combination matrix of collagens I and III has been shown to reduce graft hypertrophy and the number and depth of incisions necessary for the operation [37]. However, the use of artificial scaffolds increases the risk of immune reaction. Technical constraints during the culture and transplantation of cells, such as non-homogeneous distribution of chondrocytes, leakage of the transplanted cell suspension due to gravity and the risk of chondrocyte dedifferentiation, limit the usefulness of this technique for the production of functional hyaline cartilage and create large variations in the success of the operation [38].

These difficulties have led to the development of a third generation of autologous chondrocyte implants, composed of biomechanically stable and functional tissue matrices that integrate better into host tissues [39]. Use of scaffold-based techniques has some major advantages over scaffold-free techniques: Scaffolds can better assume the 3D structure of the defect, provide a suitable substrate for cellular adhesion, ensure the homogenous distribution of cells and prevent leakage during transplantation. Matrix-induced ACI (MACI) is an example of a scaffold-based technique in clinical use [40,41]. Unlike second-generation ACI methods, cells in this technique are seeded onto 3D porcine-derived type I/III collagen matrices and cultured for an additional three days prior to implantation. These matrices are designed in such a way that one side is porous and allows the infiltration of MSCs, while the other side exhibits high mechanical strength and has a low-friction surface that allows easier integration into the chondral cavity. The membrane patch is secured by fibrin glue during implantation, eliminating the need for tedious watertight sutures. Materials used in MACI include collagen type I/III, hyaluronan

(Hyalograft®-C, HYAFF®11; Fidia Advanced Biopolymers, Abano Terme, Italy) and fibrin (Tissucol, Baxter, Austria) scaffolds [42]. *In vitro* studies have demonstrated that bilayer collagen membranes also present an adequate environment for cell attachment and chondrogenic differentiation [43]. However, there are no clinical findings that clearly prove the superiority of MACI over existing techniques [44]: Indeed, no differences were found in the arthroscopic appearances, histological observations and rates of tissue hypertrophy between collagen I/III-based ACI-C and bilayer collagen-based MACI grafts used in the treatment of symptomatic cartilage defect cases [45]. MACI is nonetheless an attractive treatment method, as it provides a means of arthroscopic implantation that reduces invasiveness and operation times. Nonetheless, chondrocytes tend to lose their differentiated states during clonal expansion, which adversely affects their ability to synthesize functional cartilage ECM and results in large variances in the outcomes of ACI and MACI treatments. 3 days of culture in collagen matrices may result in the formation of only an immature tissue environment, leading to the dedifferentiation of cells and a corresponding decrease in their matrix synthesis capability [46]. Longer culture periods may permit chondrocytes to synthesize their own matrix, resulting in more mature and stable tissue replacements.

1.2.2 Tissue Engineering Efforts

Existing treatment techniques are insufficient for the long-term repair of cartilage and need to be complemented with engineered systems containing cartilage-mimetic material architectures, inductive signals or stem cells to produce reproducible, safe and functional tissue constructs. There are four main approaches for cartilage regeneration: cultured cell implantation, engineered tissue construct implantation, scaffoldless tissue regeneration and guided tissue regeneration. Cartilage growth, development and repair are dependent on both biomechanical and biological signals, and *in vitro* culture environments that attempt to induce cartilage repair or recapitulate the structural and biochemical elements of cartilage environment can therefore increase the success of implantation. Scaffold materials can directly alter the sensory landscape of the cells they contain, in addition to providing the mechanical cues necessary for chondrogenic differentiation. As such, a great variety of factors should be considered in tandem for the design of optimal cartilage scaffolds. In a general sense, the material should allow the transport of nutrients and waste products, facilitate the migration and development of cells, be intrinsically biocompatible and provide the biochemical signals necessary for the survival and maintenance of chondrocytes.

Scaffold surface characteristics have a direct role on controlling the adhesion, migration, and differentiation of cells [47]. Material properties such as scaffold morphology, hydrophilicity and surface charge should therefore be considered for the development of functional scaffolds that can interact with the surrounding environment. An additional factor in the design of cartilage scaffolds is the time of implantation, *i.e.* whether the construct is set to be implanted immediately or following an *in vitro* culture period. Constructs implanted immediately should be

stable in the physical environment of cartilage and protect the seeded cells until neotissue formation is completed. However, this kind of structural integrity and durability is not particularly necessary for cell-laden constructs matured in *in vitro* environments, since newly formed tissue itself may be able to withstand the native, high shear cartilage environment. The material should also be able to fill the defect site and integrate with the surrounding native tissue for the implantation to succeed. In addition, degradation rates of scaffolds in native tissue should match the formation rate of neo-tissue, as faster degradation results in shape retention issues while slow degradation intervenes with the ingrowth of neo-tissue.

Material source (natural or synthetic), physical properties, biofunctionality and tissue integration capability can affect the choice and design parameters of a scaffold. A wide range of natural and synthetic polymers have been investigated in cartilage tissue engineering efforts [48–50]. Natural materials are preferred for their low costs and similarity to the cartilage ECM, which allows their natural degradation, facilitates their interaction with cells through functional groups and ensures that the scaffold will be biocompatible. Agarose, alginate, HA, fibrin glue, chitosan, type I and II collagen and reconstituted tissue matrices are among the natural materials used in cartilage tissue engineering [51]. However, natural polymers lack the mechanical properties necessary to withstand the high-stress environment of cartilage and tend to undergo rapid degradation following implantation. Synthetic polymers, in contrast, provide tailorable physical and chemical properties through different synthesis methods and can be processed in different sizes and shapes. In addition, they present low immunogenic responses and toxicity, and tend to have lower batch-to-batch variances compared to natural materials.

1.2.2.1 Natural Polymers

Agarose and alginate are both derived from algae and provide a biocompatible three-dimensional environment that has been shown to preserve the rounded morphology of chondrocytes. Alginate and agarose are continuous, hydrogel-based materials that can transmit applied forces to encapsulated chondrocytes and allow the uniform distribution of seeded cells; this property has led to their use in studies investigating effects of dynamic loading on cell behaviour [52–55]. However, alginate is not degraded rapidly in the body and interferes with growth of neotissue. Covalent crosslinking can be performed to tune the mechanical properties, degradation kinetics and swelling ratio of alginate [56]. Photocrosslinkable alginate systems allow the non-invasive implantation of scaffolds that can fill defects of any size and geometry. In a recent study, alginate was modified with 2-aminoethyl methacrylate (AEMA) and crosslinked under 365 nm UV light with the help of a photoinitiator, creating hydrogels with adjustable degradation kinetics based on the rate of methacrylation [57].

Collagen types I and II are the most abundant proteins in the native cartilage ECM and have been used in the development of bioactive scaffolds. Collagen–derived materials bear inherent biological cues that facilitate cell attachment and can be remodeled by cells during their development. Like other natural materials, collagen has to be processed to decrease its antigenicity before use. This process removes immunogenic components within collagen and crosslinks the remaining telopeptides by aldehyde or carbodiimide chemistry. The resulting material can easily be processed into various physical configurations, such as tubes, sheets, fleeces and sponges; however, gels and fibers are the forms most commonly studied in cartilage tissue engineering [58]. The predominant collagen of cartilage is type II collagen, and chondrocytes seeded in type II collagen scaffolds were previously demonstrated to

maintain their phenotype. However, poor availability and undesirable mechanical properties of type II collagen limit its use in tissue engineering studies.

Hyaluronan is a major glycosaminoglycan component of cartilage and synovial fluid, and helps in the lubrication of joints. It is a nonsulfated glycosaminoglycan and is involved in cell differentiation, ECM organization and cell motility [58]. Hyaluronan can be derived from various animal tissues or produced by microbial fermentation. Hyaluronan can be injected to fill defects in any shape, and is therefore suited for less invasive applications however, it is quickly degraded *in vivo* by cell-secreted hyaluroidases. As with agarose and alginate, hyaluronan and HA can be crosslinked to produce porous solid platforms with higher resistances to degradation [59]. Aqueous solutions of HA can be crosslinked through covalent crosslinking or photocrosslinking. HYAFF®'7 and HYAFF®11 are the ethyl and the benzyl esters of hyaluronan, respectively, and remain intact in the body for around two months prior to their degradation by the hydrolysis of their ester bonds [60].

Fibrin is a protein involved in the blood clotting process and sees common use as an adhesive in surgery. It is composed of fibrinogen monomers, which possess two sets of three polypeptide chains that are solidified through the binding of thrombin. The stability and mechanical integrity of the resulting fibrin gel are dependent on pH and the concentrations of fibrinogen and calcium ions. Fibrin gels can be derived from the patient's own blood and subsequently utilized as an autologous scaffold. Because of its complete biodegradability and availability in injectable forms, it is popular in various tissue-engineering applications. However, it needs to be blended with different materials to enhance its mechanical properties.

Chitosan is the deacetylated form of chitin, one of the most abundant polysaccharides in nature. This polysaccharide has an intrinsic antibacterial ability, triggers mild

immunological reactions and has a structure similar to glycosaminoglycan molecules. Its highly cationic nature and resemblance to GAGs allows it to bind growth factors and adhesion proteins. Chitosan is degraded by deacetylation, and the host tissue progressively metabolizes the sugar units detached from its structure. The degradation rate of chitosan scaffolds can be modified during processing by altering the number of acetyl units. Similar to fibrin, it can be injected into target tissues due to its unique temperature-dependent gelation property: It is liquid at room temperature and gel at physiological temperature. Generally, chitosan is combined with other materials, such as PLGA and hyaluronan, to improve chondrocyte attachment, proliferation and matrix synthesis [61].

1.2.2.2 Synthetic Polymers

Synthetic polymers show predictable chemical and physical properties and can be customized easily to meet specific requirements, including degradation rates, mechanical properties and biological activities. In addition, synthetic polymers are generally cheaper than natural polymers, can be produced in large quantities and have longer shelf lives [62,63].

Short chain saturated aliphatic polyesters, including poly (glycolic acid) (PGA), poly (lactic acid) (PLA) and poly(lactic-*co*-glycolic acid) (PLGA) copolymers, are commonly used for scaffold materials because of their biodegradability and the US Food and Drug Administration (FDA) approval for their clinical use. Their degradation products are monomeric glycolic or lactic acids and can be resorbed *in vivo*. However, these products alter the local pH, resulting in insufficient tissue ingrowth and triggering inflammatory responses. Total degradation takes place within 24 months and accompanies the loss of mechanical durability. These

polymers can be produced in different shapes and forms, but for cartilage tissue engineering purposes, they are generally utilized as non-woven meshes or felt-like forms [62].

PGA is a hydrophilic polymer and enables the attachment of chondrocytes onto its surface. However, its acidic degradation products adversely affect cell proliferation and polymers implanted into the defect site undergo rapid degradation, losing 50% of their mass within two weeks [64]. For these reasons, applications of PGA are limited. PLA is similar to PGA, although its extra methyl group renders it more hydrophobic. PLA is also degraded slowlier than PGA, allowing the deposition of a replacement ECM in the defect site before the total loss of its mechanical integrity. PLGA (Poly-lactic-co-glycolic acid) is a copolymer composed of PGA and PLA monomers and can also be used as a scaffold in cartilage tissue engineering. Its overall material properties are dependent on the ratio of each polymer [65]. Polycaprolacton (PCL) is another polymer approved by FDA. It has a longer degradation time compared to PGA/PLA/PLGA; however, it also has poor wettability characteristics and has cellular interaction potential [64].

1.2.2.3 Composite Materials

Single-phase homogeneous scaffolds cannot fully replicate the structure and function of cartilage, or withstand the mechanical stresses at the defect site until the formation of new tissue. The disadvantages associated with natural and synthetic materials can be overcome by combining two or more polymers into a single material. The use of multiple polymers can improve the interaction of the scaffold material with native tissue and therefore enhance cartilage regeneration. Inert polymers in particular are coated or blended with biofunctional natural polymers in order to enhance cellular

attachment, proliferation and matrix synthesis. For example, it has been reported that filling the empty fraction of PLGA with chondrocytes in fibrin glue creates a material that exhibits homogenous cell distribution and better infiltration capacity during neotissue formation [66]. In another study, the immobilization of HA on PLGA scaffolds was shown to enhance chondrocyte attachment and differentiation, and also to prevent the dedifferentiation of chondrocytes [67].

The bioactivity of scaffolds can also be improved by the incorporation of bioactive molecules such as growth factors, adhesion proteins and short peptide sequences into their structure. The most important growth factors used in cartilage regeneration and tissue engineering approaches are the transforming growth factor β (TGF-β) family members, particularly TGF-β1 and TGF-β3. Various *in vitro* and *in vivo* studies have demonstrated that the use of TGF-beta assists in the maintenance of the chondrocyte phenotype and stimulates the synthesis of a collagen II-rich ECM [68,69]. Other growth factors used for the enhancement of cartilage regeneration are insulin-growth factor I (IGF-I), basic fibroblast growth factor (FGF-2), bone morphogenetic growth factors (BMPs), and Hedgehog (hh), wingless (Wnt) proteins.

In situ delivery of growth factors involves the covalent or non-covalent binding of the factors to the scaffold. Non-covalent binding is achieved by the physical entrapment of the growth factor within the scaffolding material. In one study, for example, basic FGF was immobilized onto the surface of PLGA after carbon dioxide plasma treatment, which facilitated the formation of ionic binding sites for the positively-charged FGF and greatly enhanced its binding to the polymer matrix [70]. Covalent binding allows the prolonged release, slow degradation and cellular internalization of the growth factor. Functional groups that are incorporated to

polymers by physical/chemical binding or copolymerization can be used for the conjugation of growth factors onto the scaffold's material [71,72].

Many research efforts focus on replicating tissue function in terms of both the structural architecture and mechanical and biological properties. Self-assembling peptides are used extensively to provide short amino acid-based biological signals to cells. Unlike long chains, the use of short chains does not sterically hinder active domains and increases the stability of the structure [73]. In one study, peptide amphiphile molecules were designed to display a TGFβ-binding epitope to sequester endogenously released TGFβ growth factor, and when implanted with MSCs, the TGFβ-binding PA significantly enhanced the recovery of microfracture-treated cartilage defects without the addition of exogenous growth factors [74]. As an alternative approach, the incorporation of cell-interacting sequences to the scaffold material is also used to elicit specific cellular responses. Methacrylated HA hydrogels have been functionalized with N-cadherin mimetic peptides to induce chondrogenic differentiation of MSCs, and results showed that the conjugation of N-cadherin mimetic peptides promoted the chondrogenesis and cartilage-specific ECM production of MSCs [75].

1.2.2.4 Physical Stimuli

Conventional cell culture methods lack the biochemical and structural characteristics of the ECM. As such, it is hard to obtain highly organized, layered and differentiated constructs. Nutrient diffusion and waste transport issues, and especially the accumulation of anabolic products, result in fluctuations in the metabolic state of the medium and affects the homogeneity of scaffolds in static cultures [76]. However, mechanical stimulation can be used during the conditioning of cell-seeded constructs

in *ex vivo* environments to improve the mechanical and functional properties of the resulting constructs [77]. Cartilage is a tissue that is constantly exposed to mechanical stimuli, and its maintenance and development are dependent on strong mechanical forces. It has been shown that extracellular matrices synthesized by chondrocytes under dynamic conditions display better compositions and zonal organization [77]. Bioreactors have been developed to apply mechanical loading regimens and create reproducible and homogeneous tissue constructs. Functional tissue engineering efforts have consequently focused on the modulation of dynamic compression, shear stress and hydrostatic pressure through bioreactors, with the aim of producing cartilage-mimetic constructs under a well-defined set of mechanical conditions [78]. Compressive loading is the main mechanical stimulus in the native cartilage environment, and especially in articulating joints. In joints, the cartilage tissue on one side physically compresses the opposing cartilage surface in a continuous manner. The most commonly used bioreactors are compression bioreactors, which generally use plates to imitate this form of contact. Dynamic compression, in which the loading is cyclical, has better outcomes than static compression in terms of ECM synthesis and chondrocyte proliferation rate. The combination of dynamic loading and growth factor application on agarose constructs have demonstrated that the two stimuli have a synergistic effect on the ECM synthesis [79].

The other type of loading exerted on chondocytes in their native environment is hydrostatic pressure. As mentioned previously, cartilage is a highly hydrated tissue and mature cartilage is composed primarily of water (70-80% by weight). During joint function, stress imparted on cartilage is distributed on cartilage surface homogeneously by water entrapped in the tissue; this effect is enhanced by the small effective pore size of cartilage tissue. As stress continues to be applied on the joint

surface, water is expelled from tissue and synovial fluid transmits the mechanical stress to water, thus decreasing friction and dissipating energy. During its normal function, cartilage is exposed to 3-10 MPa of stress at a frequency of around 1 Hz. Tissue engineering efforts using 0.1 and 15 MPa and 0.05 and 1 Hz pressures and frequencies have produced positive results for chondrocyte phenotype maintenance [80]. However, the application of constant hydrostatic pressure over long periods of time results in low cellular viability and matrix synthesis [81]. For that reason, in addition to pressure and frequency, the duration of hydrostatic pressure needs to be optimized for each construct or explant system.

The research described in this thesis aims to improve cartilage regeneration using bioactive peptide nanofibers. In order to achieve this, the composition and structural properties of native cartilage tissue was mimicked through bioactive peptide nanofibers. Glycosaminoglycan molecules are important components of both mature and developing cartilage and many regulator molecules acting on chondrogenesis rely on glycosaminoglycans. Based on the functional role of glycosaminoglycans in native cartilage tissue, in this work glycosaminoglycan mimicking peptide nanofibers were used to construct a chondrogenesis-triggering environment for progenitor cells.

CHAPTER 2

2 Growth and Differentiation of Pre-Chondrogenic Cells on Bioactive Self-Assembled Peptide Nanofibers

2.1 Synopsis

Cartilage defects are difficult to heal and current treatments are incapable of restoring the integrity of the tissue following injury. Consequently, development of novel treatment methods for cartilage tissue injuries, such as those caused by common joint diseases, is vital. Sulfated glycosaminoglycan molecules are fundamental components of both developing and mature cartilage extracellular matrices, and the interaction between regulator proteins and glycosaminoglycan molecules is of great importance in coordinating the differentiation, expansion and patterning of chondrocytes during cartilage development. In this study, we investigated the functional role of ECM on chondrogenic differentiation by emulating the cartilage ECM both chemically by presenting the functional groups of native glycosaminoglycans, and structurally through a self-assembled peptide nanofiber network. For this purpose, sulfonate, carboxylate and hydroxyl groups were integrated into the structure of self-assembled peptide nanofibers. We observed that prechondrogenic cells in insulin-free medium were able to aggregate into

cartilage-like nodule formations and deposit sulfated GAGs when cultured on GAG-mimetic peptide nanofibers. Collagen II and aggrecan expressions were likewise upregulated in these cells, further supporting the idea that the fibers stimulated chondrogenic differentiation. We therefore demonstrated that these GAG-mimetic fibers are able to modulate the maturation of prechondrogenic cells and can therefore be utilized for effective cartilage regeneration therapies.

2.2 Introduction

Cartilage tissue is regularly exposed to strong mechanical forces, but unlike other load-bearing tissues of the body, it lacks circulatory, nervous and lymphatic system input and is almost incapable of regenerating following injury. As such, diseases and injuries of cartilage tissue are exceptionally debilitating, and options for their treatment are limited [82]. Healthy cartilage is a highly structured tissue that is composed of chondrocytes and is surrounded with a specialized ECM that is largely composed of collagen and PGs. Chondrocytes are the only metabolically active units of cartilage, and are responsible for the turnover, maintenance and remodeling of the tissue. The solid fraction of cartilage tissue, which is composed of a dense collagen fibril network intertwined with a high concentration of negatively charged PGs, provides cartilage with its unique mechanical features in addition to offering biochemical signals to dictate complex cellular responses. The network of collagen fibers provides tensile strength to the tissue and counteracts the swelling pressure of PGs present in the cartilage ECM.[83]

PGs are composed of a core protein and a variable number of covalently attached glycosaminoglycan units. Glycosaminoglycans in cartilage are found in a variety of forms, including chondroitin sulfate, heparan sulfate, keratan sulfate, dermatan

sulfate and heparin.[84] Glycosaminoglycans bear a large number of sulfate and carboxyl groups, and the strongly negative charges imparted by these moieties are responsible for mediating specific protein-glycosaminoglycan interactions.[85,86] Due to the importance of protein-glycosaminoglycan interactions on cellular behavior, glycsoaminoglycans were reported as important regulator elements that guide the cell response towards migration, attachment, and differentiation during development by modulating the activity, concentration and presentation of several growth factors[15,87,88]. Many regulator molecules acting on chondrogenesis rely on heparan sulfate glycosaminoglycans [89–92]. Perlecan, a heparan sulfate PG [93], functions as a growth factor reservoir, thereby increasing local concentration of growth factors [94]. It provides signals to trigger chondrogenic differentiation [95–98]. In addition to their biological functions, PGs are highly negatively charged biomacromolecules. The carboxylate and sulfate groups on their structure provide fixed negative charge to the cartilage ECM and each PG-associated negative charge requires a mobile counter-ion to maintain tissue electroneutrality [83,99]. The mobile counter-ions (e.g. Na^+) also attract water to the tissue, resulting in a high swelling pressure that is critical for the mechanical integrity of cartilage. As such, negatively-charged groups are vital for regulating both the signaling networks and structural properties associated with cartilage, and are important models for matrix-mimicking scaffolds.

A number of studies have attempted to recapitulate the native cell microenvironment that is formed during chondrogenesis under *in vitro* conditions by manipulating a variety of signals [100–102]. In the present study, we utilized bioactive peptide nanofibers in order to construct a chondrogenesis-triggering environment. Self-assembled peptide amphiphile nanofibers are versatile scaffolds that enable the direct incorporation of various functional peptide moieties. Peptide amphiphile molecules

form nanofibers through the hydrophobic collapse of alkyl tails in aqueous environments at physiological pH [103]. The resulting higher-order structure is composed of nanofiber that are 5 nm in diameter and have pore sizes of 5-200 nm with a water content of more than 99% [104,105]. Due to these characteristics, peptide amphiphile nanofibers can mimic the native ECM in terms of structure and function by presenting bioactive signals on their surfaces [106–108].

Here, we investigated the effect of glycosaminoglycan mimetic self-assembled peptide nanofiber networks decorated with various chemical groups on the chondrogenic differentiation of chondroprogenitor ATDC5 cells. ATDC5 is a cell line derived from mouse embryonic carcinoma cells. In the presence of insulin, they show multistep chondrogenic differentiation similar to what is observed during endochondral bone formation [109]. They are easy to handle compared to MSCs and allow the straightforward tracking of chondrogenic differentiation due to their distinctive, assayable features during differentiation. Incorporating chemical groups that are also present in native glycosaminoglycan molecules on a nanofibrous network as a single system enhances the differentiate GAG-mimetic peptide nanofibers were designed to present chemical groups including sulfonate, carboxylate and hydroxyl, which are natively presented by glycosaminoglycan molecules in cartilage. The embryonic development of cartilage involves a series of complex and strictly regulated events. Before chondrogenic differentiation, stem cells undergo several processes characterized by recruitment and migration to a central core and formation of dense cell-cell interactions, which eventually results in the formation of cell aggregates [3,110,111]. Therefore, the effects of a chondro-inductive microenvironment on the differentiation of ATDC5 cells can be evaluated by analyzing the characteristic mechanisms of chondrogenic differentiation exhibited by

these cells. ATDC5 cells formed dense cell-cell interactions and cellular aggregates similar to these observed during *in vivo* chondrogenic differentiation, and deposited an extensive network of sulfated glycosaminoglycans on all bioactive peptide nanofiber systems that we have tested, without requiring external chondrogenic cues. However, when cartilage-specific gene expression profiling was examined, the glycosaminoglycan-mimetic peptide nanofiber network, which simultaneously presents sulfonate, carboxylate and hydroxyl groups, prompted collagen II, aggrecan and Sox 9 gene expression significantly more than other nanofiber systems.

2.3 Results and Discussion

2.3.1 Self-Assembled Peptide Amphiphile Nanofiber Formation

We used four different peptide nanofiber networks by mixing 3 different peptide amphiphile molecules at different ratios in order to assess the individual and synergistic effects of functional groups and the effect of overall charge. Peptide networks presented in this study mimic native GAGs by forming micrometer-long nanofibers with iterating chemical groups (containing carboxylate, hydroxyl, and sulfonate groups) presented on their surface. Lauryl-VVAGEGD-K(p-sulfobenzoyl)-S-Am (GAG-PA) carried sulfonate, carboxylate and hydroxyl groups to mimic sulfonated glycosaminoglycan molecules and named after the sulfonate group it bears, which was lacking in the other peptide molecules used in this study. Sulfonate groups are similar to the sulfate groups that form the functional residues of the polysaccharide components of the ECM, but differ from sulfate groups in terms of their stability against hydrolysis. For this reason, in our design we functionalized PA nanofibers with sulfonate groups on p-sulfobenzoic acid. This peptide system was previously designed and synthesized by our group and its activity in angiogenesis

and neural differentiation was demonstrated *in vitro*. We had also shown that this peptide nanofiber system encapsulated growth factors and increased their local concentrations.[112,113] Through this mechanism, cell differentiation was favored and improved on GAG-mimetic peptide nanofibers. In addition, in a recent study, these peptide nanofibers were shown to bind to heparin binding growth factors through their heparin binding domain and induce their activity, similar to natural heparan sulfate glycosaminoglycans [114]. Lauryl-VVAGE (E-PA) carried carboxylate and hydroxyl groups as functional units and was named according to the charged amino acid residue (Glutamic acid) at its C terminus. Lauryl-VVAGK-Am (K-PA) was a positively charged peptide amphiphile molecule and was used to induce nanofiber formation in the presence of either GAG-PA, E-PA or both through charge neutralization, the hydrophobic collapse of alkyl tail and the influence of the β-sheet forming unit VVAG (Figure 2.1a) [103]. All peptides were synthesized by solid phase synthesis and characterized by LC-MS (Figure 2.2a,c). Hydrophobic-collapse and β-sheet-driven self-assembly of oppositely-charged peptide amphiphile molecules resulted in the formation of nanofibers that are similar in structure to the native ECM. This particular geometry allows peptide nanofibers to densely present bioactive groups to cells (Figure 2.1b,c and 2.2d,e) [106]. Peptide nanofiber network 1 (NF 1) and peptide nanofiber network 2 (NF 2) contained only carboxylate and hydroxyl bearing E-PA at different concentrations. Glycosaminoglycan-mimetic nanofiber network 3 (NF 3) and nanofiber network 4 (NF 4) contained GAG-PA, which bore sulfonate, carboxylate and hydroxyl groups; however, NF 4 also contained E-PA. Each nanofiber system was formed by mixing negatively and positively charged peptide solutions at a concentration of 1 mM. All surfaces were coated with 150 μL/cm^2 peptide mixtures. Molar ratios of each peptide solution in

the mixture were determined according to the overall net charges of each nanofiber system. Net charges of E-PA, GAG-PA and K-PA were -2, -3 and +1; respectively. Overall neutral or negative charge in the gel system were obtained by adjusting the molar ratios of each positively and negatively charged PA solution in the mixture. In order to attain neutral NF 1, E-PA and K-PA were mixed at 1:2 molar ratio, while the molar ratio of E-PA and K-PA was adjusted to 2:1 in the negatively-charged NF 2, which resulted in higher carboxylate and hydroxyl amount in NF 2 compared to NF 1. In NF 3 and NF 4, which contained GAG-PA, the sulfonate amount was kept the same in both systems. For this reason, neutral NF 3 peptide nanofibers were obtained by mixing GAG-PA with K-PA alone at a 1:3 molar ratio, while negatively charged NF 4 peptide nanofibers were obtained by mixing GAG-PA, E-PA and K-PA at a 3:4:5 molar ratio. Thus, carboxylate groups were more densely presented on the NF 4 peptide nanofiber.

Table 2.1 List of Nanofiber Combinations Used in Differentiation of Chondroprogenitor ATDC5 Cells

Designations	Combinations	Net Charge
Nanofiber Network 1 (NF 1)	E-PA/K-PA	Neutral (0)
Nanofiber Network 2 (NF 2)	E-PA/K-PA	Negative (-1)
Nanofiber Network 3 (NF 3)	GAG-PA/K-PA	Neutral (0)
Nanofiber Network 4 (NF 4)	GAG-PA/E-PA/K-PA	Negative (-1)

Circular dichroism spectroscopy was employed in order to the analyze nanofiber formation behavior of peptide amphiphiles and their mixtures. E-PA and GAG-PA both had negative net charges around pH 7, and hence exhibited characteristic random coil spectra with minima around 198 nm. Positively charged K-PA had a spectrum similar to the negatively charged peptide amphiphiles, however with a

broader signal around 200 nm and a minimum around 220 nm. When K-PA solution was added to neutralize the negative charges of E-PA and GAG-PA, random coil signals immediately converted to β-sheet structures with a maximum around 200 nm and minimum around 220 nm. (Figure 2.1d) These results showed that the nanofiber formation was predominantly β-sheet driven. Peptide nanofibers were therefore found to offer a suitable network system for mimicking the ECM composition (three dimensional fibrillar network of cartilage ECM) and presenting negatively charged groups found on the GAG backbone on a synthetic macromolecule.

The mechanical properties of gels were investigated with oscillatory rheology. Due to technical limitations, gels used in rheology measurements were different than the gels used in cell culture experiments. However, mechanical properties of the bulk gel can provide a rough estimation (and comparison) of the mechanical properties of the fibrillar network, which cells sense when they are cultured on thin gels. 10 mM peptide amphiphile mixtures were prepared to form peptide hydrogels. The gel formation process was visible and the loss of fluidity could be observed by turning sample vial upside down. Storage (G′) and loss moduli (G″) were measured by oscillatory rheology at varying shear strains and constant angular frequency. Strain sweep tests showed that counter-charged PA molecules formed gels which stayed in linear viscoelastic region for strains up to 1%. Beyond this limit, gels gradually lost mechanical strength and stability. At 0.5% strain, storage moduli of the gels changed between 1-3 kPa, and loss moduli were 200-500 Pa. At this particular strain, all four combinations were similar in terms of storage and loss moduli, but the neutralized NF 3 gel was slightly stronger (Figure 2.2f).

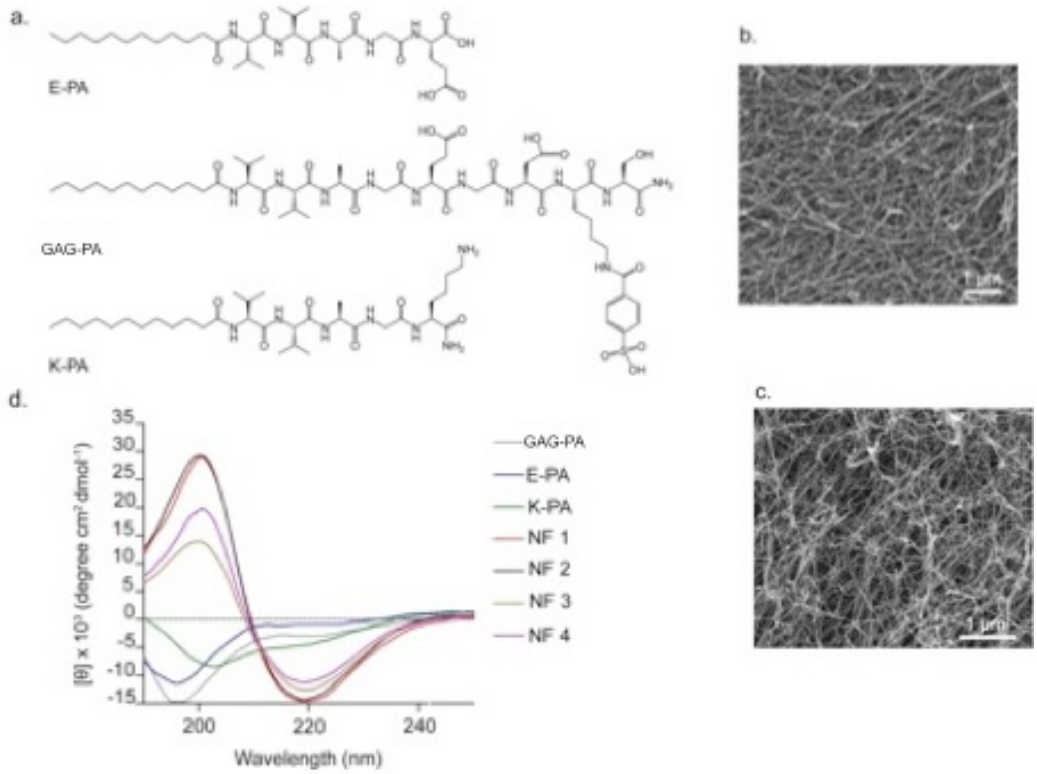

Figure 2.1 Self-Assembled Peptide Amphiphile Nanofibers.

(a) Chemical structures of peptide amphiphiles. SEM images showed the ECM-mimetic morphology of nanofiber networks NF2 (b) and NF 4 (c). (d) Circular dichroism spectra of peptide amphiphile combinations showing that nanofiber networks contain β-sheet secondary structures.

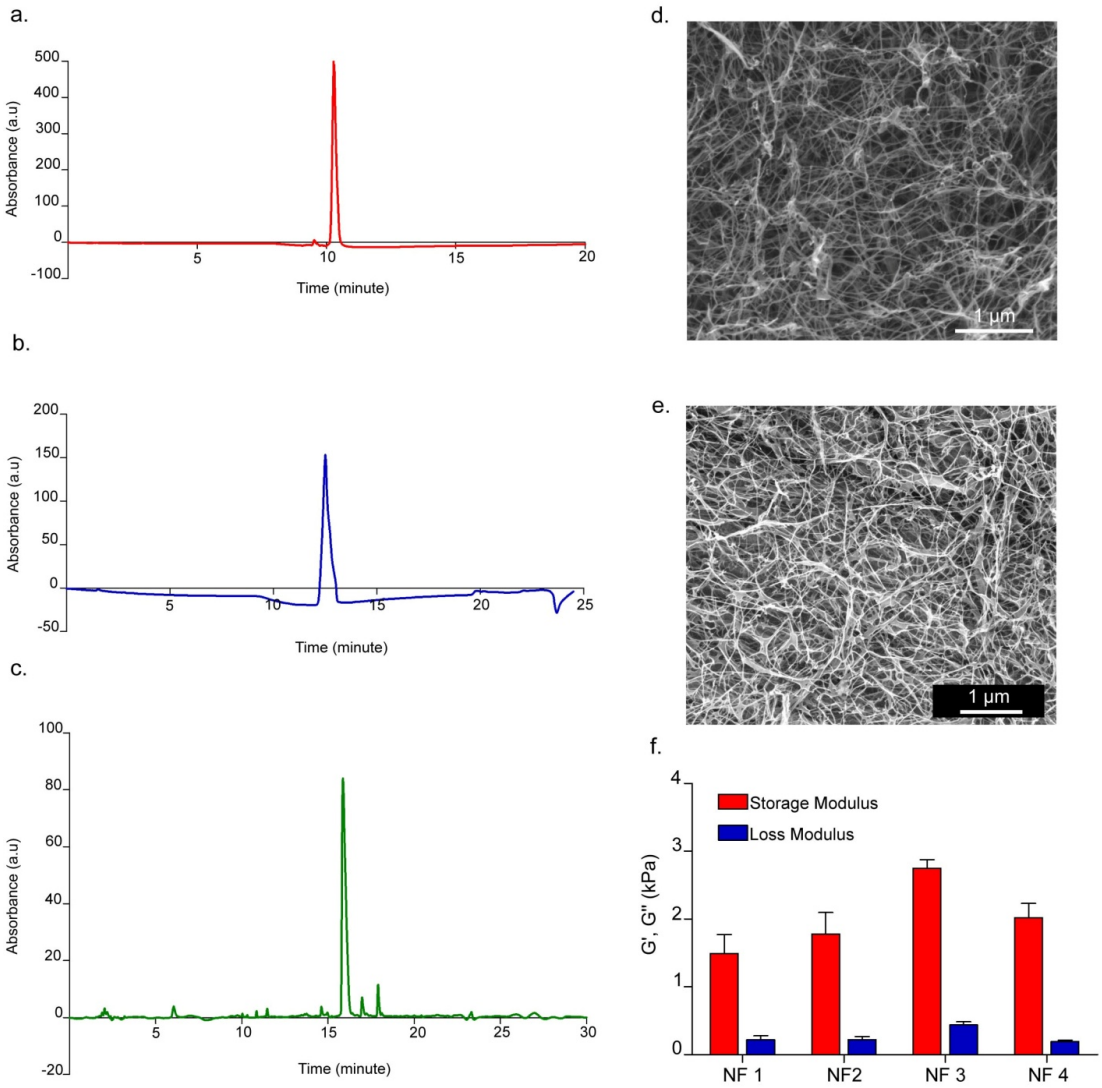

Figure 2.2 Liquid Chromatography of PA molecules.

LC of E-PA (a), K-PA (b) and GAG-PA (c) and SEM images of NF 1 (d) and NF 3 (e). Rheology measurements showed gel formation for all peptide amphiphile combinations (f).

2.3.2 Viability, Adhesion and Spreading of Cells on Peptide Nanofiber Networks

The prechondrogenic cell line ATDC5 was used as an *in vitro* model system of cartilage differentiation. Initial cellular responses were evaluated by investigating the adhesion and spreading characteristics of cells on peptide nanofibers. The interactions formed between cells and the surrounding microenvironment is crucial for the regulation of diverse cellular processes such as proliferation, migration, gene expression, differentiation and apoptosis. Thus, for a synthetic scaffold to be effective, the initial interaction of cells at the interface of the scaffold system should mimic native cell-ECM interactions to some extent. Peptide amphiphiles self-assembled into nanofibers similar to the native cell-ECM morphology and this morphology was preserved during cell culture studies (Figure 2.3). Adhesion of cells on the peptide nanofiber network system at 1 h and 3 h were studied, and the number of cells adhered on peptide nanofibers was found to be significantly greater than those that adhered on glass surfaces (Figure 2.4). The interaction of cells with peptide nanofibers was further assessed through staining the actin cytoskeleton and examining the spreading of cells. Cells seeded on peptide nanofibers managed to form prominent actin stress fibers and adhered firmly onto the peptide nanofiber networks (Figures 2.4b-i and 2.5).

Cellular viability of ATDC5 cells seeded on peptide nanofibers was assessed by Calcein AM staining. The viability of cells on peptide fibers was compared to cells that were cultured on glass surfaces at varying time points (24 h, 48 h and 72 h). There was no significant difference between cells cultured on the glass surface and peptide nanofibers and the viabilities of the cells on all surfaces were comparable. This indicates that no toxicity was induced by the material (Figure 2.4). Overall,

adhesion, spreading and viability results showed that peptide nanofibers provide a suitable microenvironment for the growth and proliferation of ATDC5 cells.

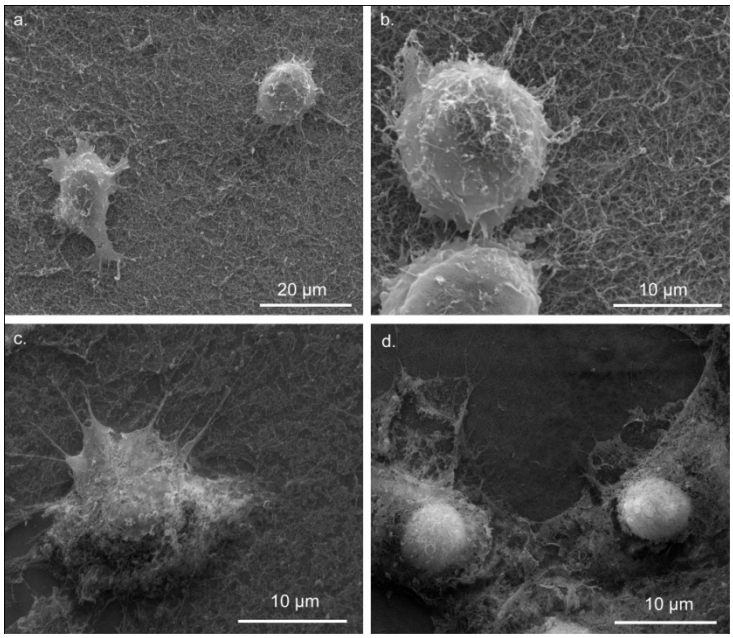

Figure 2.3 ATDC5 Cells Encounter the Nanofibrous Structure of Peptide Amphiphile Nanofibers During Cell Culture Experiments.

SEM images of ATDC5 cells seeded on PA-coated glass surfaces (a,b) after 3 h and (c,d) after 7 days.

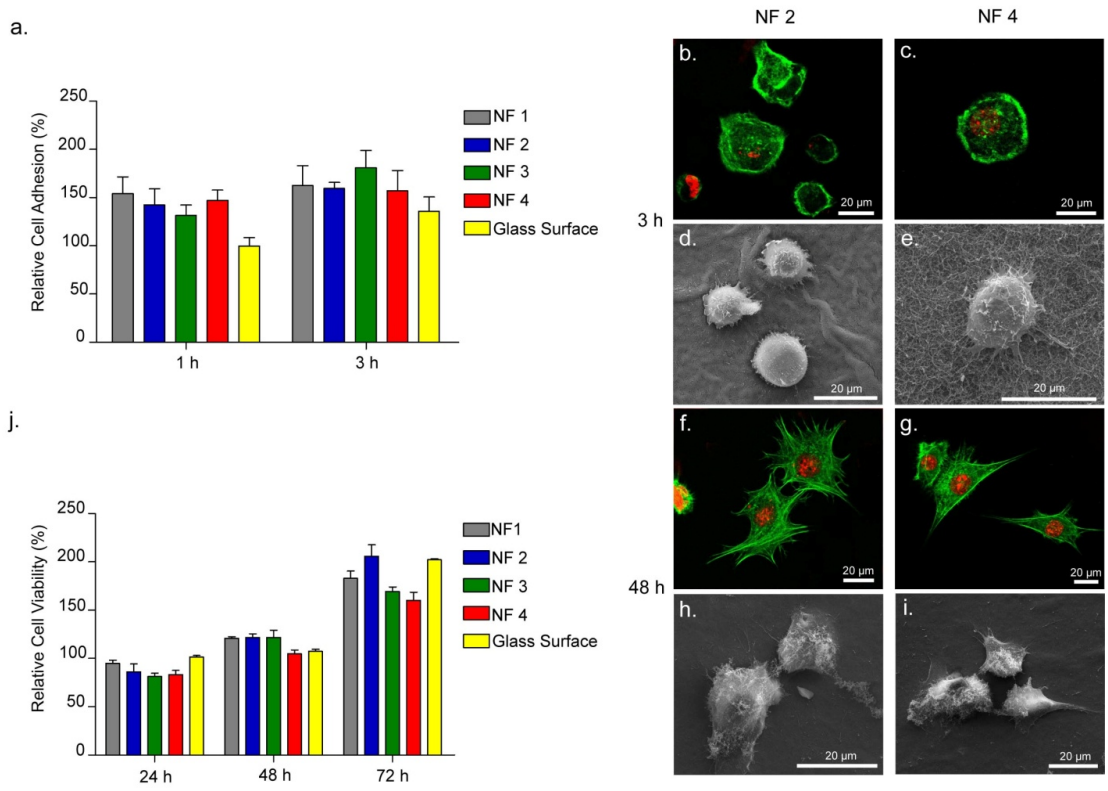

Figure 2.4 Adhesion, Spreading and Viability of ATDC5 Cells Cultured on Peptide Nanofibers.

(a) Relative adhesion of ATDC5 cells on peptide nanofibers after 1 h and 3 h. Spreading of ATDC5 cells characterized with actin fiber staining (nuclei stained with TO-PRO3 (red), actin fibers stained with TRITC-conjugated phalloidin (green)) (b, c, f, g) and SEM imaging (d, e, h, i) at 3 h and 48 h. (j) Relative cell viability on day 3, 7 and 14 showed that nanofiber networks are biocompatible.

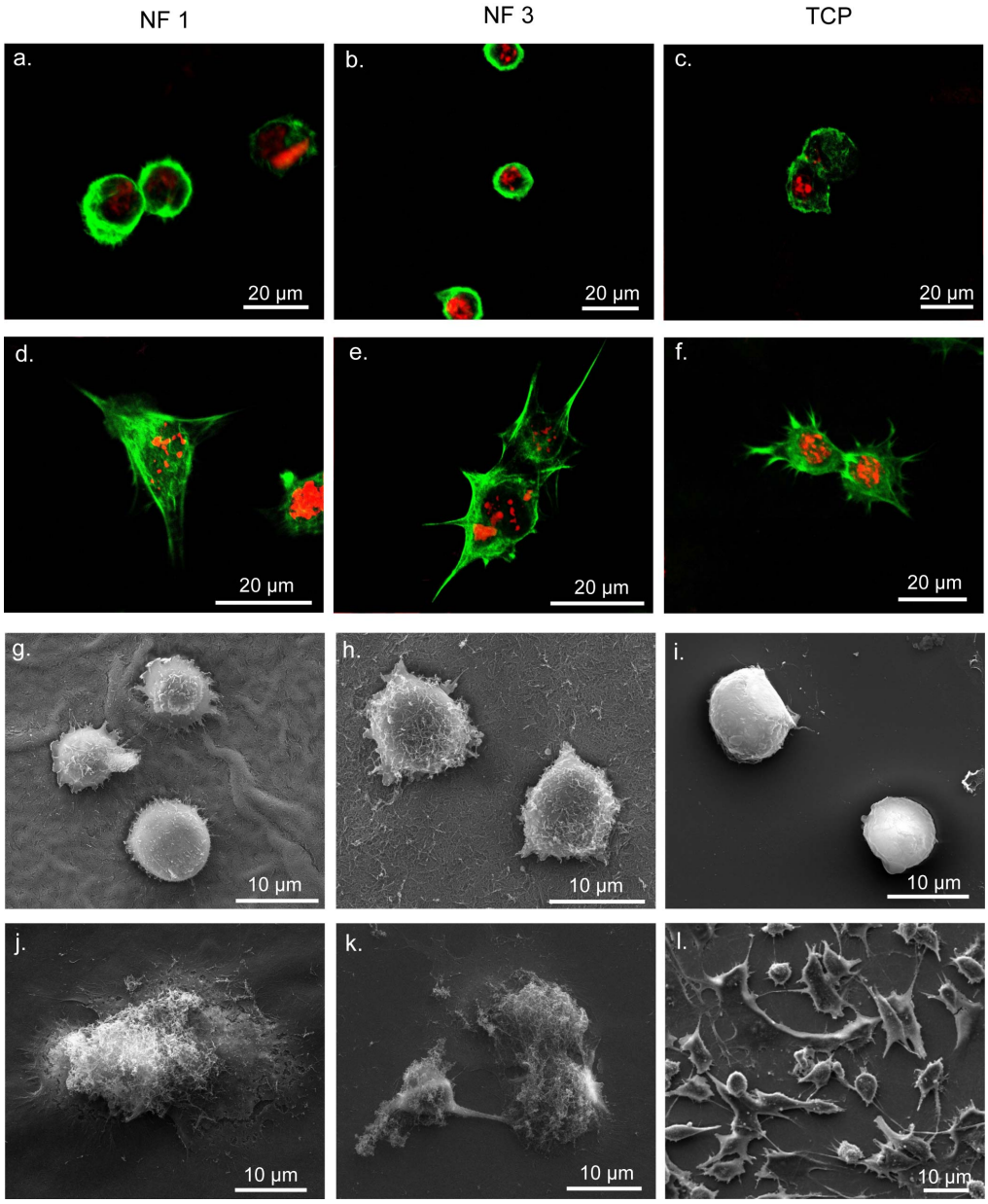

Figure 2.5 Comparable Spreading of ATDC5 Cells on Peptides vs. TCP.

Spreading of ATDC5 cells, as characterized by actin fiber staining (nuclei stained with TO-PRO3 (red), actin fibers stained with TRITC-conjugated phalloidin (green)) (a-f) and SEM imaging (g-l) at 3 h (a-c, g-i) and 48 h (d-f, j-l) of incubation.

2.3.3 Morphological Effects of Nanofiber Networks on ATDC5 Cells

Dynamic molecular-level interactions taking place between cells and the peptide nanofiber system may dictate the differentiation route and fate of cells. Thus, it is crucial to monitor newly formed tissue constructs in terms of morphology, matrix production and gene expression. In order to examine cell responses to peptide nanofibers through longer time periods, ATDC5 cells were seeded on either peptide nanofiber networks or TCPs and imaged at different time points. Cells were seeded at a high density in order to enhance spatial cell-cell contacts and better simulate the conditions experienced during native cartilage development. ATDC5 cells treated with insulin typically commit to chondrogenesis through a condensation stage, forming cartilage nodules within 21 days. ATDC5 cells commit to form nodular structures after reaching confluency, following a growth phase [109,115]. For the following differentiation studies, ATDC5 cells were cultured either in the absence or presence of insulin on both uncoated tissue culture plate (TCP) and peptide amphiphile nanofiber surfaces.

During initial seeding, cells were distributed homogeneously on peptide nanofibers or TCP, and no cell clusters were observed. Interestingly, after 36 h, cells seeded on the peptide nanofibers presented a rounded morphology similar to the cytological characteristics of chondrocytes *in vivo*, and started to move to a central core and form many independent cellular aggregates that mimic mesenchymal condensation (Figures 2.6a-h and 2.7a-h). This spontaneous response arose on each peptide nanofiber system even in the absence of insulin, which is known as an essential chondrogenic cue.

A similar trend of growth was then observed on all peptide nanofiber systems, in that the size of aggregates progressively increased while the number of aggregates

decreased after longer durations of incubation (Figures 2.6i,j and 2.7i,j). This could be caused by the formation of smaller aggregates on peptide nanofibers during earlier stages, which give rise to larger aggregates after further incubation. When cells were cultured in insulin-supplemented media, the aggregate area was slightly larger and the total number of aggregates was lower compared to aggregates formed in insulin-free media. However, when total aggregate area was considered, insulin treatment had no significant effect. Cells cultured on TCPs in the presence of insulin exhibited much smaller cartilaginous nodules (Figure 2.8). This might be caused by the fact that ATDC5 cells cultured on TCP may not have committed to chondrogenic differentiation as fast as cells cultured on peptide nanofibers.

Considering the characteristics of the aggregates, cells tended to form larger aggregates in fewer numbers (in the range of 80-330) on NF 3, 2, and 1 compared to NF 4. On the contrary, the trend was the opposite on NF 4; cells formed smaller aggregates in higher numbers (~270 to 430). The varying size and number of aggregates implied different responses of cells to different peptide networks in the context of chondrogenic differentiation. In terms of total aggregate area, results showed that there is a consistent change in each group over time (Figure 2.9). Total aggregate area was found to increase by day 7, followed by a consistent decrease after this peak (until day 9). The increase was likely due to the formation of new aggregates and the following decrease could be due to the compaction of those cell aggregates through the merging of loosely formed units. The compaction of cell aggregates is known as an inherent feature of the condensation of limb progenitor cells [116].

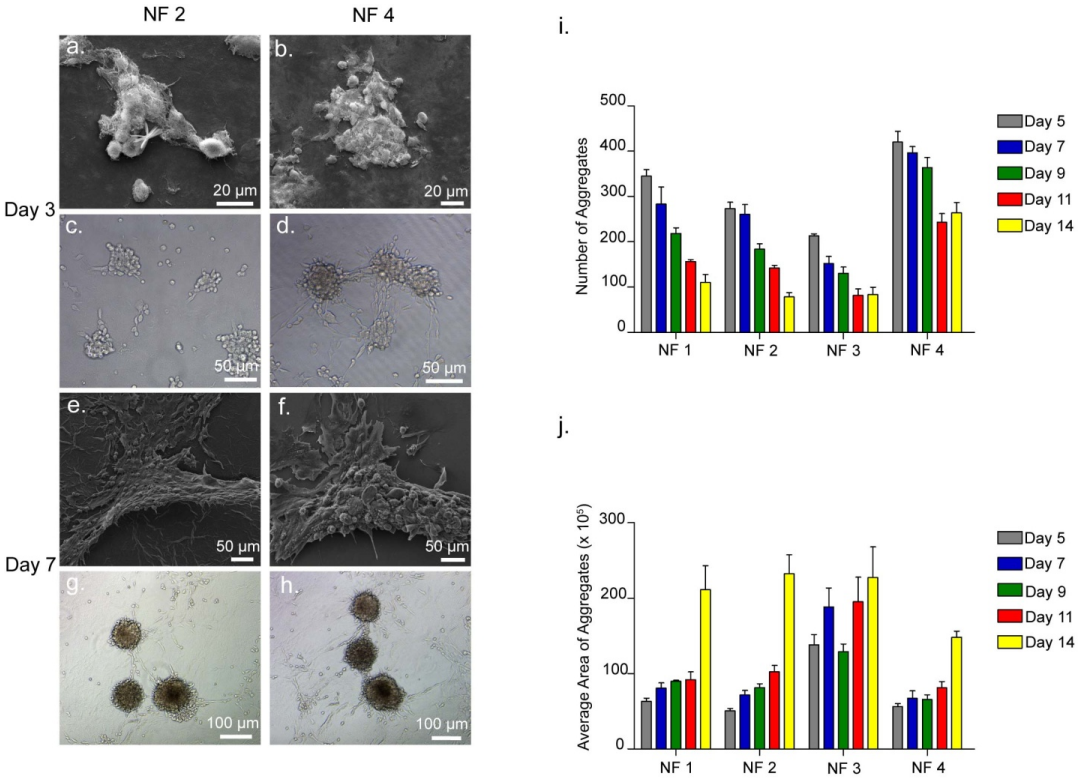

Figure 2.6 Aggregate Formation of ATDC5 Cells in the Absence of Insulin on Scaffolds.

Light microscope images (c, d, g, h) and SEM images (a, b, e, f) of aggregate formation on NF 2 and NF 4 on day 3 and 7. Number of aggregates (i) and average area of aggregates (j) of ATDC5 cells cultured on all peptide networks in media without insulin. Values represent mean ± SEM, n=3.

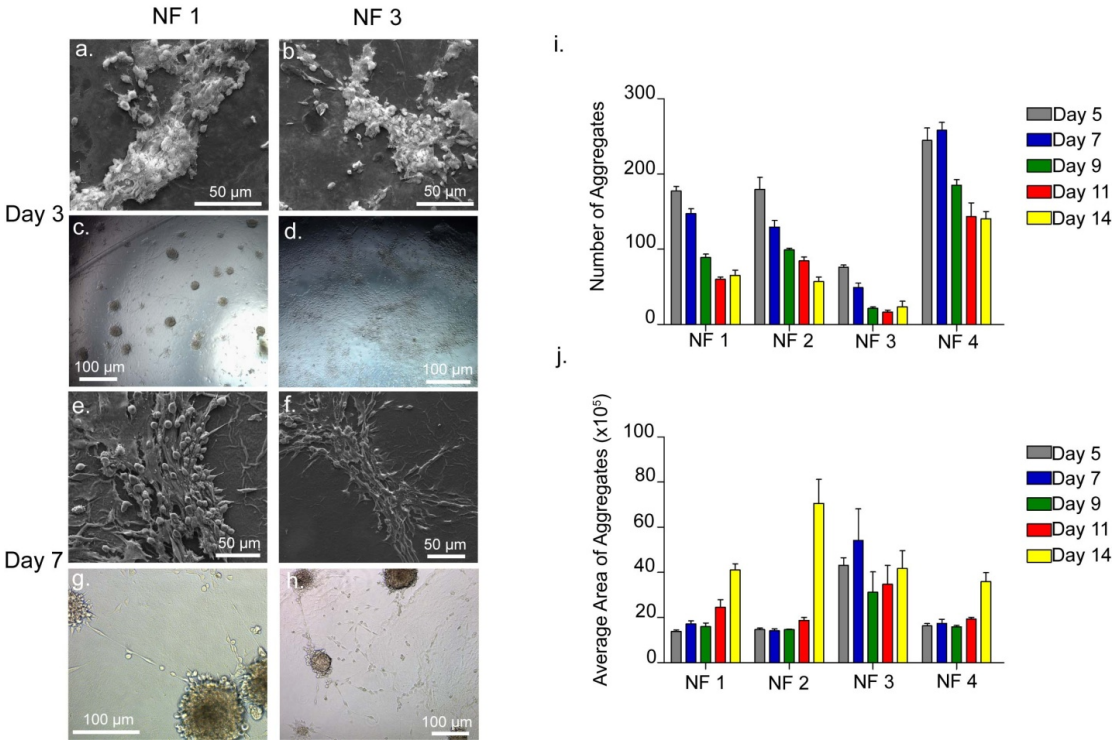

Figure 2.7 Aggregate Formation of ATDC5 Cells in the Presence of Insulin on Scaffolds.

Light microscope images (c, d, g, h) and SEM images (a, b, e, f) of aggregate formation on NF 1 and NF 3 on day 3 and 7. Number of aggregates (i) and average area of aggregates (j) of ATDC5 cells cultured on all scaffolds in media with insulin. Values represent mean ± SEM, n=3.

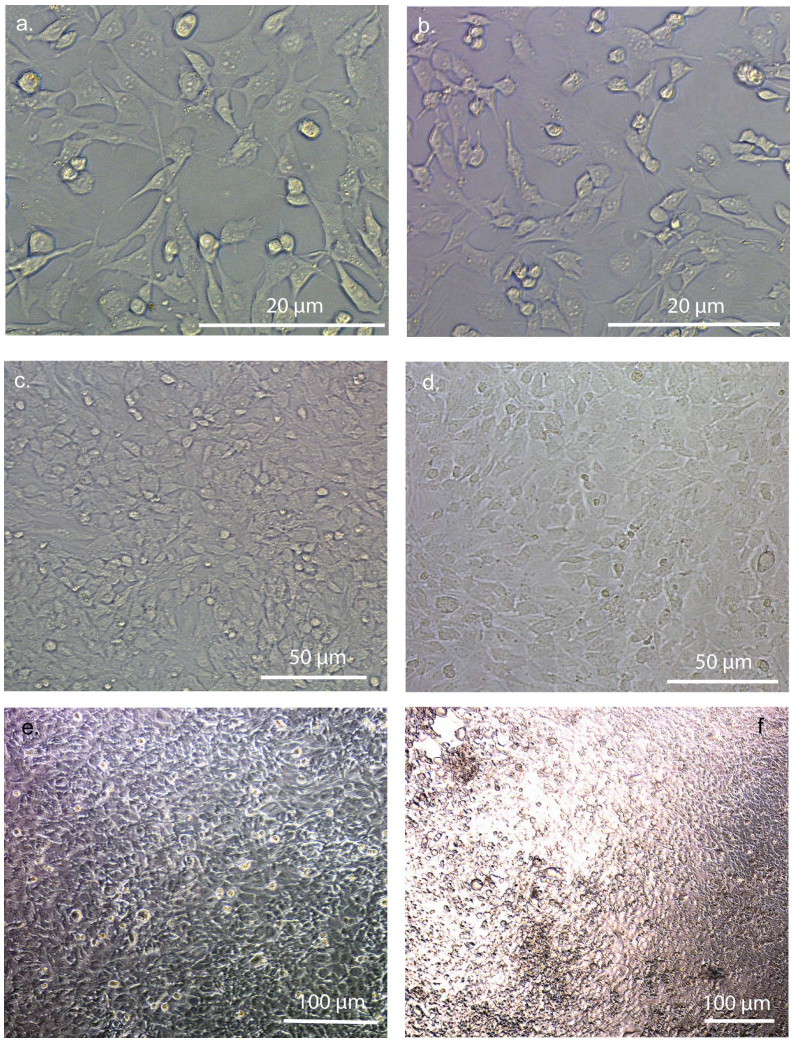

Figure 2.8 ATDC5 cells on TCP.

ATDC5 cells on TCP on day 3 (a,b), 7 (c,d) and 14 (e,f) in the absence (a,c,e) and in the presence of insulin (b,d,f).

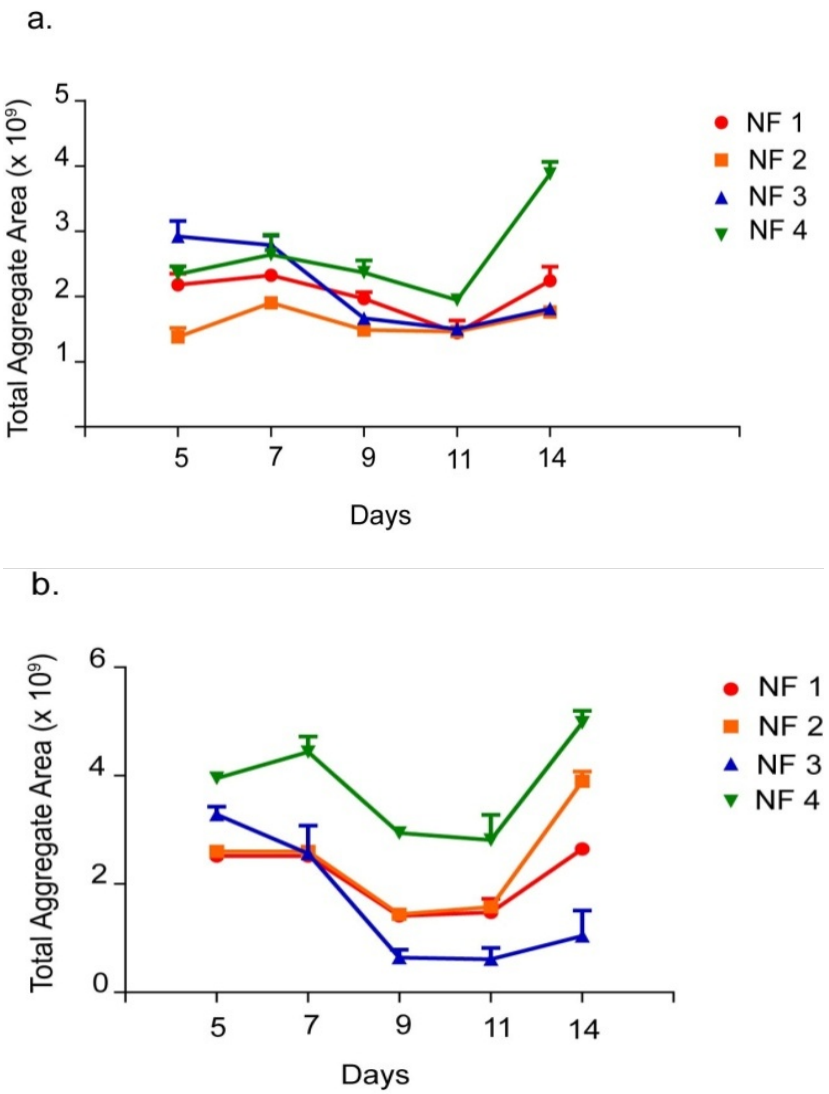

Figure 2.9 Total Aggregate Area of ATDC5 Cells Cultured on PA-Coated Surfaces.

(a) in the absence and (b) in the presence of insulin.

2.3.4 Cartilaginous Matrix Deposition

Having observed that cellular aggregates resembling cartilaginous nodules formed on peptide nanofiber networks, we decided to further characterize cellular differentiation in terms of matrix production and gene expression. The cartilage ECM is mainly composed of collagen fibers and large PG molecules, which are responsible for providing cartilage tissue with its unique mechano-physical characteristics. For this reason, we investigated the ability of ATDC5 cells to deposit glycosaminoglycans, vital components of the cartilage ECM. Cells and their exudates were stained with Safranin-O, a cationic dye that stochiometrically binds to glycosaminoglycans, to visualize sulfated GAG deposition. Cell aggregates formed on each nanofiber network stained discretely with Safranin-O with clear boundaries showing the accumulation of sulfated glycosaminoglycans (Figures 2.10a-f and 2.11a-f). No clear intensity differences were observed between cell aggregates formed on different peptide nanofibers. ATDC5 cells grown on TCPs did not form any aggregates, and stained faintly.

Even though Safranin-O staining is a common indicator for the deposition of cartilaginous matrix, it may not be sensitive enough to reflect small differences in PG content deposited on different peptide nanofibers. Thus, we quantified sulfated glycosaminoglycan production by cell aggregates on various nanofiber networks on days 3, 7 and 14 by dimethylmethylene blue (DMMB) assay, which is a rapid method for the quantification of sulfated glycosaminoglycans. DMMB assay revealed higher amounts of sulfated glycosaminoglycan deposition on peptide nanofibers compared to TCPs. This showed that the peptide nanofiber networks induced production and deposition of sulfated glycosaminoglycans to a greater extent than tissue plate controls. On day 3 and 7, there was no significant difference

between glycosaminoglycan depositions of cells cultured on different peptide networks, however, on day 14, cells cultured on NF 3 exhibited the highest (~7) GAG/DNA ratio (Figures 2.10g and 2.11g). A distinctive correlation exists between the aggregate formation and GAG deposition trends of the cells on peptide networks: When cells formed larger aggregates in fewer numbers, they accumulated more sulfated GAGs (NF 3); however, when cells formed smaller aggregates in higher numbers, they accumulated less sulfated GAGs (NF 4).

In order to further analyze the effect of peptide nanofibers on chondrogenic differentiation, cells were immunostained for cartilage-specific proteins (e.g. Collagen II and Sox 9). Cells cultured on all of the peptide nanofiber networks expressed Collagen II on days 3, 7 and 14 and Sox 9 mostly on day 3 (Figures 2.12), and we also observed staining on cells cultured on TCP (Figure 2.12 and 2.13). Since Sox 9 is a transcription factor, its expression was localized in or around the nucleus. On day 3, its expression could be observed on all groups, however, its expression level was much lower on days 7 or 14, probably due to Sox 9 being an early marker of chondrogenesis (Figure 2.15).

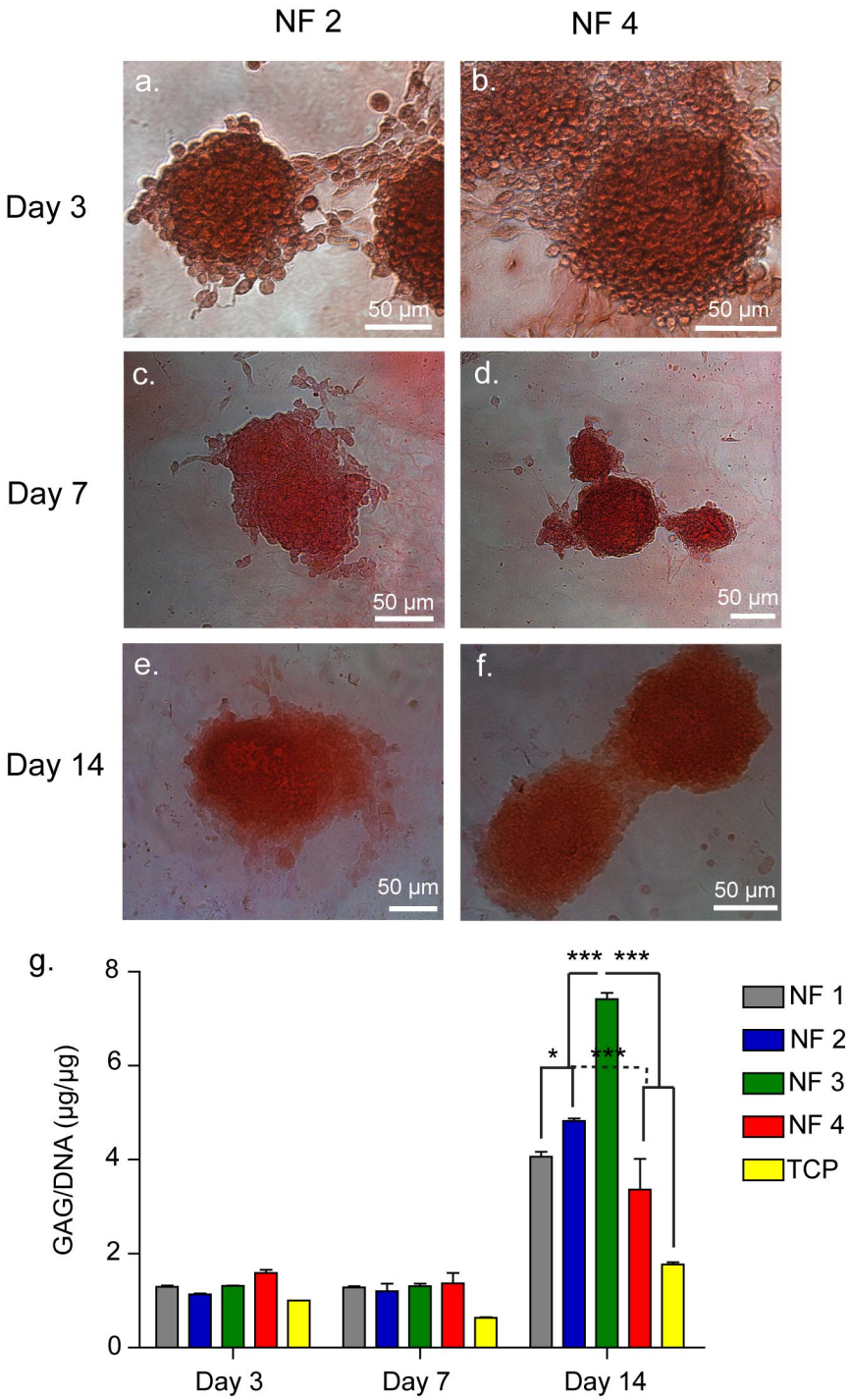

Figure 2.10 Safranin-O and DMMB Staining of ATDC5 Cells on NF 2 and NF 4, Showing GAG Incorporation.

Safranin-O staining of aggregates cultured on NF 2 network (a, c, e) and NF 4 network (b, d, f) on day 3, 7 and 14. g) DMMB assay showing sulfated glycosaminoglycan content of ATDC5 aggregates normalized to DNA content on day 3, 7 and 14.

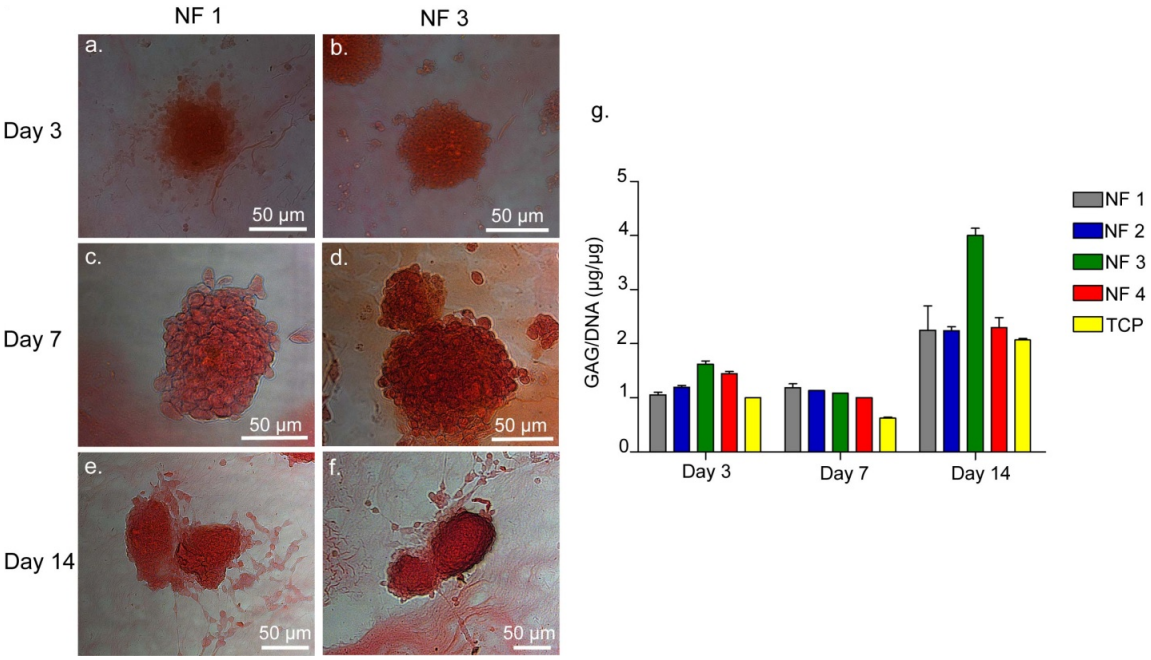

Figure 2.11 Safranin-O and DMMB Staining by ATDC5 Cells on NF 1 and NF 3 Showing GAG Incorporation.

Safranin-O staining of aggregates cultured on NF 1 scaffold (a, c, e) and NF 3 scaffold (b, d, f) in the presence of insulin on day 3, 7 and 14. g) DMMB assay showing glycosaminoglycan content of ATDC5 aggregates normalized to DNA content on day 3, 7 and 14.

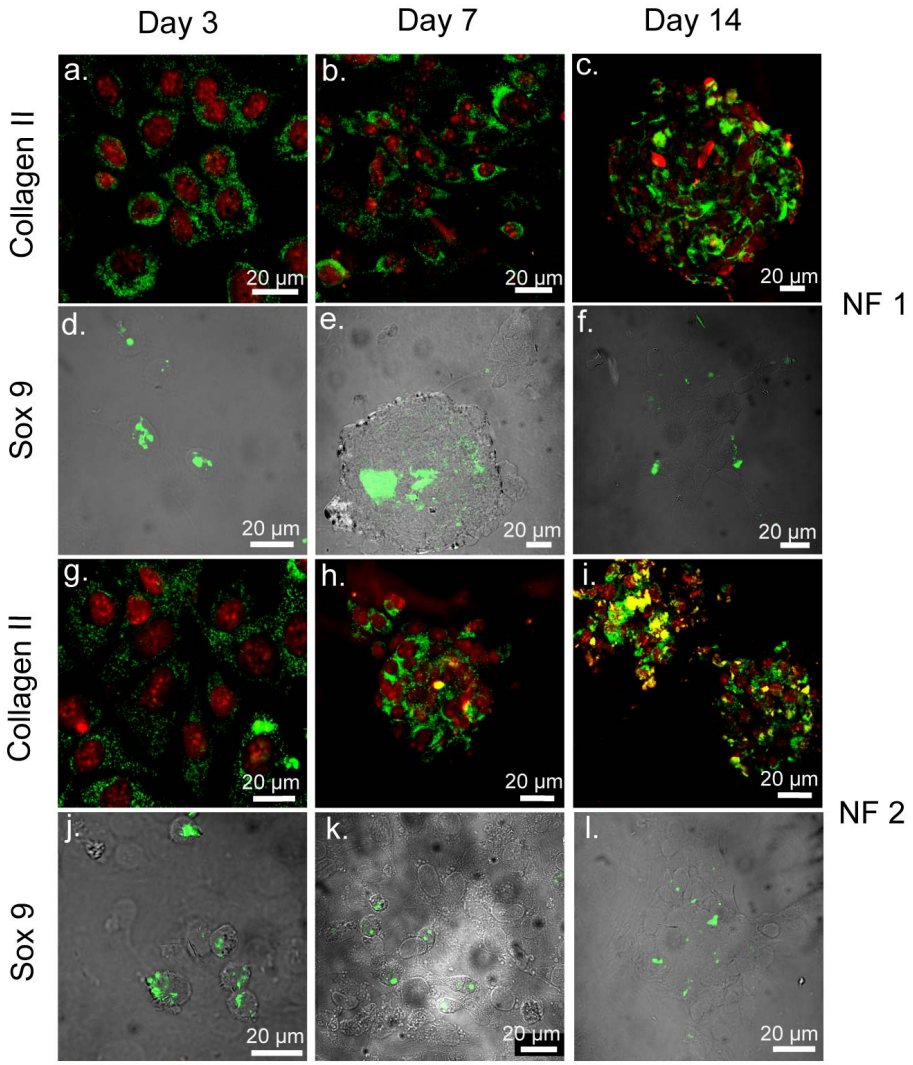

Figure 2.12 ATDC5 Cells Cultured on All Scaffolds Express Cartilage Specific Proteins on Day 3, 7, and 14.

Collagen II and Sox 9 were labeled with Cy3 secondary antibody (green) and cell nuclei were labeled with TO-PRO®-3 (red). Immunostainings showed that ATDC5 cells deposited Collagen II on all days and expressed Sox 9.

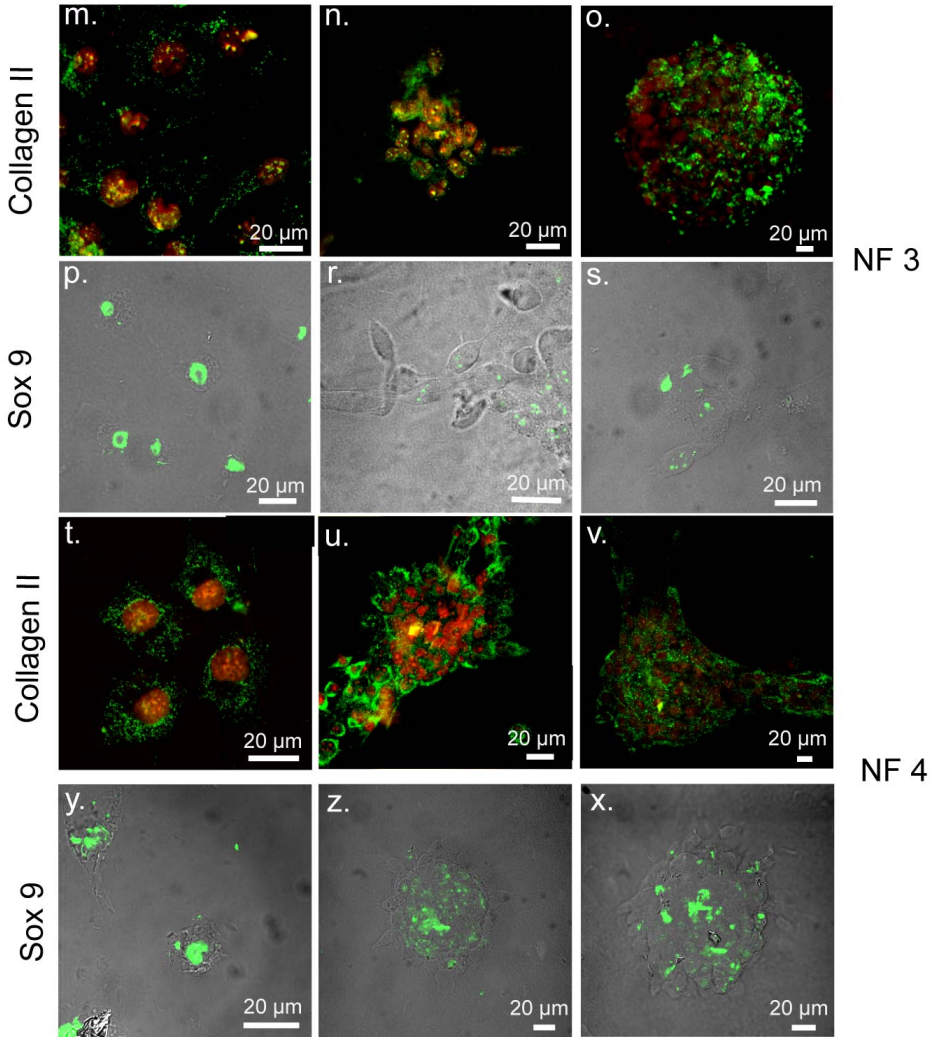

Figure 2.13 ATDC5 Cells Cultured on All Scaffolds Express Cartilage Specific Proteins on Day 3, 7, and 14.

Collagen II and Sox 9 were labeled with Cy3 secondary antibody (green) and cell nuclei were labeled with TO-PRO®-3 (red). Immunostainings showed that ATDC5 cells deposited Collagen II on all days and expressed Sox 9.

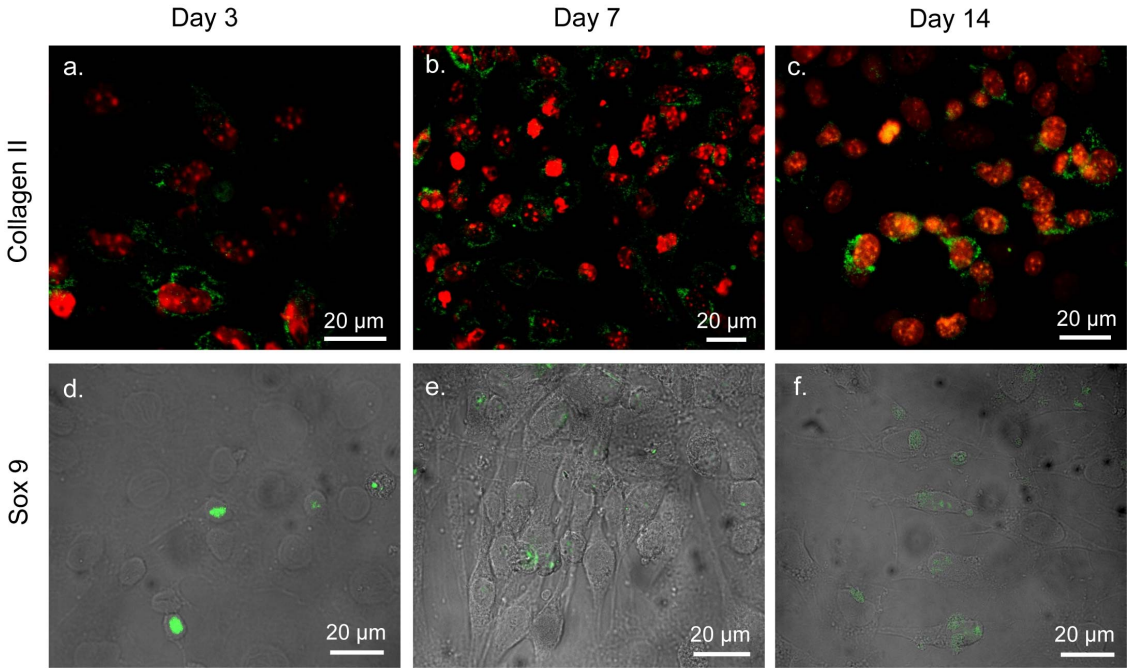

Figure 2.14 ATDC5 Cells Cultured on TCP Stained with Collagen II and Sox 9 Antibodies on Day 3, 7, and 14.

Collagen II and Sox 9 were labeled with Cy3 secondary antibody (green) and cell nuclei were labeled with TO-PRO®-3 (red)

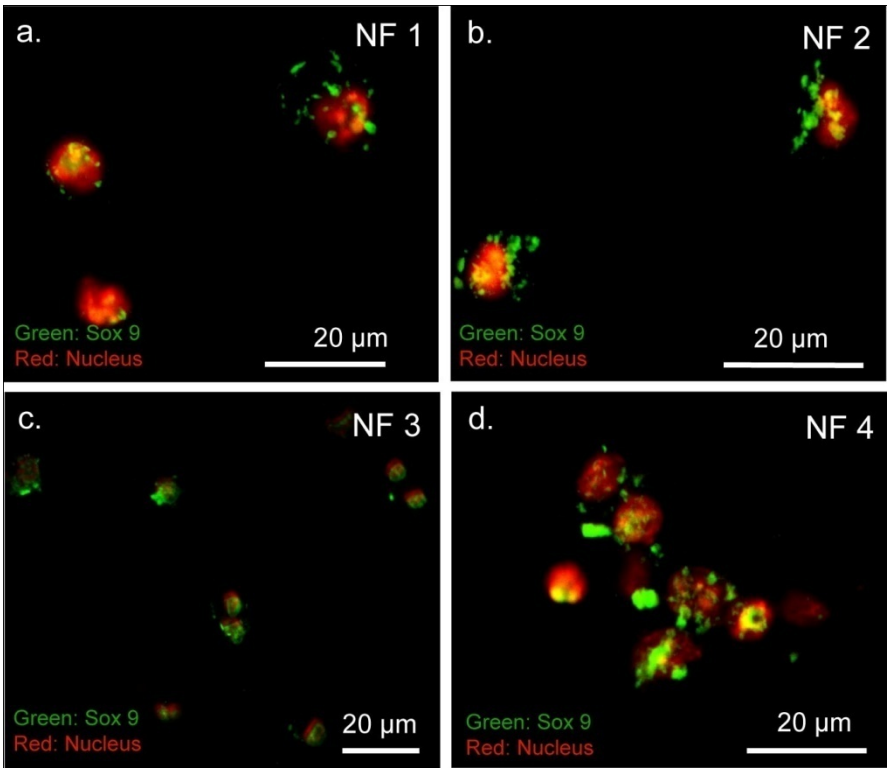

Figure 2.15 Localization of Sox 9 at or around Nucleus on Day 3.

Cells cultured on NF 1 (a), NF 2 (b), NF 3 (c) and NF 4 (d) expressed SOX 9 and showed colocalization with nuclei. Sox 9 labeled was with Cy3 conjugated secondary antibody (green) and nuclei were labeled with TO-PRO®-3 (red).

2.3.5 Gene Expression Profiles

Gene expression profiles of cells cultured on peptide network-coated and uncoated surfaces were analyzed in order to understand the differential effects of various peptide nanofiber systems on the progression of chondrogenic differentiation. The expression of cartilage-specific genes such as aggrecan, Collagen II, Sox 9 and collagen I were examined on days 3, 7 and 14. As mentioned above, Sox 9 is a key chondrogenic transcription factor that is expressed in cells undergoing cellular condensation step and regulates the expression of definitive cartilage markers like Collagen II and Aggrecan [117]. Consistent with aggregate formation and matrix deposition, Sox 9 was upregulated by at least ~1.5 fold when cells were cultured on NF 1 and NF 2 and by ~3 fold when cells were cultured on NF 3 and NF 4 in the absence of insulin on day 3. There was a significant difference between the glycosaminoglycan-mimetic peptide nanofiber networks decorated with sulfonate groups and the ones that did not have these groups on day 3 (Figures 2.16c and 2.17c). The trend continued on day 7 with modest decreases. Aggrecan expression profiles were also investigated, since aggrecan is a cartilage-specific PG core protein that is one of the downstream targets of Sox 9 in the chondrogenic differentiation pathway. Aggrecan expression was considerable (in the range of 1.82-3.38 fold) on all of the peptide nanofiber systems, yet it reached its highest value (day 3: 5.85, day 7: 8.65) on NF 4, which was significantly higher than other peptide nanofibers (Figures 2.16a and 2.17a). In parallel to aggrecan expression, collagen II expression was also upregulated by cells cultured on peptide networks (in the range of 3.29-6.68 fold) and again its highest fold change value (day 3: 31, day 7: 38) was observed when cells were cultured on NF 4 (Figures 2.16b and 2.17b). In addition, we analyzed the ratio of collagen II to collagen I, since collagen II/I ratio is another

indicator for chondrogenic differentiation. Collagen I is a chondrocyte dedifferentiation marker that is found in fibrocartilage, its expression in regenerating cartilage is therefore undesirable. Consistent with the expression of other genes, the collagen II/I ratio was significantly higher in cells cultured on the NF 4 network (Figures 2.16d and 2.17d).

Overall, aggregate formation was observed on each peptide nanofiber system and glycosaminoglycan deposition was considered to be the evidence of chondrogenic differentiation. This was validated through Safranin-O staining and quantified through DMMB assay. Gene expression analysis further revealed that cartilage-specific genes were highly expressed in cells that were cultured on peptide nanofibers compared to standard TCP. Cumulatively considering aggregate size-number, glycosaminoglycan deposition and gene expression profiles, we concluded that each peptide construct promoted chondrogenic differentiation to varying extents. ATDC5 cells formed larger aggregates in fewer numbers, deposited more sulfated GAGs and expressed cartilage specific genes in smaller quantity (aggrecan; 1.82-3.38 fold, collagen II; 3.29-6.68) on NF 3, 2 and 1. This trend was the opposite in NF 4, on which ATDC5 cells formed more aggregates in smaller sizes, deposited less sulfated glycosaminoglycans and expressed cartilage specific-genes at the highest quantity among the peptide networks tested. We conclude that high gene expression does not necessarily translate to high sulfated glycosaminoglycan deposition. On the other hand, this result does not mean that the total amount of glycosaminoglycans does not correlate with the gene expression profile, since the essay that we have utilized to measure glycosaminoglycan quantity, DMMB assay, is ubiquitously used to quantify deposited sulfated glycosaminoglycan and is not sensitive to reveal the cartilage-specific composition of glycosaminoglycan. Thus, gene expression analysis

using qRT-PCR is more reliable to assess cellular behaviors, and differentiation marker analysis results are considered more informative and accurate for the present study. The superior chondrogenic potential of NF 4 was primarily attributed to the synergistic effect of different peptide amphiphile molecules in one system, as NF 4 was composed of both E-PA and GAG-PA and contained carboxylate, hydroxyl and sulfonate groups in a single scaffold. On the other hand, the effect of overall charge might also play a role in the difference between NF 3 and NF 4, since both of these peptide networks contained sulfonate, hydroxyl and carboxylate groups. However, overall charge differences did not make a significant difference between cells cultured on NF 1 (neutral) and NF 2 (negative), both of which contained the same type of molecules. Thus, the ratio of the functional groups might play a stronger role than the overall charge of the peptide network. In addition, it is important to remark that the formation of cellular aggregates and deposition of cartilaginous matrix on each nanofiber network suggests that the nanofibrous network morphology itself may play a role in evoking the differentiation of chondroprogenitor cells.

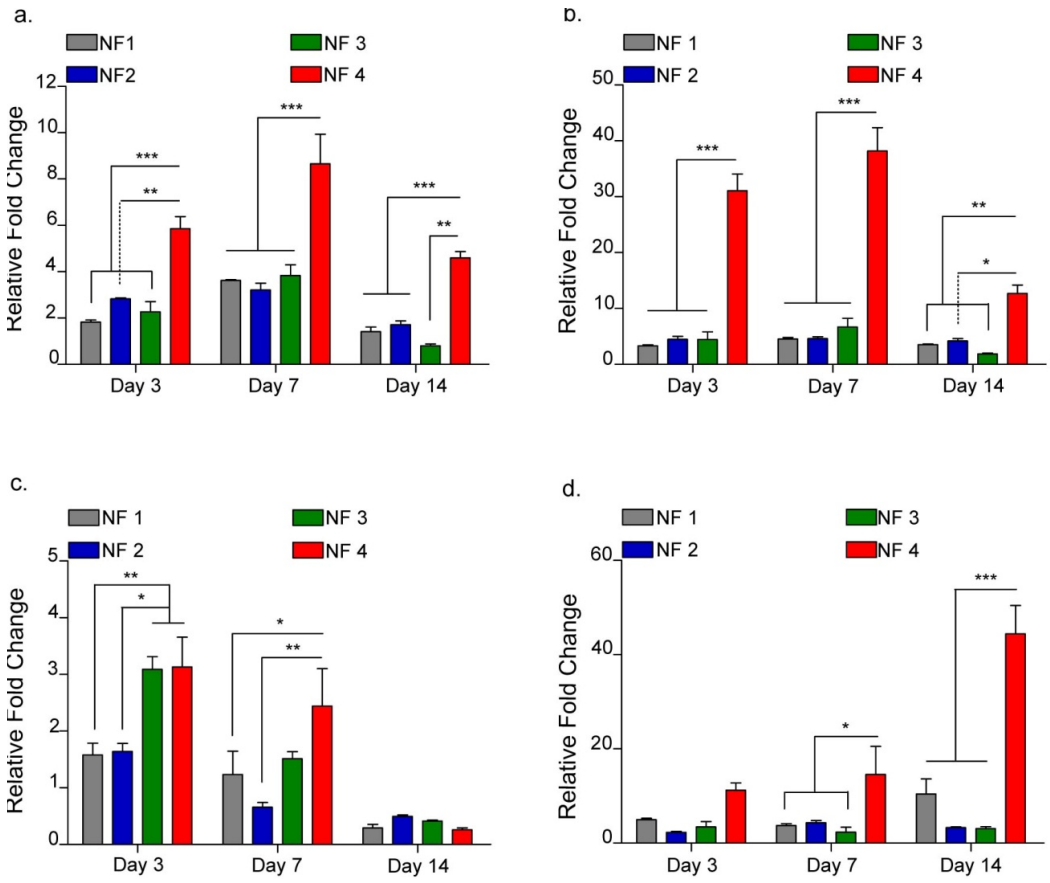

Figure 2.16 Gene Expression Analysis in the Absence of Insulin.

(a) Aggrecan gene expression. (b) Collagen II gene expression. (c) Sox 9 gene expression. (d) Collagen II/I gene expression ratio. The expression level of each gene was normalized against TCP and GAPDH was used as the internal control. Values represent mean ± SEM, n=6 (***p<0.0001, **p<0.01, *p<0.05).

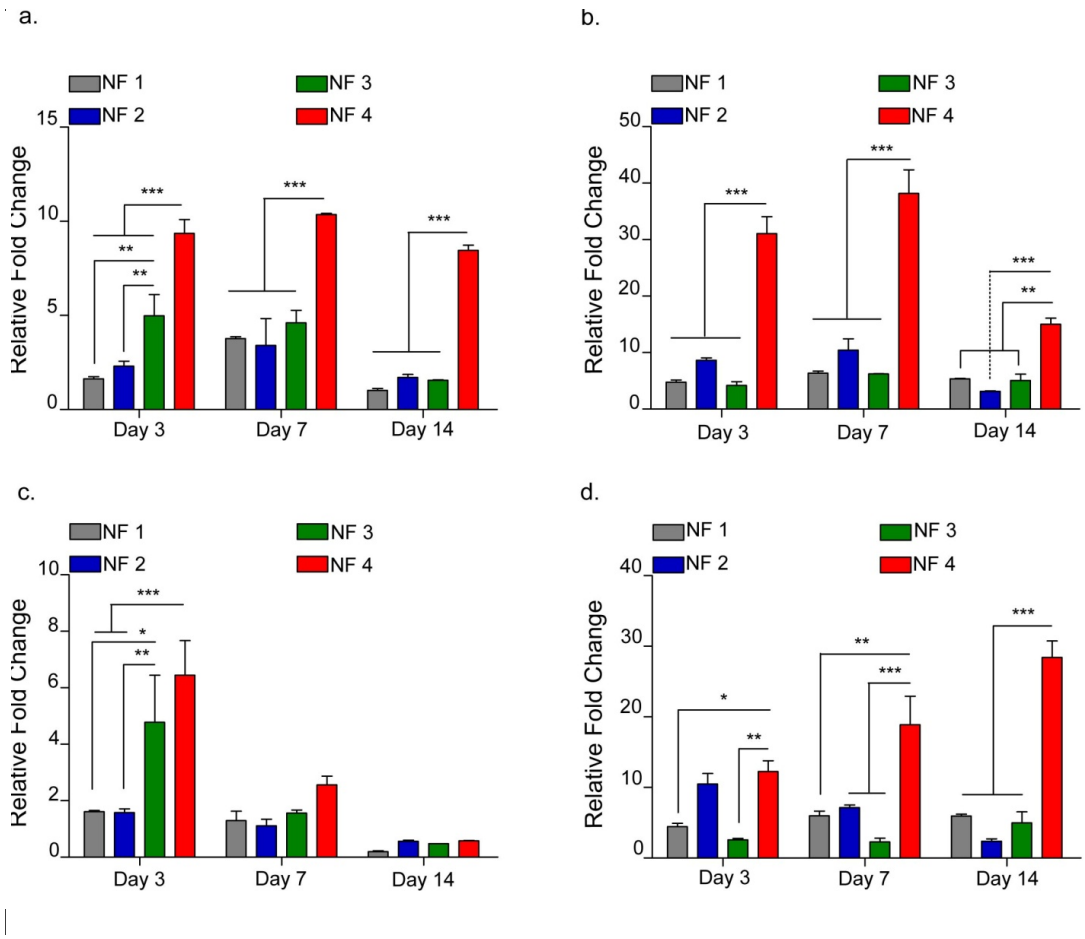

Figure 2.17 Gene Expression Analysis in the Presence of Insulin.

(a) Aggrecan gene expression. (b) Collagen II gene expression. (c) Sox 9 gene expression. (d) Collagen II/I gene expression ratio. The expression level of each gene was normalized against TCP and GAPDH was used as the internal control. Values represent mean ± SEM, n=6 (***p<0.0001, **p<0.01,*p<0.05).

2.4 Conclusion

The degeneration of cartilage is a significant health problem due to the low regeneration capacity of this tissue. The development of novel methods for the treatment of cartilage defects is therefore of great importance in the field of regenerative medicine. Here, we developed a model system using chondro-inductive glycosaminoglycan-mimetic peptide amphiphile nanofibers to enhance chondrogenic differentiation. In this model, the chondrogenic differentiation of ATDC5 cells was observed in the absence of any external bioactive factors. We developed peptide nanofiber networks equipped with differential effects of chemical groups such as hydroxyl, carboxylate and sulfonate, and although peptide nanofiber systems were different from each other in terms of chemical composition, all of formulations used supported the growth and differentiation of ATDC5 cells, as observed through the analysis of morphological changes and cartilaginous matrix deposition. However, detailed gene expression profiling clearly showed that the synergistic effects of sulfonate, carboxylate and hydroxyl groups in NF 4 formulation was more effective for inducing chondrogenic differentiation. Overall, our results showed that glycosaminoglycan-mimetic peptide amphiphile nanofiber networks provide a promising platform for cartilage regeneration by providing a chondro-inducive microenvironment.

2.5 Experimental Section

2.5.1 Materials

9-Fluorenylmethoxycarbonyl (Fmoc) and tert-butoxycarbonyl (Boc) protected amino acids, [4-[α-(2',4'-dimethoxyphenyl) Fmoc-aminomethyl]enoxy]acetamidonorleucyl-MBHA resin (Rink amide MBHA resin), Fmoc-Glu(OtBu)-Wang resin and 2-(1H-

Benzotriazol-1-yl)-1,1,3,3-tetramethyluronium hexafluorophosphate (HBTU) were purchased from NovaBiochem and ABCR. Cover glasses and TCPs (24-well) were purchased from Deckglaser and BD. All other chemicals and materials used in this study were analytical grade and obtained from Invitrogen, Fisher, Merck, Alfa Aesar, and Sigma-Aldrich.

2.5.2 Synthesis, Purification and Characterization of Peptide Amphiphile Molecules

Peptide amphiphile molecules used in this study were synthesized by standard solid phase Fmoc chemistry. Rink Amide MBHA resin (for GAG-PA and K-Pa), and Fmoc-Glu-(OtBu)-Wang resin (for E-Pa) were used as solid supports. Fmoc groups were cleaved by treating the solid phase with 20% (v/v) piperidine in DMF for 20 min. Fmoc protected amino acids were dissolved in 10 mL of DMF and activated with O-Benzotriazole-N,N,N',N'-tetramethyl-uronium-hexafluoro-phosphate (HBTU), and N-ethyl-diisopropylamine (DIEA) in a molar equivalency ratio of 2:1.95:3, respectively. Coupling of Fmoc-protected amino acid and growing peptide chains was carried out for 2 h. Fmoc groups were cleaved by treating the solid phase with 20% piperidine/DMF for 20 min. Resin was treated with 10% acetic anhydride for sealing off unreacted amines for 30 min after each coupling. After coupling all Fmoc protected amino acids, alkyl tail was attached following the same amino acid coupling protocol, using lauric acid. Peptide amphiphiles were cleaved from resin, and side chain protective groups of functional groups were removed in a cleavage step of 2 h with trifluoroacetic acid (TFA): triisopropylsilane (TIS): water at the ratio of 95:2.5:2.5. Solution containing the cleavage products was collected at a round bottom flask and resin was washed several times with DCM. Excess DCM and TFA

were removed to a large extent by rotary-evaporation. Peptide amphiphile was triturated by adding ice-cold diethylether into the solution and left overnight at -20 °C. Diethylether was decanted after centrifugation at 8000 rpm for 15 min. Product was dissolved in ddH_2O, frozen at -80 °C and freeze-dried for two days.

Peptide amphiphiles were purified by reverse phase HPLC system equipped with Zorbax Extend-C18 21.2 x 150 mm column for E-PA and GAG-PA. Pure peptide amphiphile was eluted applying a linear gradient of acetonitrile for 30 min. Molecular mass and purity of peptide amphiphiles were confirmed with Agilent 6530-1200 Q-TOF LC-MS equipped with ESI-MS. Purity by peptide content was monitored at 220 nm. Zorbax Extend-C18 21.2 x 150 mm column was used for K-PA, and Zorbax Extend C18 column was used for GAG-PA and E-PA. 0.1% formic acid in water served as the aqueous phase while 0.1% formic acid in acetonitrile gradient served as the organic phase.

2.5.3 Analysis of Structural and Mechanical Characteristics of Peptide Nanofibers

Oscillatory rheology measurements were performed with an Anton Paar Physica MCR301. For all measurements 25 mm parallel plate was used with 0.5 mm gap. Total gel volume was adjusted to fill the whole cylindrical space between the stage and the plate. 10 mM PA solutions were freshly prepared, and sonicated for 30 min. After loading one PA solution at the center of the stage, counter charged PA solution was added on it drop wise. Upper plate was brought to 0.5 mm position and gel was incubated in this position for 15 min before measurement. For strain sweep measurements, angular frequency was kept constant at 10 rad/s, and strain was increased between 0.1-100%. Storage and loss moduli were recorded at each strain.

Circular Dichroism studies were performed with 0.3 mM aqueous solutions of peptide amphiphiles diluted from 1 mM stock solutions by using J-815 Jasco spectrophotometer. All spectra were obtained at a wavelength interval of 190-300 nm. Spectra were obtained at a digital integration time of 4 s, bandwidth of 1 nm, and data pitch of 0.1 nm. Three subsequent spectra were averaged for each sample.

2.5.4 Cell Culture

2.5.4.1 Monolayer Culturing

ATDC5 cells were cultured as monolayer cultures in 1:1 mixture of DMEM and Ham's F12 medium supplemented with 5% fetal bovine serum, 10 μg mL^{-1} holo-transferrin and 3 x 10^{-8} M sodium selenite in TCPs at standard culture conditions (at 37 °C under 5% CO2). In order to induce chondrogenic differentiation maintenance medium was supplemented with 10 μg mL^{-1} of insulin.

2.5.4.2 Cell Seeding and Cultivation on Peptide Nanofiber Networks

Before cell culture experiments, TCPs were coated with 1 mM peptide amphiphile solutions. Coated plates were left under laminar flow hood for overnight incubation to dry solvent and sterilized under UV lamp for 30 min prior to cell seeding. ATDC5 cells were seeded at a density of 5 x 10^3 cells/cm^2 in either insulin-supplemented media or insulin-free media on peptide networks or TCPs.

2.5.5 *In vitro* Adhesion, Spreading and Cell Viability

Adhesion of ATDC5 cells was assessed at 1 h and 3 h after seeding cells on each peptide network and glass surface. Prior to experiment, cells were pre-treated with 50 μg/mL cyclohexamide in serum-free DMEM medium supplemented with 4 mg/mL BSA for 1 h at 37 °C and 5% CO2 in order to eliminate the effect of endogenous

proteins in initial cell attachment onto surfaces. In this set of experiments, peptide amphiphiles were coated on glass surfaces, and cells were seeded on either coated or uncoated glass surfaces for achieving better resolution during subsequent imaging procedures after staining.

After 1 h and 3 h culture of cells, unbound cells were washed with PBS and remaining adhered cells were stained with 1 μM Calcein AM. Adhered cells were imaged under fluorescence microscope and counted by using Image J. Quantified data was normalized against glass surface.

In order to monitor spreading characteristics of ATDC5 cells on peptide nanofibers, cells were stained with TRITC conjugated phalloidin that maps local actin filaments and imaged with confocal microscope or examined under scanning electron microscope (SEM). Cells were seeded on peptide nanofibers and uncoated glass surfaces with ATDC5 expansion medium. After 3 h and 48 h of culture, they were fixed with 4% paraformaldehyde/PBS for 10 min and permeabilized for 15 min with 0.1% Triton X-100/PBS. F-actin was stained with TRITC-phalloidin and cell nuclei were stained with TO-PRO®-3 iodide. The stained cells were examined under confocal microscope. For imaging cells under SEM, cells were washed with PBS and attached cells were fixed with 2% gluteraldehyde/PBS for 2 h. Following three washing steps with PBS, samples were dehydrated in graded ethanol solutions starting with 20% ethanol and continuing up to absolute ethanol for 10 min at each step. Samples were dried with Tourismis Autosamdri®-815B critical point drier, coated with 6 nm Au/Pd and imaged by FEI Quanta 200 FEG SEM.

On day 1, 2 and 3, viability of ATDC5 cells seeded on nanofiber networks were quantified by Calcein AM staining (Molecular Probes, Invitrogen). After cell seeding in ATDC5 expansion medium, cultures were incubated under standard conditions. At

indicated time points, cells were first washed with PBS to remove dead cells and then stained with 1 μM Calcein AM (n=3 per group). Viable cells were imaged under fluorescence microscope and counted by using Image J. Quantified data was normalized to glass surface.

2.5.6 Differentiation Analysis

2.5.6.1 Morphology Screening

Cells were cultured on peptide nanofibers for 18 days (three wells for each peptide nanofiber), during which 10 random images were taken from each well periodically. Size measurements of aggregates (area, perimeter, major, minor) and number of aggregates were quantified with ImageJ for each frame. For each well, 10 frames were pooled to determine the number of aggregates per well and the average area of aggregates. Average area of each aggregate formed on each well was calculated according to: Average area of aggregates = Total area of aggregates (within ten frames) / Number of aggregates (within ten frames). Mean values and standard deviations were obtained from 3 wells.

2.5.6.2 Analysis of Sulfated Glycosaminoglycan Production

The sulfated glycosaminoglycan content produced by cells on peptide nanofibers or TCP was analyzed with both Safranin-O staining and DMMB assay, which determine glycosaminoglycan production, on days 3, 7 and 14. For Safranin-O staining, cells were washed with PBS and fixed with 4% paraformaldehyde for 15 min at room temperature. In order to eliminate nonspecific binding, cells were blocked with 2% BSA/PBS for 30 min after washing fixed cells with PBS. Then cells were treated with 0.1% (w/v) Safranin-O in 0.1% (v/v) in acetic acid for 5 min at

room temperature. Extensive washing with PBS was performed after Safranin-O treatment to remove unbound dye.

For DMMB assay, cell cultures were digested in papain digestion buffer (100 mM sodium phosphate buffer/10 mM Na_2EDTA/ 10 mM L-cysteine/0.125 mg/mL papain) overnight at 65 °C. Total DNA per well was measured with Qubit dsDNA quantitation kit (Invitrogen) according to manufacturer's instructions. Total dsDNA was used to normalize sulfated glycosaminoglycan content. For DMMB assay diluted chondroitin sulfate standards (from 0 to 35 μg mL^{-1}) were used to generate standard curve. 100 μL of DMMB solution (16 mg L^{-1} 1,9-DMMB, 40 mM glycine, 40 mM NaCl, 9.5 mM HCl, pH 3.0) was added on 40 μL of papain digested solutions and standard samples and optical density (OD) of the solutions was read using 595 nm filter on microplate reader. The absorbance of the cell-free control groups was subtracted from the absorbance values of the experimental groups.

2.5.6.3 Immunofluorescence Staining and Imaging

Immunocytochemistry was used to analyze expression of collagen II and Sox 9 proteins. Cells were seeded at a density of 2.5 x 10^4 cells/cm^2 on peptide nanofibers or glass surfaces in cell culture media with or without insulin. After harvesting on days 3, 7 and 14, cells were fixed in 4% paraformaldehyde/PBS for 10 min and permeabilized in 0.1% Triton X-100 for 15 min. In order to reduce nonspecific binding, samples were incubated with 10% (w/v) bovine serum albumin/PBS for 30 min and treated with either collagen II primary antibody (Abcam) at 1:200 dilution and Sox 9 primary antibody (Thermoscientific) at 1:300 dilution overnight at 4 °C. Then, samples were incubated with Cy3 conjugated goat anti-rabbit secondary antibody at 1:500 dilution for 1 h at room temperature. Extensive washing with PBS

was performed between each step. All samples were counterstained with 1 μM TO-PRO-3 (Invitrogen) in PBS for 15 min at room temperature and mounted with Prolong Gold Antifade Reagent (Invitrogen). Negative controls were obtained by omitting primary antibody and incubating with 1% normal goat serum/PBS. Samples were imaged using confocal microscope (Zeiss LSM510).

2.5.6.4 Gene Expression Analysis

Gene expression profiles for chondrocyte differentiation (Sox 9, collagen II and aggrecan), and dedifferentiation (collagen I) were assessed by quantitative RT-PCR analysis. ATDC5 cells were seeded at a density of 2.5 x 10^4 cells/cm^2 on peptide nanofibers and total RNA was isolated using TRIzol (Invitrogen) according to manufacturer's instructions. Yield and purity of extracted RNA were assessed by Nanodrop 2000 (Thermoscientific). Primer sequences were designed using Primer 3 software (Table 1). cDNA synthesis from RNA and qRT-PCR were performed using SuperScript® III Platinum® SYBR® Green One-Step qRT-PCR Kit according to manufacturer's instructions. Reaction conditions were briefly as follows: 55 °C for 5 min, 95 °C for 5 min, 40 cycles of 95 °C for 15 s, 60 °C for 30 s, and 40 °C for 1 min, followed by a melting curve to confirm product specificity. The reaction efficiencies for each primer set were evaluated with standard curve using 5-fold serial dilutions of total RNA. For analysis of the expression data, primary gene expression data was normalized by the expression level of GAPDH. Comparative Ct method was used to analyze the results.

2.5.7 Statistical Analysis

All data are presented as mean ± SEM (standard error of the mean). The significance of differences between groups was determined with either one-way or two-way

analysis of variance (ANOVA). Differences were considered significant when $p<0.05$.

CHAPTER 3

3 Glycosaminoglycan-Mimetic Peptide Networks Promote the Chondrogenic Differentiation of Mesenchymal Stem Cells

3.1 Synopsis

Glycosaminoglycans are one of the most significant ECM components of cartilage tissue and provide bioactive signals to resident stem cells and chondrocytes for the development and functional regeneration of cartilage. Sulfated glycosaminoglycans in particular are notable for binding to growth factors and enhancing their functionality by enabling growth factor-receptor interactions. The functional groups of native glycosaminoglycans can be used to replicate this capacity on a bioactive scaffold matrix and modulate the biological activity of cells. In this study, we used peptide amphiphile nanofibers functionalized with the chemical groups of native glycosaminoglycan molecules to induce the chondrogenic differentiation of rat mesenchymal stem cells (rMSC). MSCs cultured on GAG-mimetic environments formed cartilage-like nodules and deposited cartilage-specific matrix components by day 7, suggesting that the GAG-mimetic peptide nanofibers effectively facilitated their commitment into the chondrogenic lineage. The degree of chondrogenic differentiation could be modulated by altering the extent of nanofiber sulfonation. The GAG-mimetic peptide nanofiber network presented here serves as a bioactive and bioinductive platform for stem cell-based cartilage regeneration studies.

3.2 Introduction

MSCs are commonly used for cell-based regenerative therapies due to their availability, ease of culture and capacity for self-renewal and multi-lineage differentiation [118,119]. The commitment and maturation of stem cells are strictly regulated through soluble and physical factors found in the tissue microenvironment, which should be provided to facilitate their *in vitro* differentiation into specific lineages. As such, various medium components are used to direct the lineage commitment of stem cells in natural and synthetic scaffolds [120–123]. In addition to soluble factors, cellular differentiation can also be altered by the chemical composition and biomechanical properties of the extracellular environment. Tissues such as bone and cartilage are especially reliant on a specific set of biochemical and mechanical cues for their repair; consequently, scaffolds for cartilage regeneration must present an adequate combination of physical characteristics and soluble factors to produce an ideal environment for chondrogenic differentiation.

MSCs have been reported to undergo *in vitro* chondrogenesis and deposit cartilage-specific matrix molecules in a variety of natural and synthetic materials, especially in the presence of an appropriate set of growth factors [124]. Growth factors can be provided to the culture environment through several means: they may *e.g.* be physically encapsulated within the matrix, added into the culture medium, released over time by growth factor release vectors or covalently attached to the scaffold in random or specific orientations [125–128]. However, growth factors are expensive and sensitive, and often lose their bioactivity during sterilization procedures. In addition, they have a narrow pH-tolerance and are susceptible to proteolytic degradation, which leads to their rapid clearance under *in vivo* conditions [129]. The clinical use of

growth factors is also a contentious issue, as some are known to be proto-oncogenic [130,131]. New generation biomaterials that can use the endogenously produced growth factors to facilitate chondrogenic differentiation could therefore enhance the efficiency and clinical potential of regenerative scaffolds [132,133].

The bioactivity of growth factors is regulated through their interactions with ECM elements. In particular, sulfated glycosaminoglycans are capable of facilitating the immobilization and release of growth factors through their negatively-charged sulfate and carboxylate groups. A number of recent studies have demonstrated that growth factor sequestration can also be performed by biomaterial scaffolds that incorporate glycosaminoglycans in their structure, allowing these materials to modulate the biological responses of cells [134–137]. The addition of heparan sulfate, heparin, or dermatan sulfate enhanced the formation of chondrogenic cell aggregates and the sulfate-bearing domain of perlecan was responsible for the *in vitro* aggregation and chondrogenic activation of C3H10T1/2 cells [96]. However, the use of heterogeneous combinations of glycosaminoglycans in unknown ratios prevents the in-depth analysis of structure-function relationships and complicates the clinical use of these materials due to concerns involving off-target effects [138,139]. In addition, glycosaminoglycans are often covalently crosslinked to hydrogels, which introduces toxic side products into the material matrix, restricts the conformation of scaffold-bound biomolecules and weakens the overall biological functionality of the system. A "reductionist glycosaminoglycan-mimetic approach" involving the use of small chemical groups has been proposed as an alternative to the crosslinking of glycosaminoglycans and was shown to be effective: sulfate/sulfonate groups, for example, have been demonstrated to induce the chondrogenic differentiation of stem cells and chondroprogenitors under *in vitro* conditions [140].

In this manuscript, we report the induction of chondrogenic differentiation in MSCs on a glycosaminoglycan-mimetic environment produced through the supramolecular assembly of peptide amphiphile (PA) molecules that present specific functional epitopes in high densities across one-dimensional arrays [106,112,113,141]. Peptide amphiphile molecules contain an alkyl tail attached to their peptide component and, in aqueous environments, the hydrophobic collapse of the alkyl tail drives the self-assembly of these molecules into hydrogels [142,143]. Peptide amphiphile molecules functionalized with sulfonate, carboxylate and hydroxyl groups self-assemble into nanofiber networks with structures similar to that of the native ECM and provide suitable platforms for the culture of MSCs. The chondrogenic differentiation of MSCs was shown to be enhanced when cultured on glycosaminoglycan-mimetic platforms through the analysis of sulfated glycosaminoglycan deposition patterns and cartilage-specific gene and protein expressions. We also showed that the extent of chondrogenic differentiation was dependent on the degree of epitope density presented on nanofiber system.

3.3 Results and Discussion

3.3.1 Characterization of Peptide Amphiphile Nanofibers

In this study, we aimed to mimic the function of heparan sulfate glycosaminoglycans in the ECM by incorporating functional units found in native glycosaminoglycans, such as carboxylate, sulfonate and hydroxyl groups, into a peptide nanofiber network. High-aspect ratio nanofibers were produced by mixing oppositely charged peptide amphiphile molecules at molar ratios given at Table 3.1. The amphiphilic nature of peptide amphiphile molecules facilitated the formation of one-dimensional nanofibers through the hydrophobic collapse of the alkyl tails, intermolecular

hydrogen bonding of hydrophobic amino acids in the β-sheet configuration and electrostatic interactions between charged amino acids [103,112]. This particular geometry allows the presentation of high-density functional epitopes on the outer periphery of the peptide nanofibers. Three different peptide amphiphile molecules were used to form three different nanofiber networks. Lauryl-VVAGE (E-PA) carried carboxylate and hydroxyl groups as its functional units, while glycosaminoglycan mimetic Lauryl-VVAGEGD-K(p-sulfobenzoyl)-S-Am (GAG-PA) carried sulfonate, carboxylate and hydroxyl groups and Lauryl-VVAGK-Am (K-PA) was a positively charged peptide amphiphile molecule used to induce nanofiber formation with negatively-charged peptide amphiphiles (Figure 3.1a). The GAG-PA molecule carrying sulfonate, carboxylate and hydroxyl groups was previously designed by our group and its activity in angiogenesis and cellular differentiation had been demonstrated [113,114]. Furthermore, it was shown that glycosaminoglycan mimetic peptide nanofiber networks encapsulate growth factors and increase their local concentrations [141].

Nanofiber networks were formed by mixing PA molecules at different concentrations to adjust the presentation of functional groups at different ratios. E-PA/K-PA did not contain sulfonate groups and served as a control for sulfonate functionality, while GAG-PA/K-PA and GAG-PA/E-PA/K-PA bore all the functional group types and were used as GAG-mimetic nanofiber networks; however, GAG-PA/E-PA/K-PA contained less sulfonate groups (1x) compared to GAG-PA/K-PA (2x) (Table 3.1). In all of these systems, we observed dense and interconnected organizations of nanofibers, which formed networks that closely resemble the structure of the native ECM (Figure 3.1c). β-sheets were the dominant secondary structure of nanofibers, as

evidenced by circular dichroism spectra showing a maximum around 200 nm and minimum around 220 nm (Figure 3.1b).

Table 3.1 Molar Ratios Used in the Preparation of Peptide Amphiphile Networks.

Nanofibrous Network Composition	Molar Mixing Ratio
E-PA/K-PA	2 : 2
GAG-PA/E-PA/K-PA	1 : 1 : 2
GAG-PA/K-PA	2 : 2

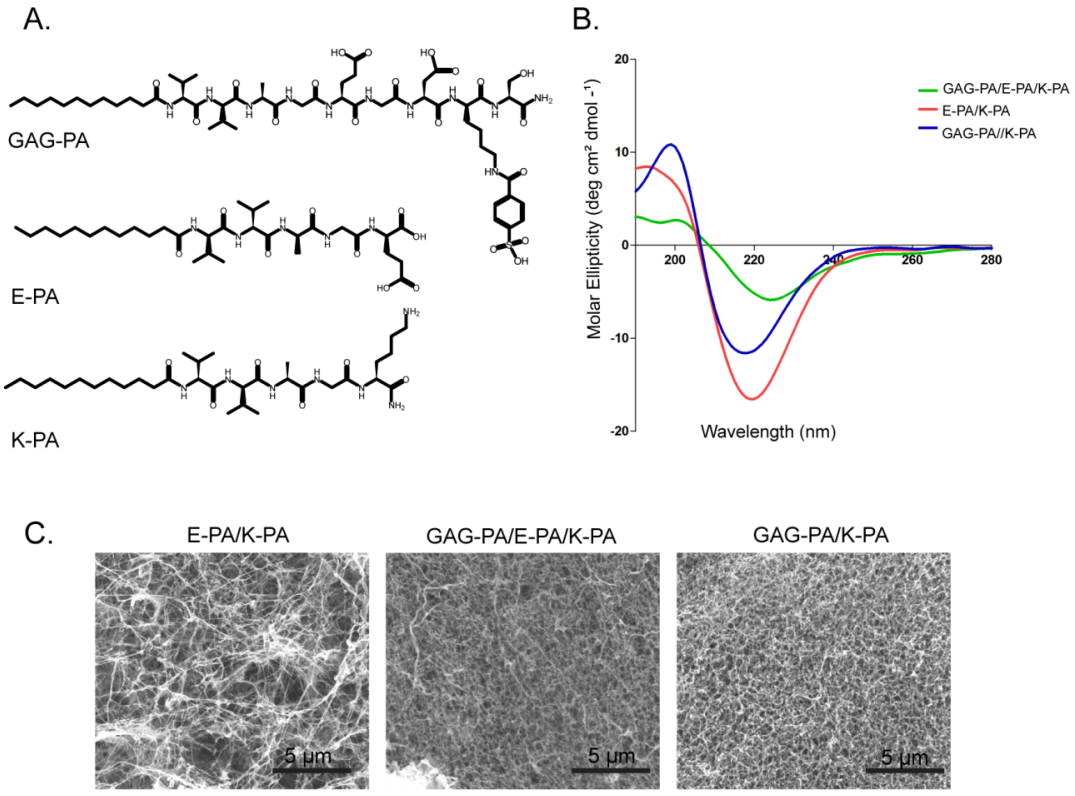

Figure 3.1 Self-assembly of Peptide Amphiphile Molecules into Nanofibrous Networks.

(a) Chemical presentation of peptide amphiphile molecules. Lauryl-VVAGEGDKS-OH (GAG-PA), Lauryl-VVAGE-OH (E-PA) and Lauryl-VVAGK-Am (K-PA). (b) Circular dichroism spectra of the nanofibers, showing β-sheet-associated peaks. (c) SEM images showing the ECM mimetic morphology of nanofiber networks.

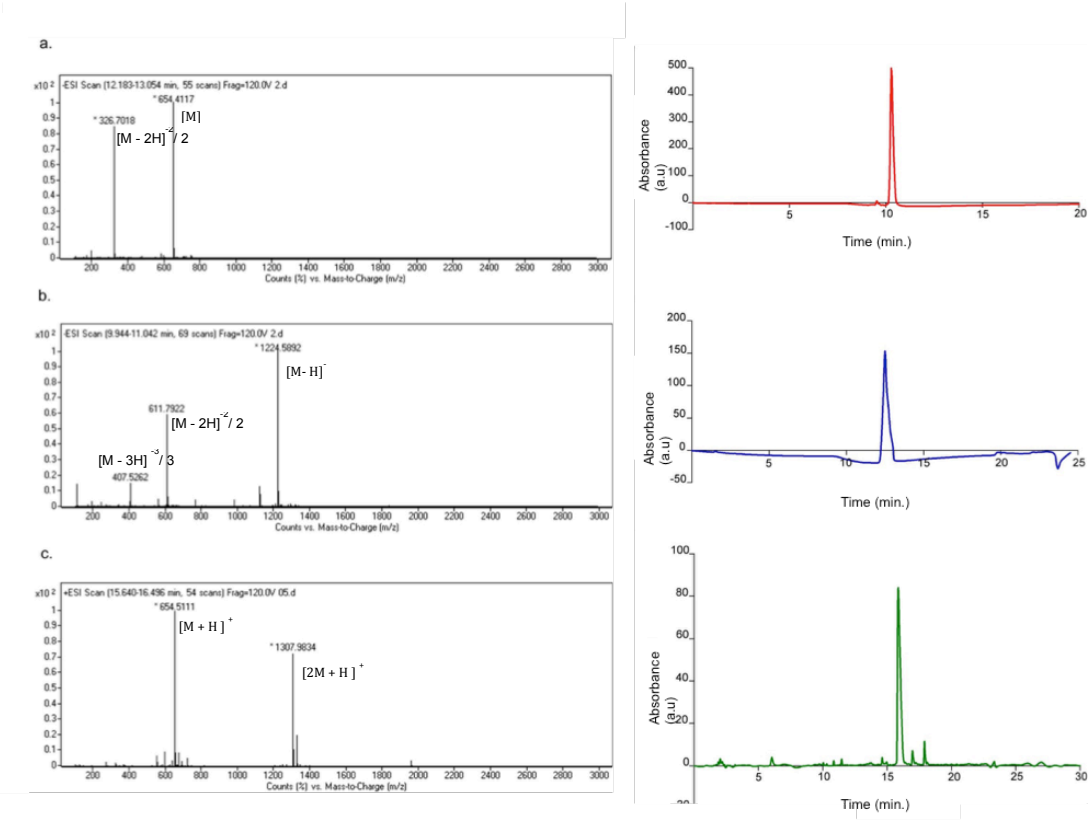

Figure 3.2 Liquid Chromatography-Mass Spectrometry (LC-MS) Analysis of PA Molecules.

E-PA (a), GAG-PA (b) and K-PA (c)

3.3.2 Cellular Behavior on Nanofiber Networks

We investigated the biocompatibility of nanofiber networks by examining the viability of MSCs cultured on peptide scaffolds for 24 h. Calcein AM staining was performed to determine the number of viable cells and bare TCPs were used as control. Lower numbers of cells were stained with Calcein AM for MSCs cultured on nanofiber groups at 24 h compared to MSCs on bare TCP surface (Figure 3.3a,b). In accordance with viability results, the proliferation rate of MSCs on nanofiber scaffolds was also lower compared to bare TCP (Figure 3.3c). The relative lack of proliferating cells may explain the lower number of viable cells on nanofiber scaffolds, as the decreased proliferation of MSCs would lead to a lower total number of cells present on nanofiber scaffolds at 24 h. It is known that stem cells decrease their proliferation rates under environments that are inductive for their differentiation[144]. The response of MSCs cultured on nanofiber scaffolds may be directed toward differentiation from the onset of their seeding, which would result in a decrease in the number of proliferating cells. Differences in proliferation rates at 24 h might also be the result of heterogeneity in the initial MSC population and the plastic properties of MSCs, which are known to play a role in the phenotypic and functional variances observed in cultures on different surfaces[145].

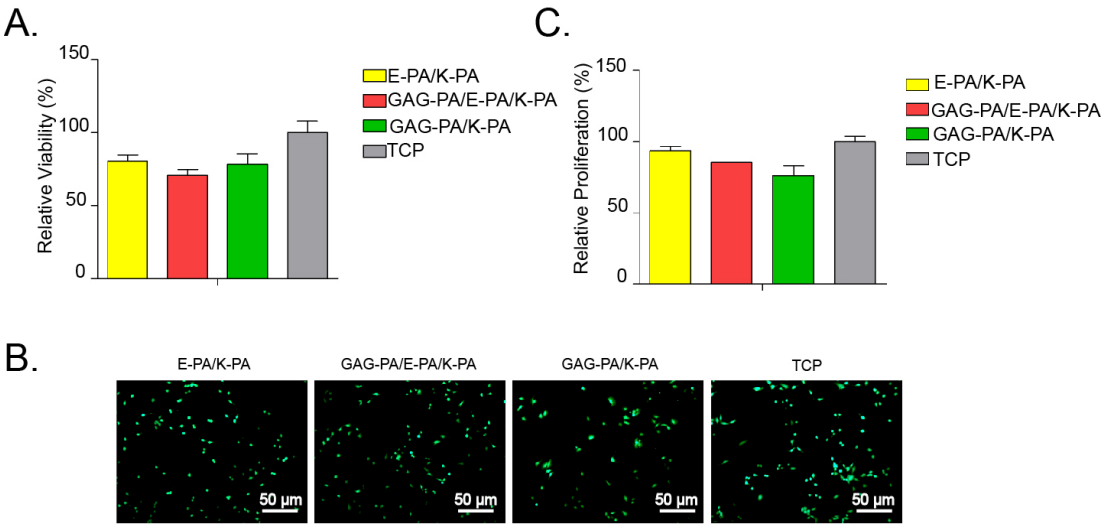

Figure 3.3 Viability and Proliferation of MSCs on Nanofiber Networks at 24 h.

(a) Relative viability and (b) proliferation rates of MSCs on nanofiber networks and bare culture plates. (c) Representative Calcein-AM stained micrographs of MSCs at 24 h.

3.3.3 Nanofiber Networks Promote MSC Aggregation and Deposition of Cartilage ECM Components

We next analyzed the chondrogenic differentiation potential of MSCs on nanofiber networks bearing different functional epitopes. MSCs that commit to the chondrocytic lineage rapidly lose their fibroblastic morphology, deposit sulfated glycosaminoglycans and increase cell-cell interactions, as evidenced by aggregate formation [3,146,147]. At day 7, MSCs on nanofiber networks displayed morphological similarities to chondrocytes, acquiring a rounded morphology and forming aggregate units (Figure 3.4). These cell aggregates were distinct and homogenously distributed on GAG-PA/E-PA/K-PA and E-PA/K-PA systems. In contrast to these groups, aggregates formed on GAG-PA/K-PA were smaller in size. As such, differences in cellular responses may exist with respect to nanofiber composition. On bare culture plates, MSCs preserved their fibroblastic/spindle shapes over 7 days even in the presence of chondrogenic medium (Figure 3.4).

The deposition of glycosaminogycans was examined by Safranin-O staining and DMMB (DMMB) assay on day 7. Discrete staining on or around cellular aggregates was clear for MSCs on nanofiber networks and indicated the accumulation of glycosaminoglycans in both maintenance and chondrogenic media, whereas cells on bare culture plates were stained less prominently (Figure 3.5a). Quantitatively, the accumulation of glycosaminoglycans was higher (in maintenance medium ~10 folds, in chondrogenic medium ~11 folds) in cells on GAG-PA/E-PA/K-PA compared to cells cultured on uncoated TCPs. These results suggest that GAG-PA/E-PA/K-PA promoted GAG deposition by differentiating MSCs (Figure 3.5b). We also observed that GAG deposition in cells cultured on GAG-PA/E-PA/K-PA peptide nanofiber systems was higher than cells on GAG-PA/K-PA and E-PA/K-PA, suggesting the

importance of ligand density: The optimal density among these three formulations appears to be GAG-PA/E-PA/K-PA for the induction of chondrogenic differentiation of MSCs. In addition, the increased GAG production in both sulfonate containing groups, GAG-PA/E-PA/K-PA and GAG-PA/K-PA, compared to the group that does not contain sulfonate, E-PA/K-PA, further reveals the importance of the presence of sulfonate groups and presentation density of charged groups.

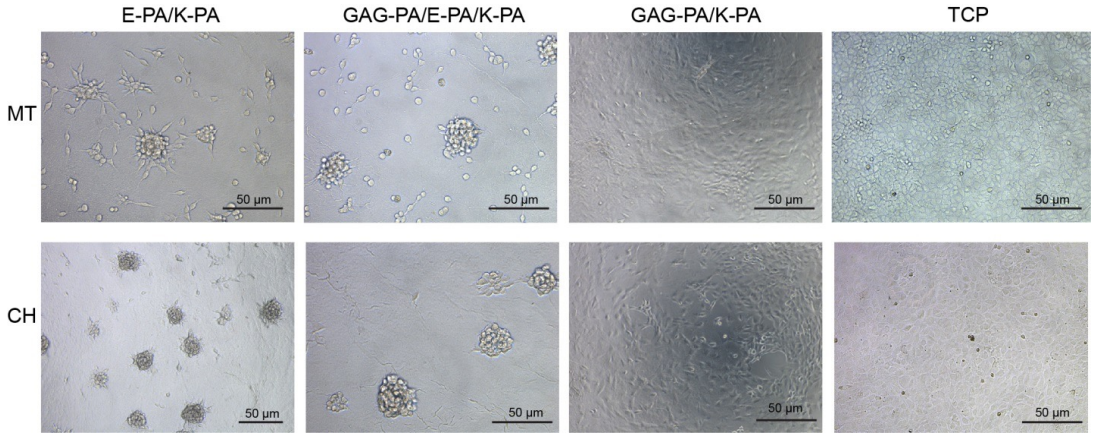

Figure 3.4 Morphological Changes of MSCs on Day 7 Cultured in Either Maintenance or Chondrogenic Medium.

(MT; maintenance medium, CH; chondrogenic medium)

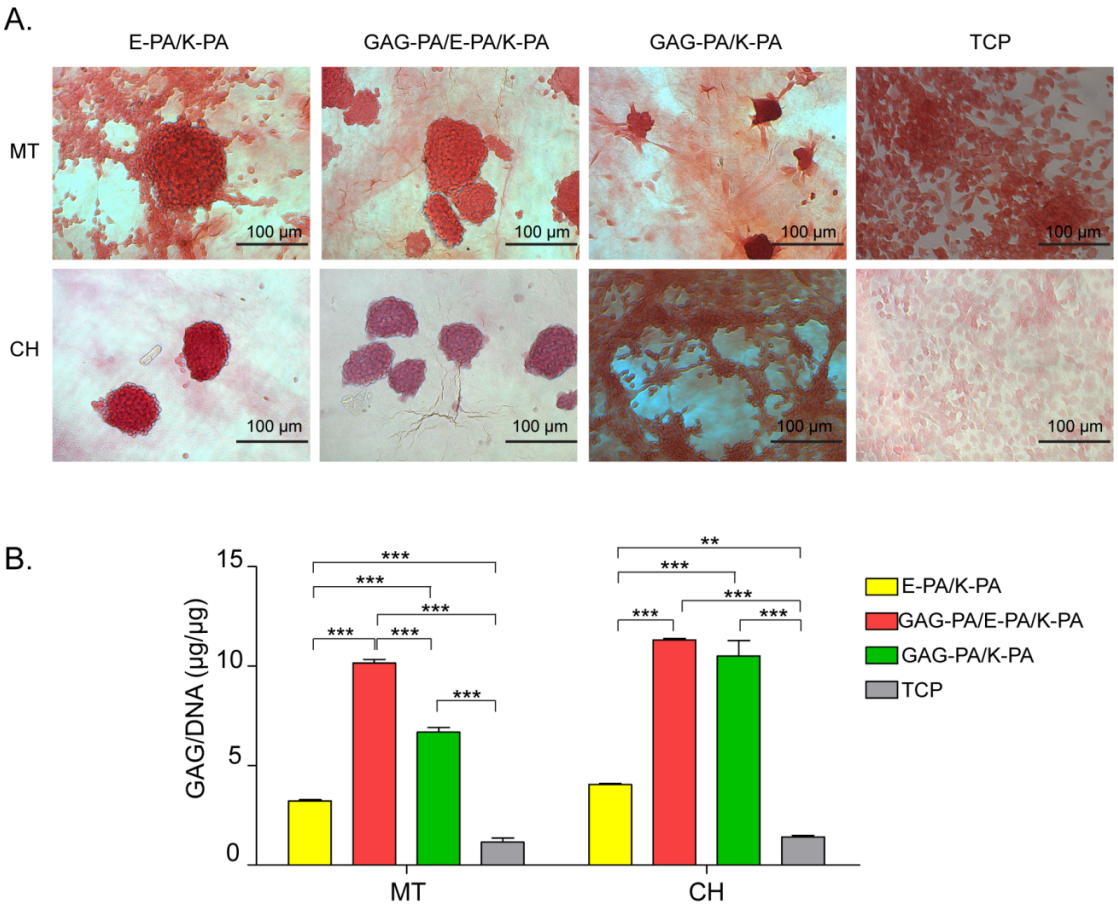

Figure 3.5 Glycosaminoglycan Deposition of MSCs on Nanofiber Networks or TCP on Day 7.

(a) Safranin-O staining and (b) DMMB Assay on day 7 for cells cultured in either chondrogenic (CH) or maintenance (MT) medium. GAG content was normalized to DNA content and expressed as µg/µg. Values represent mean ± SEM, n = 3 (***p < 0.0001, **p < 0.01, *p < 0.05)

3.3.4 Gene Expression Profiles of MSCs Confirm Chondrogenic Lineage Commitment

To further investigate the importance of sulfonate densities on MSC differentiation, we also performed Collagen II, Aggrecan and Collagen I expression analyses of MSCs cultured on different combinations of GAG-PA/E-PA/K-PA networks with different epitope densities (Table 3). Morphological observation clearly showed that MSCs formed aggregates within 3 days following their seeding on peptide nanofibers, suggesting a rapid commitment to the chondrogenic lineage. Morphological changes were confirmed by gene expression pattern analyses on both day 3 and day 7. MSCs exhibited an upregulation of Collagen II (Day 3 = ~4 folds, Day 7 = ~15 folds) and Aggrecan (Day 3 = ~6 folds, Day 7 = ~12 folds), two predominant components of cartilage ECM, on GAG-PA/E-PA/K-PA nanofiber networks at days 3 and 7 (Figure 3.6a, b). With respect to the reference gene, GAPDH, the relative expression of Collagen II and Aggrecan were significantly higher compared to other groups. Collagen II/I ratio is another widely used differentiation index and is expected to be higher than 1 for cells committing to the chondrogenic lineage [148]. The collagen phenotype of differentiated chondrocytes is marked by the synthesis of Collagen II, while the MSC or dedifferentiated phenotype primarily produces Collagen I. As such, differentiating cells increase their Collagen II expression while decreasing Collagen I expression. In agreement with Collagen II and Aggrecan expression results, the Collagen II/I ratio was higher for MSCs cultured on GAG-PA/E-PA/K-PA at days 3 (~7 folds) and 7 (~95 folds) (Figure 3.6a,b). When cells were cultured in maintenance media (which includes no chondrogenic cues, but contains serum to encourage cell proliferation), the GAG-

PA/E-PA/K-PA group also showed an upregulated expression of Collagen II (~7 folds) and higher fold changes of Collagen II/I (~32 folds) at day 7 (Figure 3.7).

MSCs on nanofiber networks displaying sulfonate epitopes at higher (H-1.33x) and lower (L-0.66x) stoichiometric ratios than GAG-PA/E-PA/K-PA network (1x) showed lower expression of chondrogenesis-related markers (Table 3.2) (Figure 3.8). This result showed that epitope density affects cellular behavior in both ways; as such, MSCs decrease the expression of chondrogenic markers when cultured on networks presenting sulfonate groups in both denser and sparser forms. As such, we note that it is necessary for cells to access optimal densities of bioactive epitopes to evoke cellular responses, as was shown previously in the literature [149]. These results are also in agreement with studies investigating the impact of sulfation and importance of its pattern on the regulation of cellular activities [150,151].

Table 3.2 Molar Ratios Used in the Preparation of Peptide Amphiphile Scaffolds.

Nanofibrous Network Composition	Molar Mixing Ratio
GAG-PA/E-PA/K-PA-L	0.66 : 1.33 : 2
GAG-PA/E-PA/K-PA	1 : 1 : 2
GAG-PA/E-PA/K-PA-H	1.33 : 0.66 : 2

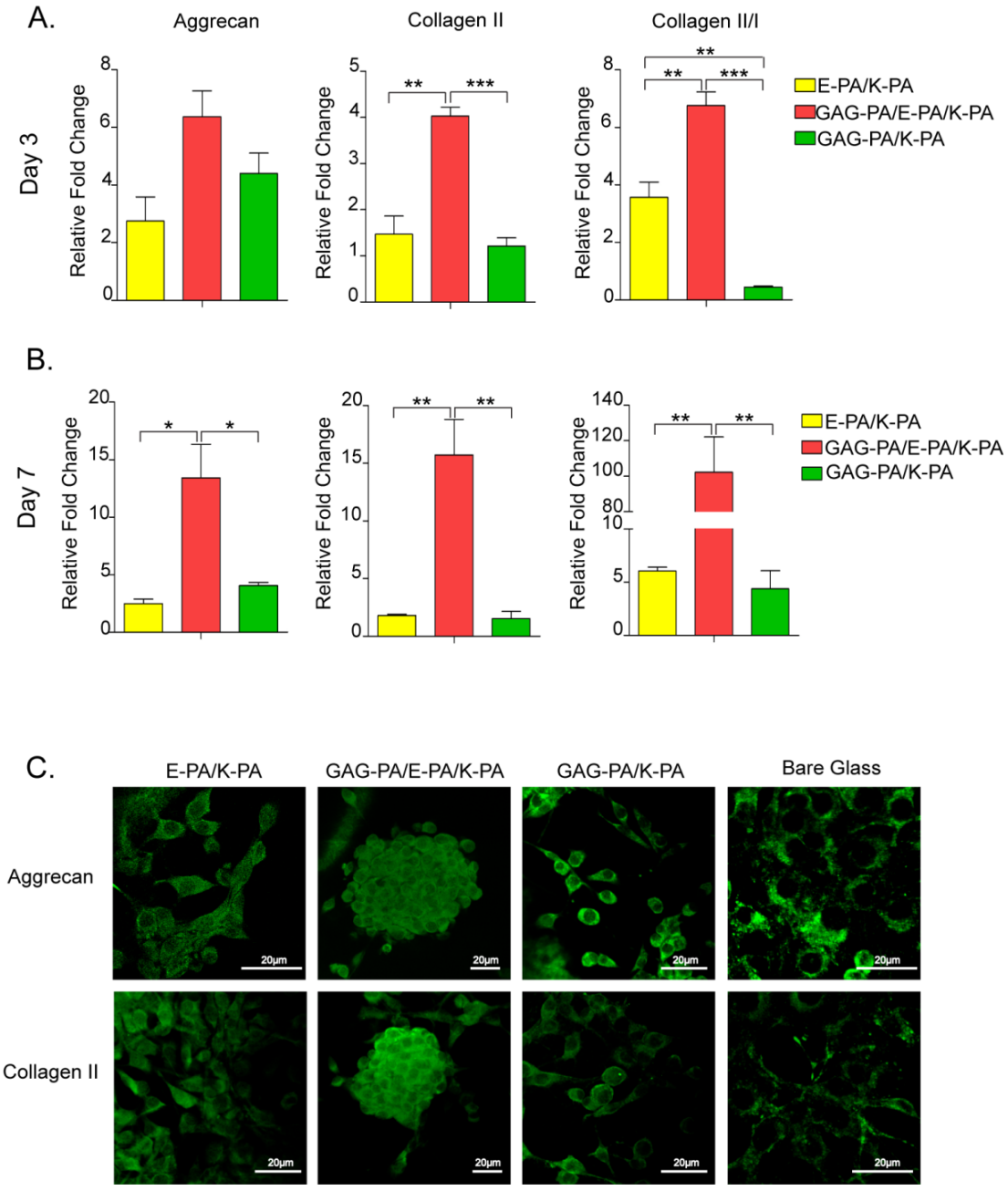

Figure 3.6 Cartilage-Specific Gene and Protein Expression in Chondrogenic Medium at Day 3 and 7.

(a,b) Aggrecan. Collagen II and Collagen II/I expression of MSCs on nanofiber networks on day 3 and 7 in chondrogenic medium. The expression level of each gene was normalized against TCP and GAPDH was used as internal control. Values

represent mean ± SEM, $n = 3$ (***$p < 0.0001$, **$p < 0.01$, *$p < 0.05$). C) Aggrecan and Collagen II protein expression of MSCs on day 7 in chondrogenic medium.

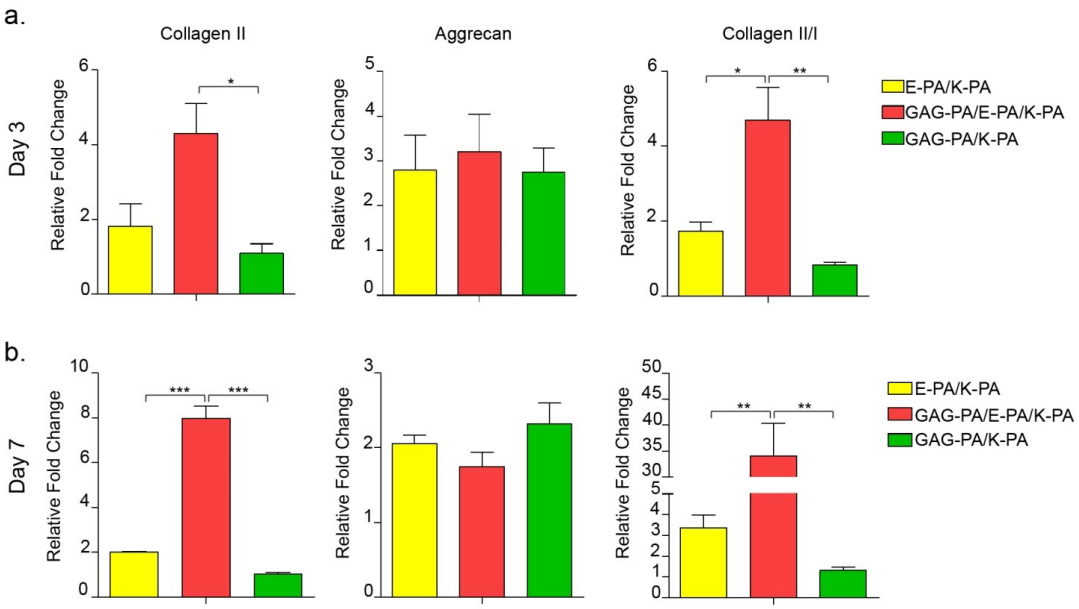

Figure 3.7 Cartilage-Specific Gene Expression in Maintenance Medium at Day 3 and 7.

(a,b) Aggrecan. Collagen II and Collagen II/I expression of rMSCs on nanofiber networks on day 3 and 7 in maintenance medium. The expression level of each gene was normalized against TCP and GAPDH was used as internal control. Values represent mean ± SEM, $n = 3$ (***$p < 0.0001$, **$p < 0.01$, *$p < 0.05$).

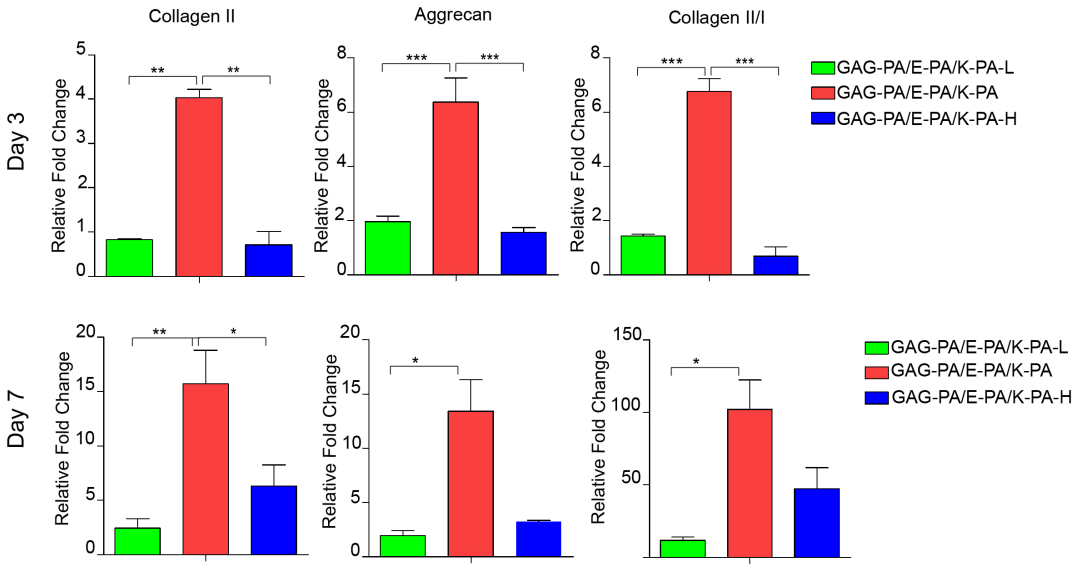

Figure 3.8 Cartilage-Specific Gene Expression on Bioactive Nanofibers with Different Epitope Concentrations.

Aggrecan, Collagen II and Collagen II/I expression of rMSCs on nanofiber networks (GAG-PA/E-PA/K-PA-L, GAG-PA/E-PA/K-PA and GAG-PA/E-PA/K-PA-H) on day 3 and 7 in chondrogenic medium. The expression level of each gene was normalized against TCP and GAPDH was used as internal control. Values represent mean ± SEM, $n = 3$ (***$p < 0.0001$, **$p < 0.01$, *$p < 0.05$).

3.4 Conclusion

We studied the impact of synthetic GAG-mimetic extracellular environments on the *in vitro* chondrogenic differentiation of MSCs. Our main motivation stems from the biofunctional role of glycosaminoglycan molecules in the promotion of chondrogenic differentiation in stem cells. Prior reports showed that heparin and heparin-incorporating biomaterials were able to induce lineage commitment in stem cells through growth factor sequestration and presentation [152,153]. The incorporation of glycosaminoglycan functional groups into a biomaterial may replicate these properties through the localization of endogeneous growth factors by charge interactions, which in turn provides a way to locally amplify biomolecular signals for cellular differentiation.

We investigated three different peptide nanofiber networks, each of which displayed structural and fibrous characteristics similar to these found in the ECM. The design of PA networks relies on incorporation of charged groups of native glycosaminoglycan molecules onto PA molecules to enhance the localization of positively-charged, endogenously released bioactive factors [154]. To examine the influence of each functional group found in glycosaminoglycan molecules in detail, we used networks that bear carboxylate, sulfonate and hydroxyl groups at different stoichiometric ratios. E-PA/K/PA, which includes carboxylate and hydroxyl groups, served as a negative control for sulfonate groups and GAG-PA/K-PA, a peptide scaffold that contains both sulfonate and carboxylate groups at higher stoichiometric ratios compared to GAG-PA/E-PA/K-PA, was used to investigate the effect of ligand density. Results showed that the superior chondrogenic potential of GAG-PA/E-PA/K-PA can largely be attributed to the synergistic effect of carboxylate, sulfonate

and hydroxyl groups in one system at a suitable density. This result is in accordance with our previous study with ATDC5 cells, which suggested that the synergistic effect of sulfonate, carboxylate, and hydroxyl groups was highly effective for inducing chondrogenic differentiation using peptide nanofibers [155]. Future studies may consider more specific GAG-mimetic PA molecule designs for improved control over growth factor sequestration and release.

3.5 Experimental Section

3.5.1 Materials

9-Fluorenylmethoxycarbonyl (Fmoc) and tert-butoxycarbonyl (Boc) protected amino acids, [4-[α-(2',4'-dimethoxyphenyl) Fmoc-aminomethyl]enoxy]acetamidonorleucyl-MBHA resin (Rink amide MBHA resin), Fmoc-Glu(OtBu)-Wang resin and 2-(1H-Benzotriazol-1-yl)-1,1,3,3-tetramethyluronium hexafluorophosphate (HBTU) were purchased from NovaBiochem and ABCR. Cover glasses and TCPs (24-well) were purchased from BD. All other chemicals and materials used in this study were purchased from Invitrogen, Fisher, Merck, Alfa Aesar or Sigma-Aldrich.

3.5.2 Synthesis, Purification and Characterization of Peptide Amphiphile Molecules

Peptide amphiphile molecules were synthesized by standard solid phase Fmoc chemistry. GAG-PA and K-PA were synthesized by using MBHA Rink Amide resin and E-PA was synthesized by using Fmoc-Glu-(OtBu)-Wang resin as solid supports. Fmoc groups were cleaved by treating the solid phase with 20% (v/v) piperidine in DMF for 20 min. Fmoc-protected amino acids were dissolved in 10 mL of DMF and activated with O-Benzotriazole-N,N,N',N'-tetramethyl-uronium-hexafluoro-

phosphate (HBTU) and N-ethyl-diisopropylamine (DIEA) at a molar ratio of 2:1.95:3, respectively. Peptide was synthesized by coupling of Fmoc-protected amino acids for 2 h per residue. Fmoc groups were cleaved by treating the solid phase with 20% piperidine/DMF for 20 min. Resin was treated with 10% acetic anhydride for sealing off unreacted amines for 30 min after each coupling. After the completion of the peptide chain, an alkyl tail was attached following the same amino acid coupling protocol, using lauric acid. Peptide amphiphiles were cleaved from resin, and side chain protective groups of functional groups were cleaved for 2 h with trifluoroacetic acid (TFA): triisopropylsilane (TIS): water at the ratio of 95:2.5:2.5. Solution containing the cleavage products was collected in a round bottom flask and resin was washed several times with DCM. Excess DCM and TFA were removed to a large extent by rotary-evaporation. The peptide amphiphile solution was triturated with ice-cold diethylether and left overnight at -20 °C. Diethylether was decanted after centrifugation at 8000 rpm for 15 min. The solid peptide product was dissolved in ddH_2O, frozen at -80 °C and freeze-dried for two days.

Peptides were purified by using a reverse phase HPLC system equipped with a Zorbax Extend-C18 21.2 x 150 mm column for E-PA and GAG-PA. Pure peptide amphiphile molecules were eluted applying a linear gradient of acetonitrile for 30 min. Purities and molecular masses of peptide amphiphiles were confirmed with an Agilent 6530-1200 Q-TOF LC-MS equipped with an ESI-MS. Purity by peptide content was monitored at 220 nm. A Zorbax Extend-C18 21.2 x 150 mm column was used for K-PA, and Zorbax Extend C18 column was used for GAG-PA and E-PA. 0.1% formic acid in water served as the aqueous phase while 0.1% formic acid in acetonitrile gradient served as the organic phase.

An aqueous solution of peptide amphiphiles was prepared in double distilled water at pH 7.4. Mixing of two oppositely charged PA solutions at 10 mM in specified volumetric ratios (Table 3.1) resulted in the formation of peptide hydrogels. Hydrogel morphology was assessed by using scanning electron microscopy (SEM). Briefly, peptide hydrogels were prepared on silicon wafer and incubated at room temperature for 15 min. After the formation of gels, samples were dehydrated in gradually increasing ethanol/water solutions and dried using a Tourismis Autosamdri-815B critical point drier. Dried samples were coated with 3 nm Au/Pd and visualized under high vacuum with a FEI Quanta 200 FEG SEM equipped with an ETD detector.

Peptide self-assembly was assessed by circular dichroism analysis of 0.3 mM aqueous solutions of PA molecules diluted from 1 mM stock solutions. Circular dichroism spectra were acquired using J-815 Jasco spectrophotometer at a wavelength interval of 190-300 nm. Spectra were obtained using a digital integration time of 4 s, bandwidth of 1 nm and data pitch of 0.1 nm. Three consecutive spectra were averaged for each sample and expressed as mean residue ellipticity and converted to the unit of degree cm^2 $dmol^{-1}$.

3.5.3 rMSC Culture Conditions and the Preparation of Nanofibrous Networks for *In Vitro* Culture

rMSCs (Invitrogen) were expanded in maintenance medium consisting of DMEM supplemented with 10% (v/v) FBS (Invitrogen), 1% (v/v) GlutaMAX (Invitrogen) and 1% penicillin-streptomycin (Invitrogen). All experiments were conducted with cells between passages 7-9. Cells were maintained at humidified incubators with 5% CO_2 and at 37 °C. Cells were passaged at 80% confluency by Trypsin-EDTA

(0.025%) (Invitrogen) and reseeded at 3000 cells/cm^2. The culture medium was replaced every 3-4 days.

rMSCs were seeded on PA-coated surfaces or culture plates for in vitro analysis. Coating was performed using oppositely charged 1 mM PA solutions 150 μL/cm^2 (Table 3.1). Coated plates were left under laminar flow hood to dry for 16 h and sterilized under UV irradiation for 30 min prior to cell seeding.

3.5.4 Viability and Proliferation Assays

Cellular viability was assessed by Calcein AM (Invitrogen) staining. rMSCs were seeded at a density of 250 cells/cm^2 and cultured for 24 h prior to staining. At the time of assay, medium was discarded and dead cells were washed with PBS. Live cells were stained with Calcein AM for 30 min at room temperature; viable cells were subsequently imaged under light microscope and counted using Image J software. Cell viability was normalized against cell counts in uncoated culture plates.

Proliferating cells were detected by Click-iT EdU assay (Molecular Probes) at day 1. rMSCs were seeded on nanofibers or uncoated culture plate at a density of 250 cells/cm^2 in maintenance medium. After 6 h, maintenance medium was changed with maintenance medium supplemented with 10 mM EdU. At the time of assay, cells were fixed with 4% paraformaldehyde in PBS and permeabilized with 5% Triton-X. Cells were treated with Alexafluor-488 conjugated azide to detect the incorporation of EdU in replicating DNA strands. Cells stained with Alexafluor-488 were imaged by fluorescence microscopy and quantified with Image J software. Proliferation rates of cells on PA-coated surfaces were normalized against cells cultured on uncoated culture plate.

3.5.5 Glycosaminoglycan Imaging and Quantification

Glycosaminoglycan deposition was assessed through Safranin-O staining. Safranin-O is a cationic dye that binds to negatively charged sulfated glycosaminoglycans. For Safranin-O staining, cells were washed with PBS and fixed with 4% paraformaldehyde for 15 min at room temperature. To eliminate nonspecific binding, fixed cells were blocked with 2% BSA/PBS for 30 min after washing with PBS. Cells were then treated with 0.1% (w/v) Safranin-O in 0.1% (v/v) acetic acid for 5 min at room temperature. Extensive washing with PBS was performed after Safranin-O treatment to remove unbound dye.

Quantification of sulfated glycosaminoglycans was performed using a biochemical DMMB assay. Briefly, cell cultures were digested in papain digestion buffer (100 mM sodium phosphate buffer/ 10 mM Na_2EDTA/ 10 mM L-cysteine/ 0.125 mg/mL papain) overnight at 65 °C. Total DNA per well was measured with Qubit dsDNA quantification kit (Invitrogen) according to manufacturer's instructions. Total dsDNA was used to normalize the sulfated glycosaminoglycan content. Diluted chondroitin sulfate standards (from 0 to 35 μg mL^{-1}) were used to generate a standard curve for the DMMB assay. A total of 100 μL of DMMB solution (16 mg L^{-1} 1,9-DMMB, 40 mM glycine, 40 mM NaCl, 9.5 mM HCl, pH 3.0) was added on 40 μL of papain-digested solutions and standard samples, and optical densities (ODs) of the solutions were measured using a 595 nm filter on a microplate reader. The absorbance of the cell-free control groups was subtracted from the absorbance values of the experimental groups.

3.5.6 Gene Expression Analysis

Gene expression profiles of differentiating rMSCs were assessed by quantitative real time PCR (qRT-PCR). Before qRT-PCR experiments, RNA from each sample was extracted by using TRIzol reagent (Invitrogen) according to manufacturer's instructions. Yield and purity of extracted RNAs were assessed by Nanodrop 2000 (Thermoscientific). cDNA synthesis from RNA and qRT-PCR were performed using SuperScript III Platinum SYBR Green One-Step qRT-PCR Kit (Invitrogen) according to manufacturer's instructions. Reaction conditions were briefly as follows: 55 °C for 5 min, 95 °C for 5 min, 40 cycles of 95 °C for 15 s, 60 °C for 30 s, and 40 °C for 1 min, followed by a melting curve to confirm product specificity. The reaction efficiencies for each primer set (Table 3.3) were evaluated with a standard curve using 5-fold serial dilutions of total RNA. Each run was internally normalized to GAPDH, and each group was normalized to the expression levels of MSCs cultured in maintenance medium. A comparative Ct method with efficiency correction was used to analyze the results. Expression ratios greater than 1 indicate the upregulation of the gene of interest, while ratios less than 1 correspond to its downregulation.

Table 3.3 Primers Used for qRT-PCR Expression Analyses

Gene	Primer Sequence: Forward/Reverse	Product Size (bp)
Col I	5'-TGACTGGAAGAGCGGAGAGT-3'	151
	5'-GTTCGGGCTGATGTACCAGT-3'	
Col II	5'-ACTTGCGTCTACCCCAACC-3'	123
	5'-GCCATAGCTGAAGTGGAAGC-3'	
Aggrecan	5'-GGTCACTGTTACCGCCACTT-3'	175
	5'-CCCCTTCGATAGTCCTGTCA-3'	

3.5.7 Immunostaining and Imaging

rMSCs cultured on peptide coated or uncoated glass surfaces at day 7 were fixed in 4% paraformaldehyde/PBS for 10 min and permeabilized in 0.1% Triton X-100 for 15 min. For blocking, samples were incubated with 10% (w/v) bovine serum albumin/PBS for 30 min and treated with collagen II primary antibody (Abcam) at 1:200 dilution or aggrecan antibody at 1:200 dilution (Abcam) overnight at 4 °C. Cells were then washed with PBS and incubated for 1 h at room temperature with Goat Anti-Rabbit IgG H&L (Alexa Fluor® 488). All samples were counterstained with 1 μM TO-PRO-3 (Invitrogen) in PBS for 15 min at room temperature and mounted with Prolong Gold Antifade Reagent (Invitrogen). Negative controls were obtained by omitting the primary antibody and incubating the samples with 1% normal goat serum/PBS. Samples were imaged using confocal microscopy (Zeiss LSM510).

3.5.8 Statistical Analysis

All data are presented as means ± standard error of means (s.e.m). One-way ANOVA and Bonferronni post-test were performed to test the significance of observed differences between the study groups. A p value of less than 0.05 was considered to be statistically significant, except where noted.

CHAPTER 4

4 Supramolecular Glycosaminoglycan-like Self-Assembled Glycopeptide Nanofibers Induce Chondrogenesis and Cartilage Regeneration

4.1 Synopsis

Glycosaminoglycans and glycoproteins are vital components of the ECM, directing tissue homeostasis and cell proliferation, differentiation and migration. Here, we demonstrate the synthesis and characterization of supramolecular glycosaminoglycan-like glycopeptide nanofibers mimicking the bioactive functions of natural HA molecules. The self-assembly of glycopeptide amphiphile molecules enables the organization of glucose residues in close proximity on a nanoscale structure forming a supramolecular glycosaminoglycan-like system. Our *in vitro* culture results indicate that the glycopeptide nanofibers are recognized through CD44 receptors and promote the chondrogenic differentiation of MSCs. We analyzed the bioactivity of glycosaminoglycan-like glycopeptide nanofibers in chondrogenic differentiation and injury models, as HA, a type of glycosaminoglycan, is a major component of articular cartilage. The capacity of glycopeptide nanofibers to enhance *in vivo* cartilage regeneration was demonstrated in a microfracture-treated osteochondral defect-healing model. Glycopeptide nanofibers were shown to act as a cell-instructive synthetic counterpart to HA, and can be used in stem cell-based cartilage regeneration therapies.

4.2 Introduction

Adult cartilage tissue lacks the innate repair responses required for its complete regeneration. Many processes involved in cartilage development are lost or partially activated in the mature tissue, which prevents the recovery of cartilage injuries and allows their progressive degeneration into [28,156]. Therefore, the repair of cartilage defects is a topic of great interest for the field of regenerative medicine. The complete and functional repair of any tissue requires an adequate supply of progenitor cells to produce a specialized ECM by recapitulating the tissue development process, which is characterized by cellular self-organization and lineage commitment through molecular specification [3]. Consequently, the modulation of cellular behavior through bioactive signals is an effective means of enhancing tissue repair. MSCs are suitable progenitors for the repair of cartilage, and can follow the natural course of early cartilage development when stimulated by critical signals found in the cell microenvironment. Bone marrow-stimulating techniques utilize the patient's own population of MSCs to facilitate the repair of cartilage tissue [157]. However, this generally leads to the deposition of a mechanically weak layer of fibrous cartilage [158], suggesting that bioactive signals required for the production of hyaline cartilage ECM are lacking at the site of injury. Therefore, a suitable set of bioactive signals should be supplied to the defect site for the production of a healthy ECM and the maintenance of the chondrogenic phenotype by differentiating MSCs.

Due to its inherent capacity for cellular recognition, regulatory role in developmental condensation and high abundance in the native cartilage ECM, HA is used as an inductive microenvironment for the enhancement of cartilage repair [75,159,160]. Mesenchymal condensation, an essential stage of chondrogenesis, is tightly regulated

by the distribution and organization of HA molecules, and specific HA-cell interaction coincides with the onset of condensation [161]. HA mediates the crossbridging of cells into condensate units by binding to its transmembrane cell surface receptor, CD44. Downstream effectors of this receptor are responsible for initiating chondrogenesis [162], and the perturbation of HA-CD44 interactions may halt or delay the chondrogenic differentiation of MSCs [75]. HA-cell interactions therefore play a major role in chondrogenesis and the subsequent maintenance of the chondrogenic phenotype.

Although HA has been shown to enhance chondrogenesis under both *in vitro* and *in vivo* conditions, it nonetheless bears the limitations and drawbacks of naturally derived materials. In addition to the high costs and potential batch-to-batch variances associated with their extraction, polysaccharides derived from animals may also cause chronic immunogenic responses when introduced to the human body [163–165]. Furthermore, crosslinking reagents used to produce HA derivatives are also toxic, and while polymer-based hydrogels have been developed, toxicity and degradability issues associated with these materials prevent their application in *in vivo* systems [166]. Although protein-glycosaminoglycan conjugates offer improved scaffold properties in cartilage, bioactivity pertaining to the core protein is often lost [167]. However, there have been attempts to develop supramolecular glycopeptide nanostructures and use them as biocompatible materials in biological applications. So far, various glycosyl units have been incorporated into Fmoc- or naphthalene conjugated amphiphilic di- or tripeptides to obtain self-supportive glycopeptide gels through noncovalent forces. However, the attachment of the saccharide unit to the peptide backbone was achieved by using different chemical approaches, none of which involved the glycosylation

bonds found in natural systems [168–171]. Previously, glycopolypeptide hydrogels were also used as synthetic scaffolds for cartilage tissue engineering [172].

In this chapter, a self-assembled glycopeptide nanofiber system is described to serve as an analogue of HA. The co-assembly of a Ser-linked β-D-glucose containing amphiphilic glycopeptide and a carboxylic acid-bearing peptide amphiphile results in the formation of a synthetic HA-emulating system. The self-assembled glycopeptide nanofibers were observed to interact with MSCs through CD44 receptors and induce chondrogenic differentiation in a manner similar to native HA. In addition, an *in vivo* microfracture-treated osteochondral defect model was used to evaluate the effect of glycopeptide nanofiber hydrogels in promoting the formation of hyaline-like cartilage as opposed to fibrous cartilage.

4.3 Results and Discussion

4.3.1 Interactions of mMSCs with Glycopeptide Nanofibers is Mediated Through CD44 Receptors

We evaluated the similarity of glycopeptide nanofibers to HA by studying the recognition of glycosaminoglycans through the CD44 receptor, which is responsible for cellular recognition and commitment to the chondrogenic differentiation pathway. Glc-PA/E-PA, HA/K-PA, K-PA/E-PA and standard polystyrene culture plate groups were used for mMSC cultures. HA/K-PA served as a biological positive control, while K-PA/E-PA was a nanofibrous gel control bearing the same functional units as Glc-PA/E-PA, except for the glycoamino acid residue.

In vitro viability and proliferation rates of mouse mesenchymal stem cells (mMSC) were evaluated to ensure that cell survival was not adversely affected on nanofibrous networks. Cellular viability was at comparable levels on days 1, 2 and 3 of culture,

suggesting that the nanofibrous networks are biocompatible. The rate of proliferation of mMSCs was also comparable to control at 24 h and 48 h of culture (Fig. 4.1a,b). Cells were able to interact with the nanofibrous network and changed their morphology following their seeding onto the peptide nanofibers, as shown by scanning electron microscopy images on day 7 (Figure 4.1c). Hyaluronidase-1 (Hyal-1) expression was studied on day 2 of culture to determine whether cells recognize the Glc-PA/E-PA matrix through CD44 receptor-mediated interactions in a similar manner to the CD44-HA binding process. Hyal-1 is one of the main enzymes for the cleavage of HA and has been reported to be upregulated in response to the binding of CD44 to HA [173,174]. The mRNA expression of Hyal-1 was enhanced in cells on Glc-PA/E-PA and HA/K-PA, while no significant changes were observed for K-PA/E-PA. The blocking of CD44 by anti-CD44 antibody significantly downregulated the Hyal-1 expression of cells on Glc-PA/E-PA and HA/K-PA (Figure 4.1e).

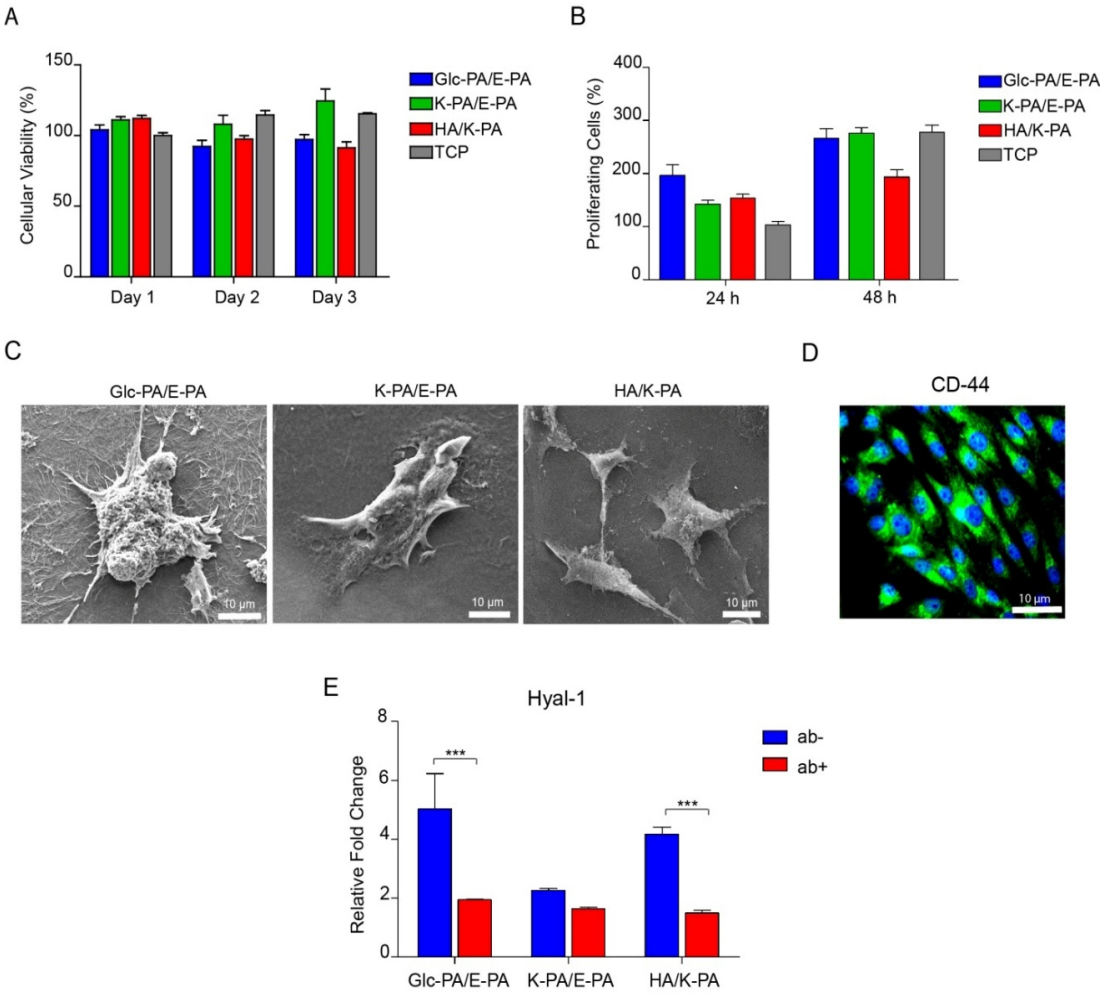

Figure 4.1 *In vitro* Viability, Proliferation and Morphology of mMSCs Cultured on Glc-PA/E-PA, K-PA/E-PA, and HA/K-PA.

(a) Cellular viability on day 1, 2 and 3; represented as percentiles by normalization to mMSCs on culture plate (b) Number of proliferative cells detected at 24 h and 48 h. (c) SEM images showing the morphology and interaction of cells on Glc-PA/E-PA, K-PA/E-PA and HA/K-PA. (d) Expression of CD44 in mMSCs as an indicator of stem cell characteristics. (Green: CD44, blue: nuclei) (e) Hyal-1 gene expression, analyzed 36 h after anti-CD44 incubation (anti-CD44 treatment indicated with ab+, no treatment indicated with ab-). Expression ratio was normalized to GAPDH and calibrated to cultured cells on TCP. Error bars indicate SEM, n = 3, **p<0.05.

4.3.2 Early Chondrogenesis of mMSCs is Promoted on Glycopeptide Nanofibers and Hyaluronic Acid Networks

To assess the influence of glycopeptide nanofibers on the chondrogenic differentiation of mMSCs, we cultured cells on nanofibrous networks over a course of 14 days and examined cellular glycosaminoglycan production and the expression levels of genes and proteins involved in chondrogenesis during this time period. One of the key features of chondrogenic differentiation in mMSCs is the elevated level of cell-cell interactions [175]. Long-term culture of mMSCs revealed that cells on nanofibrous networks undergo condensation to increase cell-cell contacts (Figure 4.2). This spontaneous aggregation of cells eliminates the necessity of micromass culture to induce *in vitro* chondrogenic differentiation. The mMSCs on Glc-PA/E-PA also exhibited a rounded morphology, which differs from their normal spindle/fibroblastoid shape, in both chondrogenic and growth media. This morphology was observed on days 3 through 14, suggesting that the cells preserve their phenotype over time (Figure 4.2).

Time-dependent tracking of sulfated glycosaminoglycan deposition and gene expression levels revealed that mMSCs on Glc-PA/E-PA committed to the chondrocytic lineage at a very early stage. On day 3, the mMSCs on Glc-PA/E-PA were found to deposit significantly higher amounts of glycosaminoglycans than those cultured on HA/K-PA, K-PA/E-PA and culture plate in both chondrogenic and growth media (Figure 4.3). Expression profiles of chondrogenesis markers showed that mMSCs on Glc-PA/E-PA displayed significantly higher fold changes (Collagen II = ~10, Aggrecan = ~14, Sox = ~38) in chondrogenesis-associated genes following 3 days of culture in chondrogenic medium, which is in accordance with the GAG deposition results. A similar result was observed, although to a lesser extent

(Collagen II = ~2.5, Aggrecan = ~3, Sox = ~5), in cells cultured in growth medium (Figure 4.3 and 4.4). These results suggest that Glc-PA/E-PA and the inducer molecules in chondrogenic differentiation medium may have a synergistic effect on chondrogenic differentiation. It is also remarkable that Glc-PA/E-PA is effective enough to trigger chondrogenesis even in the absence of a chondrogenic medium.

The mMSCs on HA/K-PA showed a different pattern of glycosaminoglycan accumulation and Collagen II and Sox 9 expression, both of which had increased at day 7 in chondrogenic and growth media (Figure 4.3 and 4.4). At day 14, glycosaminoglycan deposition and Collagen II expression of cells on HA/K-PA were significantly higher than Glc-PA/E-PA and control groups in growth medium (Figure 4.5). Moreover, Sox 9 expression also peaked at day 14 for HA/K-PA treated cells in both growth and chondrogenic media (Figure 4.3c and 4.5a). However, aggrecan expression did not show significant upregulation by cells on HA/K-PA throughout the experimental period, which can be attributed to the scaffold-mediated suppression of aggrecan expression (Figure 4.3 c). The overall pattern of sulfated glycosaminoglycan production matches the pattern of chondrogenic marker expression in both Glc-PA/E-PA and HA/K-PA samples, suggesting that signals received from both nanofibrous network types similarly instruct mMSCs for cartilage-like ECM deposition.

Sulfated glycosaminoglycan deposition patterns were further investigated by the visualization of glycosaminoglycan distribution on or around cellular aggregations through Safranin-O staining at days 3, 7 and 14 (Figure 4.3a and 4.4a,c). Gradual increases in staining intensity, in concert with increases in aggregate sizes, could be used to follow the ongoing differentiation process on Glc-PA/E-PA and HA/K-PA through 14 days. We also investigated cartilage-specific protein expressions by

immunolocalization with fluorescence-conjugated antibodies on day 14. The extensive staining of Collagen II, Aggrecan and Sox 9 in cells cultured on Glc-PA/K-PA further supports the strong trend for chondrogenic differentiation on this hydrogel, while cells on HA/K-PA, K-PA/E-PA and TCP showed less prominent staining for cartilage marker proteins (Figure 4.3d and 4.5b).

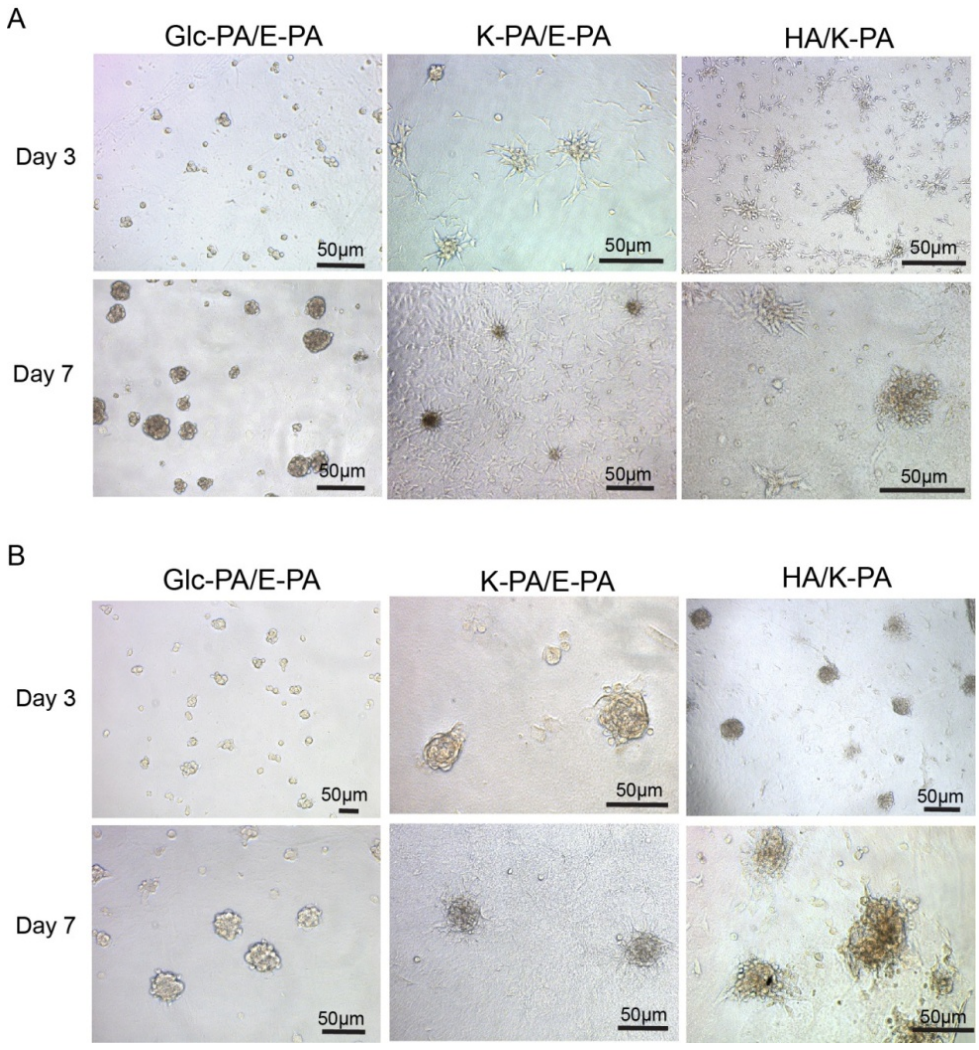

Figure 4.2 mMSC Morphology and Cluster Formation on Glc-PA/E-PA, K-PA/E-PA and HA/K-PA

(a) in maintenance medium or (b) in chondrogenic differentiation medium on days 3 and 7

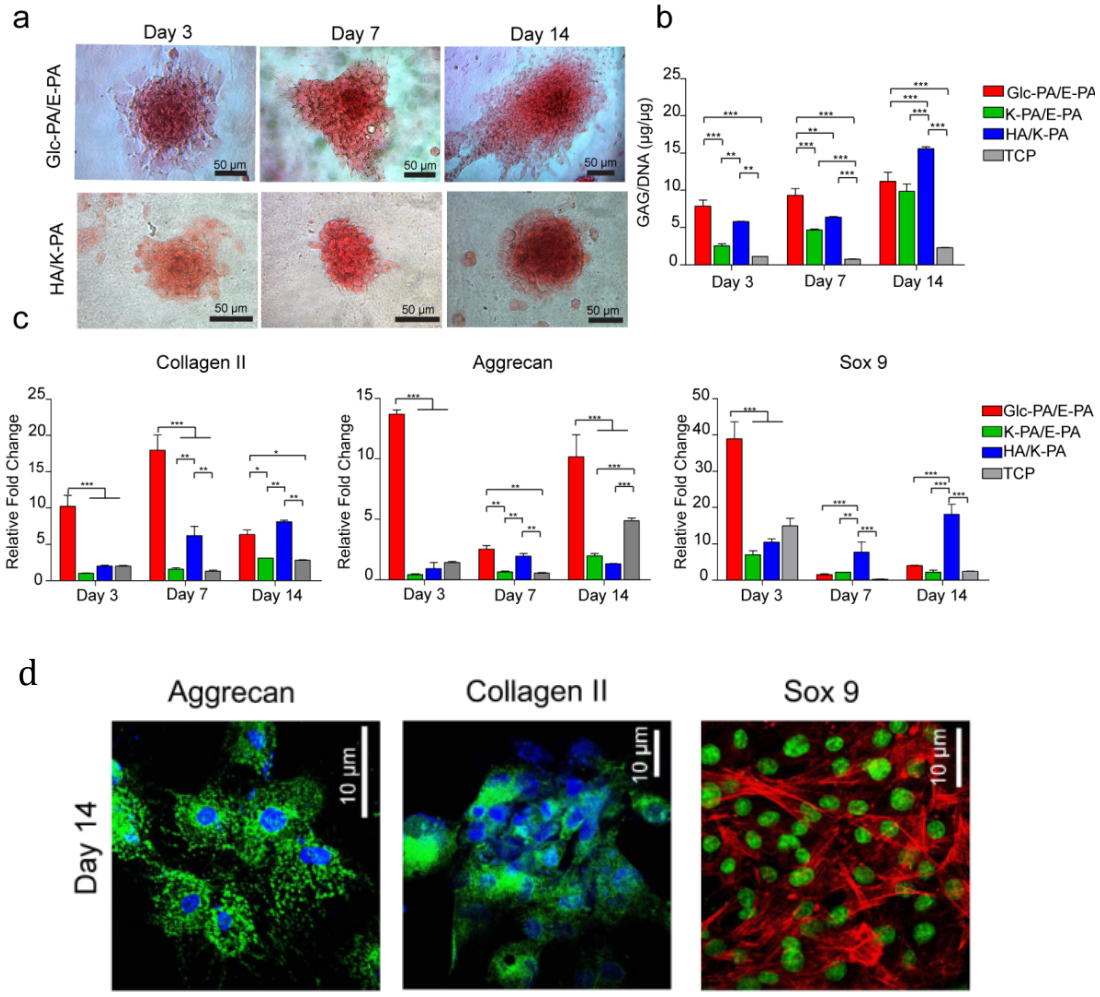

Figure 4.3 Glycopeptide Nanofibrous Networks Enhance the Chondrogenic Differentiation of mMSCs.

a,b, Glycosaminoglycan (GAGs) deposition was analyzed by Safranin-O staining and DMMB assay. Safranin-O stainings (a) and DMMB assay for quantification of GAGs (normalized to DNA amount) (b) demonstrate the elevated production of GAGs by mMSCs cultured on Glc-PA/E-PA and HA/K-PA on days 3, 7 and 14 in chondrogenic medium. c, Gene expression analyses performed for Collagen II, Aggrecan and Sox 9 genes on days 3, 7 and 14 in chondrogenic medium. Expression ratios were normalized to GAPDH and calibrated to cultured cells on TCP in maintenance media. d, Immunolocalization of Aggrecan, Collagen II and Sox 9 protein expressions of mMSCs on glycopeptide nanofibers on day 14 in chondrogenic medium. Error bars in b,c indicate SEM, n = 3, **p<0.05, *p<0.01.

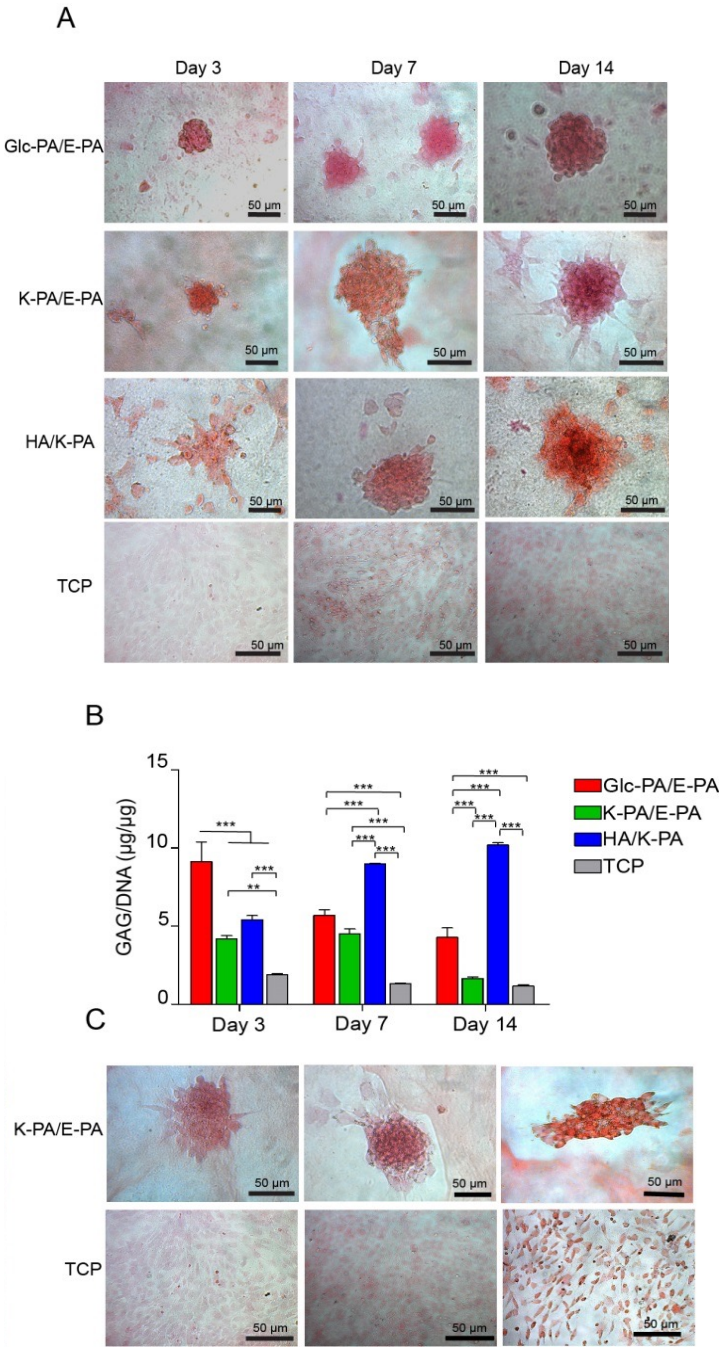

Figure 4.4 Glycosaminoglycan (GAG) Accumulation by mMSCs Cultured on Glc/E-PA, K-PA/E-PA, HA/K-PA and Culture Plate on Day 3, 7 and 14.

(a) Safranin-O staining showing the intensity and distribution of GAGs produced by mMSCs cultured in maintenance medium and (c) in chondrogenic medium. (b) Quantification of GAGs by DMMB assay on day 3, 7 and 14. GAG concentrations were normalized to DNA. Error bars indicate SEM, n = 3, **p<0.05

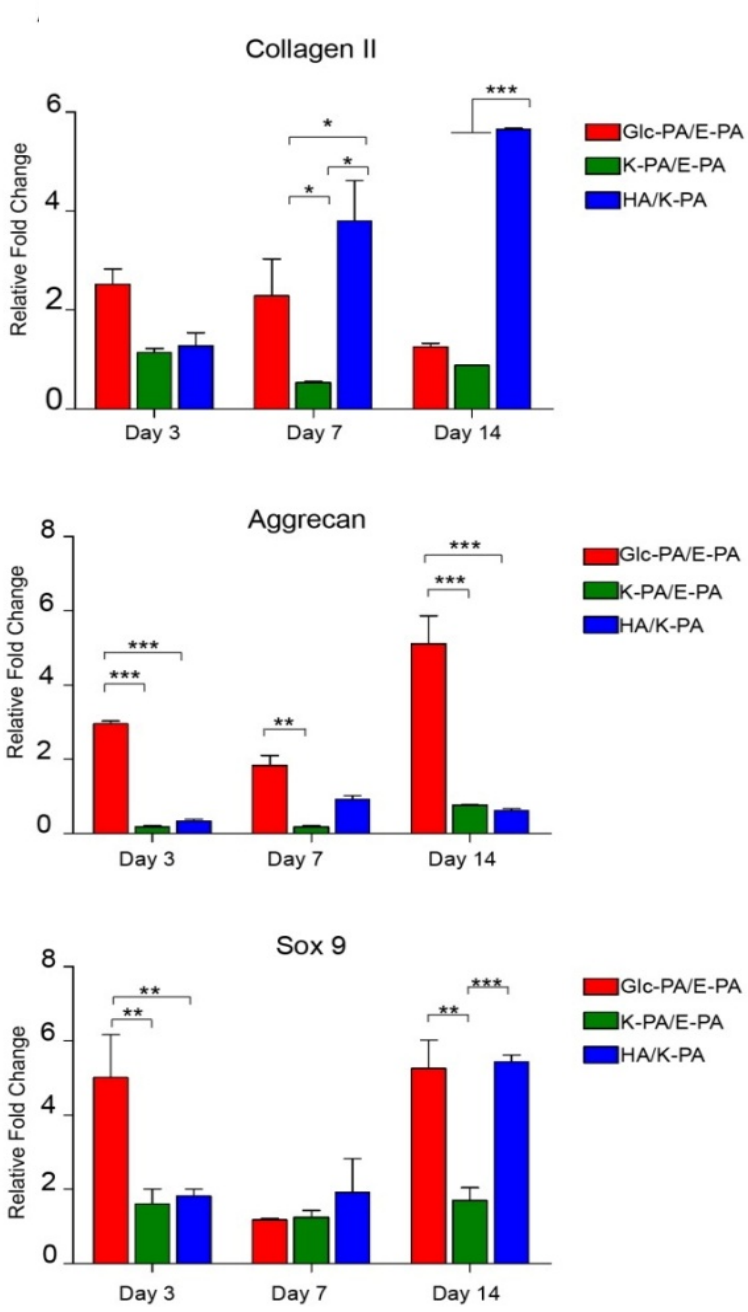

Figure 4.5 Gene Expression Levels of Collagen II, Aggrecan and Sox 9 of mMSCs Cultured in Maintenance Medium on Days 3, 7 and 14.

Expression ratios were normalized to GAPDH and calibrated to cultured cells on TCP in maintenance media.Error bars indicate SEM, n = 3, **p<0.05.

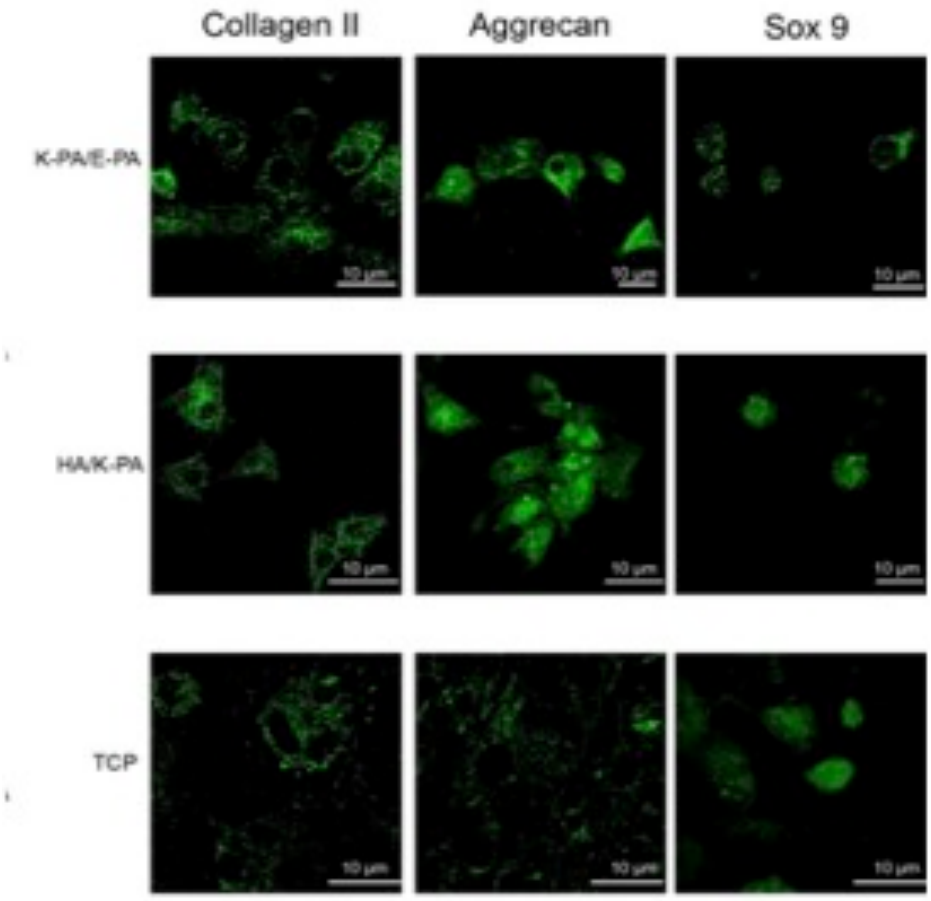

Figure 4.6 Immunostaining of Collagen II, Aggrecan and Sox 9 Expressed by mMSCs Cultured on K-PA/E-PA, HA/K-PA and Culture Plate on Day 14 in Chondrogenic Differentiation Medium.

4.3.3 CD44 Blockade Downregulates the Expression of Sox 9 on Both Glycopeptide and Hyaluronic Acid Nanofibers

To study hydrogel-CD44 interactions and the subsequent signaling responsible for the early induction of the mMSCs towards chondrogenesis, we analyzed the changes in the expression of Sox 9, a transcription factor that activates chondrogenesis-related pathways, following CD44 blockage. On Glc-PA/E-PA nanofibers, mMSCs treated with anti-CD44 had significantly decreased Sox 9 expression compared to non-treated mMSCs on day 3 in both growth and chondrogenic media (Figure 4.6 and 4.7). Similarly, mMSCs on HA/K-PA also displayed decreased Sox 9 expression following anti-CD44 treatment on day 3. However, CD 44 blocking clearly did not affect Sox 9 expression of mMSCs cultured on K-PA/E-PA and TCP (Figure 4.6a,b). This finding is consistent with Hyal-1 expression patterns and suggests that the mMSCs recognize functional units of Glc-PA/E-PA in a similar way with HA/K-PA, directing their differentiation accordingly.

,

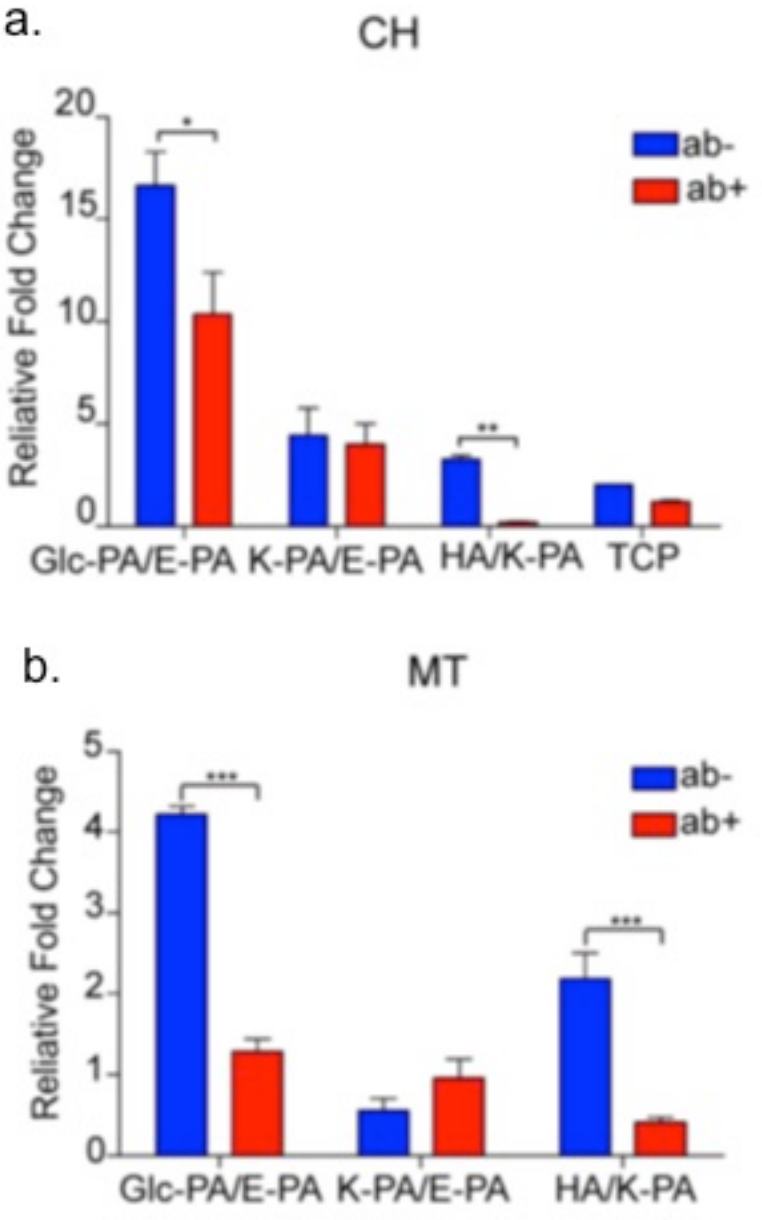

Figure 4.7 CD44 Blocking Downregulates Sox 9 Expression of mMSCs on Glycopeptide Nanofibrous Networks on Day 1.

Sox 9 expression analysis was performed at day 1 using mMSCs cultured in two different media: chondrogenic differentiation (a) and maintenance medium (b) (anti-CD44 treatment indicated with ab +, no treatment indicated with ab -). Expression ratio was normalized to GAPDH and calibrated to cultured cells on TCP in maintenance media. Error bars indicate SEM, n = 3, **p<0.05, *p<0.01.

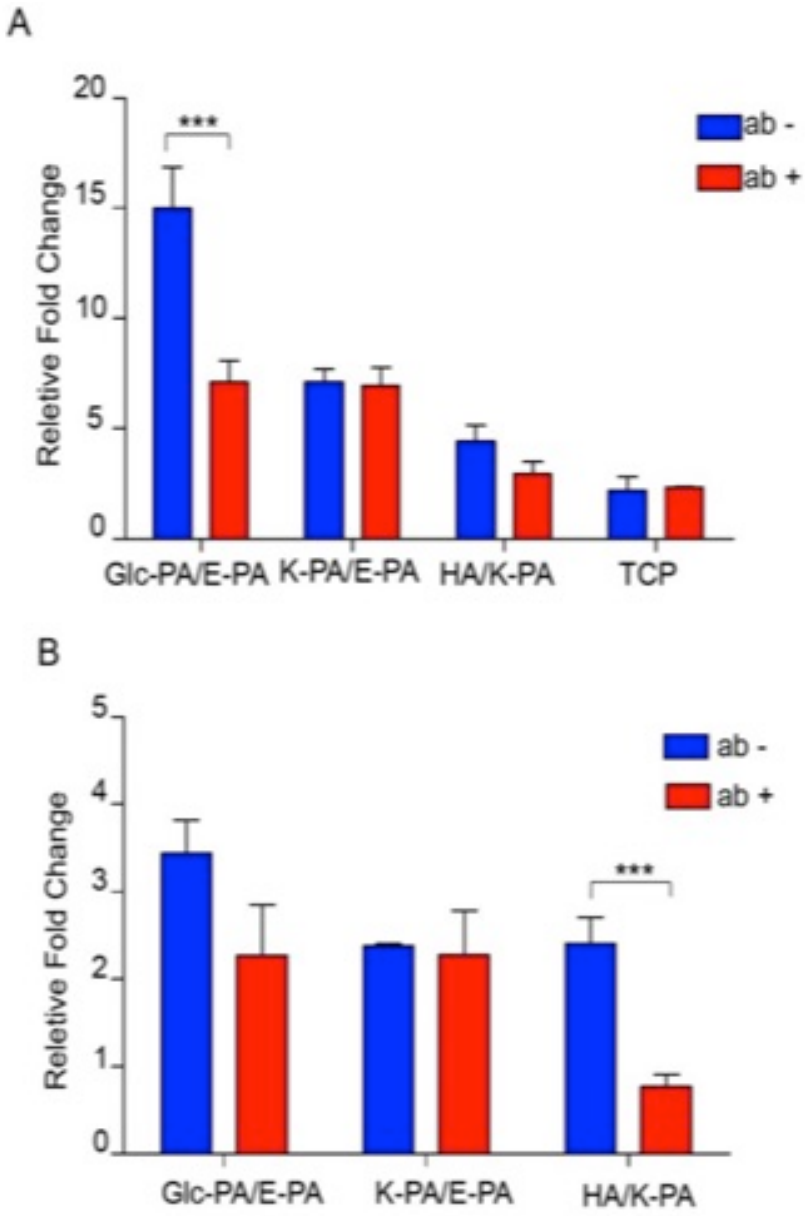

Figure 4.8 Effect of CD44 Inhibition on the Expression of Sox 9 by mMSCs Cultured on Glc/E-PA, K-PA/E-PA, HA/K-PA and Culture Plate on Day 3.

mMSCs cultured in two different culture media; (a) chondrogenic differentiation or (b) maintenance media in the presence (indicated as ab+) or absence of anti-CD44 (indicated as ab-) Sox 9 expression levels were assessed on day 1 and normalized to GAPDH. Error bars indicate SEM, n = 3, **p<0.05.

4.3.4 Regeneration of Osteochondral Defects was Improved by Glycopeptide Nanofiber Gel Treatment

To evaluate the capacity of glycopeptide gels to direct the recovery of damaged articular cartilage, we performed regeneration experiments using a model based on the microfracture treatment of full thickness osteochondral defects. In this model, the subchondral bone is bled to allow the recruitment of bone marrow-derived MSCs into the defect site, initiating the regeneration process. The ability of the glycopeptide nanofiber gels to promote the differentiation of transported MSCs was compared to a clinically utilized formulation of hyaluronic acid (Hyalgan®), and a saline-treated group was included as control. Defects were created in the trochlear groove of each knee and treated with Glc-PA/E-PA, Hyalgan®, or saline following microfracture. Animals were sacrificed 12 weeks post-operation.

Consecutive sections from each sample were stained with Safranin-O and counterstained with Fast Green/Haemotoxylin to qualitatively assess the characteristics of regenerated tissue. Newly-formed tissue thickness and integration to surrounding tissue, GAG and collagen II-rich matrix deposition and cellular morphology and density were analyzed in detail for each section. All samples, except for one Hyalgan-treated sample, showed full closure of the defect site. No tissue necrosis or infiltration by immune cells was observed in any of the samples. Samples treated with Hyalgan® and saline generally exhibited a weak vertical and basal integration to surrounding tissue, with fissures and partial detachment (Fig. 6a,b). Moreover, weak Safranin-O stainings and loose tissue arrangements in these groups indicated the presence of fibrous cartilage with apparent surface irregularities, including disruption and delamination. Spherical chondrocytes were distributed in a limited part of the regenerated tissue, and hypocellularity was observed at the site of

integration (Figure 4.8a). Collagen II immunostainings showed that cells in saline-treated groups deposited relatively low amounts of collagen, especially at the uppermost part of the regenerated tissue (Figure 4.8b).

The non-matching distributions of collagen II and sGAG in Hyalgan®-treated samples indicated the heterogeneous nature of the regenerated tissue (Figure 4.8a,b). In contrast, defect sites filled with Glc-PA/E-PA nanofiber gel completely integrated to the surrounding tissue at two lateral sites, and basally integrated to the subchondral bone. The regenerated tissue was smooth, displayed no evidence of abrasive damage and closely matched the surrounding tissue in appearance. Chondrocytes were generally distributed in columnar structures, as is observed in lacunae, and showed zonal organization (i.e. were spindle-shaped in the superficial zone and rounded at the mid-zone). The strong and evenly distributed staining of collagen II and Safranin-O suggests that the regenerated tissue was dominated by hyaline-like cartilage and closely matched the morphology and composition of the surrounding tissue.

The characteristics of the regenerated tissue were also scored for quantitative assessment. A validated 24-point O'Driscoll scoring system optimized for cartilage repair in animal studies was used for this purpose [176]. This test encompasses four major categories; the nature of the predominant tissue, structural characteristics, cellular evidence of degeneration and degenerative changes in adjacent cartilage. Results were derived from six animals each for the saline-treated, Hyalgan® and Glc-PA/E-PA groups and yielded the following means: 12.55 ± 6.02, 11.64 ± 5.02 and 17.31 ± 4.83, respectively (Figure 4.8c and Table 4.1). A higher score and lower standard deviation was achieved in Glc-PA/E-PA treated groups, while Hyalgan®-treated groups showed a lower score that was statistically indistinguishable from the

saline-treated group. We also investigated the number of cells stained positively with collagen II in regenerated tissues. The ratio of collagen II-positive cells was significantly higher in Glc-PA/E-PA treated group, with abundant distribution in the mid-zone of newly formed tissue, compared to the saline-treated or Hyalgan®-treated group (Figure 4.8d and 4.9). *In vivo* experiments overall suggested that Glc-PA/E-PA treatment results in the complete regeneration of the defect site with hyaline-like characteristics within a 12-week period, which provides further support for the capacity of glycopeptide nanofibers for facilitating the early induction of chondrogenesis.

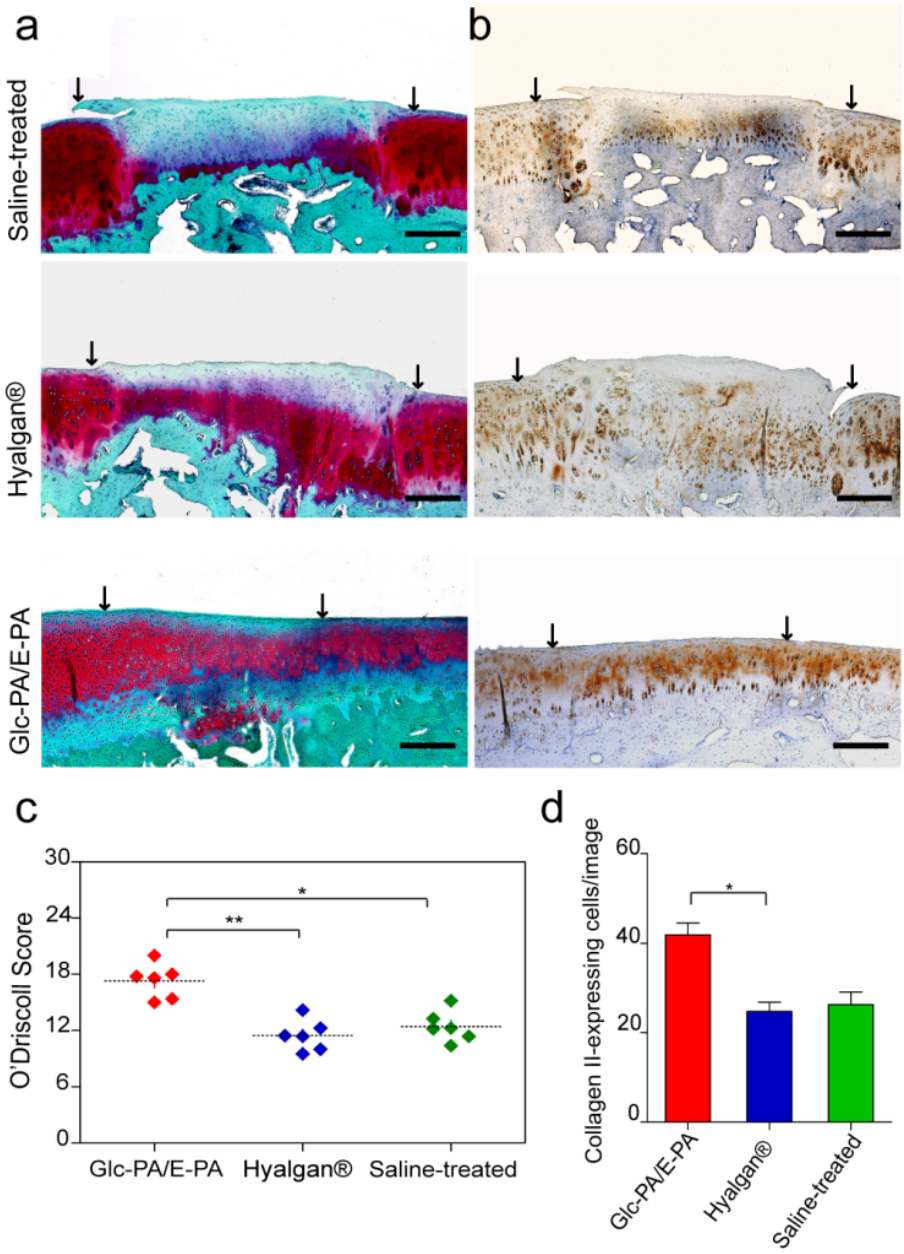

Figure 4.9 Hyaline Cartilage Formation Predominates in Groups Treated with Glycopeptide Nanofiber Gels Following Microfracture.

Histological assessment was performed 12 weeks after treatment. Tissue sections stained with Safranin-O (a) and Collagen II immunostain (b). c, O'Driscoll scoring system was used to evaluate repair tissue characteristics. Each square shape represents a single sample belonging to the relevant treatment group. d, Quantitative analysis of collagen II expressing cells in the defect sites of each treatment group. Error bars indicate SEM, n = 3, **p<0.05, *p<0.01.

Table 4.1 Histological Scores for Sham, Hyalgan and Glycopeptide Hydrogel Groups

Category	Saline-treated		Hyalgan®		Glc-PA/K-PA	
	Mean	**SD**	**Mean**	**SD**	**Mean**	**SD**
Cellular morphology	1.86	0.76	1.91	0.75	2.24	0.64
Safranin O staining	2.00	0.67	1.50	0.80	2.41	0.63
Surface regularity	1.44	1.15	1.36	0.73	2.24	0.64
Structural integrity	0.82	0.72	0.68	0.57	1.45	0.51
Thickness	0.82	0.48	1.05	0.65	1.24	0.51
Bonding to the adjacent tissue	1.32	0.61	1.18	0.59	1.86	0.35
Hypocellularity	1.89	0.63	1.77	0.53	2.31	0.66
Chondrocyte clustering	1.25	0.65	1.14	0.77	1.52	0.57
Freedom from degenerative changes in adjacent tissue	1.14	0.36	1.05	0.21	2.03	0.33
Total	12.55	6.02	11.64	5.60	17.31	4.83

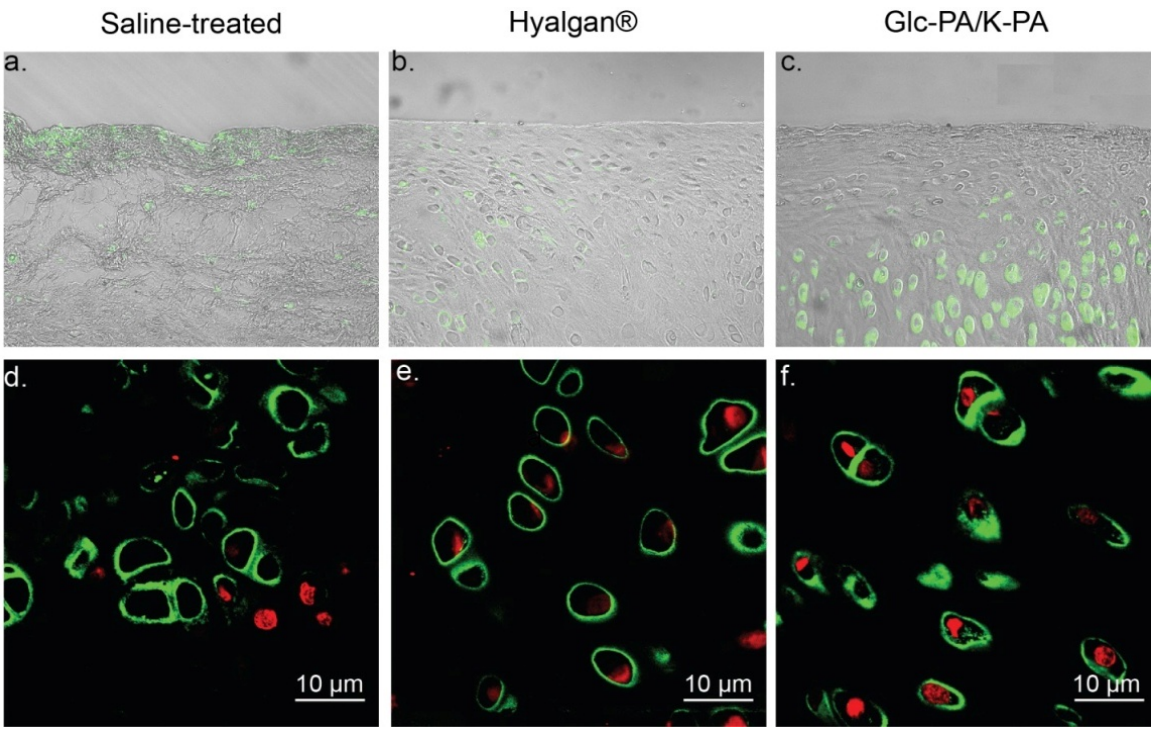

Figure 4.10 Immunofluorescence Collagen II Staining on Sections of mMSC Cultures in 3D Glc/E-PA, HA and Treatment-Free Sections.

(a) DIC (differential inference constrast) images show morphology and distribution collagen II positive cells and (b) dark field image shows a closer view of cells in defect sites. (Green; Collagen II)

4.4 Conclusion

Mature cartilage tissue is unable to reinitiate its developmental mechanisms after injury and requires exogenous manipulation for functional regeneration [50,177]. HA is one of the most prominent regulatory components of mature and developing cartilage ECM [178]. In developing cartilage, the HA-rich ECM regulates the formation of condensation units that will later serve as templates for the cartilage anlagen [84,3,161]. Moreover, several reports have shown that HA molecules initiate and enhance the *in vitro* chondrogenic differentiation of stem cells, and that CD44 binding is necessary for this process [75,162]. The modulation of CD44 and its downstream elements provides an effective means of initiating and maintaining the chondrogenic differentiation of MSCs. In this chapter, we report a supramolecular design involving glycopeptide nanofibers that present functional chemical units found in the native HA. These nanofibers stimulate the early commitment of mMSCs into the chondrogenic lineage through CD44 interactions, thereby replicating the function of native HA networks.

The combination of β-D-glucose-containing amphiphilic glycopeptide and carboxylic acid-bearing peptide amphiphile molecules allows the imitation of the chemical signature and high charge density of HA. This GAG-like nanofibrous system morphologically mimics the fibrous ECM responsible for regulating cell adhesion and protein adsorption processes. A combination of these factors allows the glycopeptide nanofiber matrix to provide a biocompatible and cell-inductive environment for the culturing of MSCs. Our *in vitro* results suggest that mMSCs recognize glycopeptide nanofibers through HA receptors, and this interaction leads to their early commitment to the chondrogenic lineage. Cellular recognition of Glc-

PA/E-PA by CD44, as the main adhesion receptor for HA, was also shown by *in vitro* studies. mMSCs primarily use CD44 for HA binding, and the HA-CD44 interaction has been reported to upregulate the expression of Hyal-1. As such, we tracked Hyal-1 expression of cells following the blocking of CD44 receptors with an anti-CD44 antibody. The downregulation of Hyal-1 expression following CD44 blockade confirmed the possibility that the mMSCs recognize glycopeptide nanofibers in a similar manner to the native HA.

Subsequently, differentiation analysis demonstrated that the differentiation of mMSCs occurs at an earlier stage and is enhanced on glycopeptide nanofibers, even in the absence of chondrogenic factors. HA promotes chondrogenesis through its interaction with CD44, and the inhibition of this interaction results in the downregulation of cartilage related markers. The expression of Sox 9, the master transcription factor of the chondrogenic differentiation pathway, was downregulated in mMSCs cultivated on Glc-PA/E-PA following CD44 blocking, while no difference in expression was observed in K-PA/E-PA control. A similar response to Glc-PA/E-PA group was observed in cells grown on HA/K-PA following CD44 blockage, suggesting that the biochemical composition of Glc-PA/E-PA and HA/K-PA are similar. As such, the Glc-PA/E-PA nanofiber is capable of mimicking the function of HA through its chemical composition, which elicits cellular responses similar to the native hyaluronic acid molecules through CD44 signaling pathways.

Our *in vivo* results also supported these *in vitro* findings and demonstrated that hyaline cartilage formation is enhanced by Glc-PA/E-PA treatment in a microfracture-treated cartilage defect model. In addition to the biochemical cues provided by the hydrogel, the structure of the Glc-PA/E-PA matrix itself may assist in maintaining a high concentration of cells at the defect site by facilitating the

adhesion of MSCs transferred from bone marrow during microfracture. Moreover, Glc-PA/E-PA treatment may stabilize blood clots and promote the early mechanical stability of the defect site.

In conclusion, our findings support the hypothesis that a molecularly designed supramolecular mimic of hyaluronic acid can interact with MSCs through CD44 receptors and facilitate their commitment to the chondrogenic lineage without the need for exogenous growth factors. A key aspect of the current design is that it can be used in place of naturally-derived hyaluronic acid to eliminate the potential health hazards associated with natural scaffolds. Our *in vivo* results also suggest that glycopeptide nanofibers can be used for less invasive and cell-free *in situ* cartilage regeneration approaches by inducing the chondrogenesis of MSCs released from bone marrow following microfracture.

4.5 Experimental Section

4.5.1 mMSC Culturing and Preparation of Nanofibrous Networks for *In Vitro* Culture

mMSCs were expanded to passage 3 in maintenance medium consisting of DMEM with 10% (vol/vol) FBS (Invitrogen), 1% (vol/vol) GlutaMAX (Invitrogen) and 1% penicilin-streptomycin (Invitrogen). All experiments were conducted with cells within passage 3-8. Cells were maintained in humidified incubators at 5% CO_2 at 37 °C. Cells were passaged when they reached 80% confluency through detachment by Trypsin-EDTA (0.025%) (Invitrogen) and reseeding at 3000 cells/cm_2.

For in vitro analysis, mMSCs were cultured on TCP or surfaces coated with Glc-PA/E-PA, K-PA/E-PA or HA/K-PA. Coating was performed with 1 mM PA solutions or hyaluronic acid solution prepared from sodium salt (Sigma, Cat no:

42686). Coated plates were left under laminar flow hood to dry for 16 h and sterilized under UV irradiation for 30 min prior to cell seeding.

4.5.2 Viability, Proliferation and SEM imaging

Cellular viability was assessed by colorimetric MTT assay (Sigma, Cat no:.TOX-1). Cells were seeded at a density of 250 cells/cm_2, and cultured for 24 h, 48 h and 72 h at parallel plates. At the time of the assay, cells were incubated with (3-(4,5-dimethylthiazol-2-yl)-2,5 diphenyltetrazolium bromide (MTT) reagent (Sigma-Aldrich) for 3 h at standard cell culture conditions. Viable cells form a purple formazan product through the reduction of the MTT reagent. Cell viability was quantified by the spectrophotometric measurement of solubilized formazan products at 590 nm. Viability was normalized against the TCP.

Proliferating cells were detected by Click-iT EdU assay (Molecular Probes) at days 1 and 2. mMSCs were seeded on nanofibers or culture plate at a concentration of 250 cells/cm_2 in maintenance medium. After 6 h, maintenance medium was exchanged with maintenance medium supplemented with 10 mM EdU. At the time of the assay, cells were fixed with 4% paraformaldehyde/PBS and permeabilized with 5% Triton-X. To detect incorporated EdU in proliferating cell DNA, cells were treated with Alexa Fluor-488-conjugated azide. Cells stained with Alexa Fluor-488 were imaged by fluorescence microscope and quantified with Image J software. Proliferation rate of cells on Glc-PA/E-PA, K-PA/E-PA and HA/K-PA was normalized to cells on TCP.

For SEM imaging, mMSCs were cultured for 7 days in maintenance medium, culture plate wells were washed with PBS and the attached cells were fixed with 2% gluteraldehyde/PBS for 2 h. Following three washing steps with PBS, samples were

dehydrated in a series of ethanol solutions starting with 20% ethanol and proceeding to absolute ethanol for 10 min at each step. Samples were dried with a Tourismis Autosamdri-815B critical point drier, coated with 6 nm Au/Pd and imaged with a FEI Quanta 200 FEG SEM.

4.5.3 Glycosaminoglycan Quantification

Quantification of sulfated glycosaminoglycans was performed by a biochemical DMMB assay (2). Cell cultures were digested in papain digestion buffer (100 mM sodium phosphate buffer/10 mM Na_2EDTA/10 mM l-cysteine/0.125 mg/mL papain) overnight at 65 °C prior to analysis. Total DNA per well was measured with a Qubit dsDNA quantitation kit (Invitrogen) according to manufacturer's instructions. Total dsDNA amount was used to normalize the sulfated glycosaminoglycan content. Diluted chondroitin sulfate standards (from 0 to 35 μg mL^{-1}) were used to generate standard curves for the DMMB assay. A total of 100 μL of DMMB solution (16 mg L^{-1} 1,9-DMMB, 40 mM glycine, 40 mM NaCl, 9.5 mM HCl, pH 3.0) was added to 40 μL of papain-digested solutions and standard samples, and optical densities (ODs) of the solutions were measured using a 595 nm filter on a microplate reader. The absorbance of the cell-free control groups was subtracted from the absorbance values of the experimental groups.

4.5.4 Gene Expression Analysis

Gene expression profiles for analyzing chondrogenic differentiation were assessed by quantitative real time PCR (qRT-PCR). Before qRT-PCR experiments, RNA from each sample was extracted with TRIzol reagent (Invitrogen) according to manufacturer's instructions. The yield and purity of extracted RNA were assessed with Nanodrop 2000 spectrophotometer (Thermo Scientific). cDNA synthesis from

RNA and qRT-PCR were performed using SuperScript III Platinum SYBR Green One-Step qRT-PCR Kit according to manufacturer's instructions. Reaction conditions were briefly as follows: 55 °C for 5 min, 95 °C for 5 min, 40 cycles of 95 °C for 15 s, 60 °C for 30 s, and 40 °C for 1 min, followed by a melting curve to confirm product specificity. The reaction efficiencies for each primer set (Table 4.2) were evaluated with a standard curve using 5-fold serial dilutions of total RNA. Each run was internally normalized to GAPDH, and each group was normalized to the expression levels of MSCs cultured in maintenance medium. A comparative Ct method with efficiency correction was used to analyze the results. An expression ratio of greater than 1 indicates upregulation, while a ratio less than 1 corresponds to the downregulation of the gene of interest.

Table 4.2 Primers Used for qRT-PCR Expression Analysis

Gene	Primer Sequence: Forward/Reverse	Product Size (bp)
Col I	5′-TGACTGGAAGAGCGGAGAGT-3′ 5′-GTTCGGGCTGATGTACCAGT-3′	151
Col II	5′-ACTTGCGTCTACCCCAACC-3′ 5′-GCCATAGCTGAAGTGGAAGC-3′	123
Aggrecan	5′-GGTCACTGTTACCGCCACTT-3′ 5′-CCCCTTCGATAGTCCTGTCA-3′	175
Sox 9	5′-AGGAAGCTGGCAGACCAGTA-3′ 5′-CGTTCTTCACCGACTTCCTC-3′	193
Hyal-1	5′-ATGCCCTTTACCCCAGTATT-3′ 5′-TGGGGGTCTCTGGAAACTAT-3′	216

4.5.5 Immunostaining and Imaging

mMSCs were fixed in 4% paraformaldehyde/PBS for 10 min and permeabilized in 0.1% Triton X-100 for 15 min. For blocking, samples were incubated with 10%

(w/v) bovine serum albumin/PBS for 30 min and treated with collagen II primary antibody (Abcam) at 1:200 dilution, Sox 9 primary antibody (Thermoscientific) at 1:300 dilution or aggrecan antibody at 1:200 dilution (Abcam) overnight at 4 °C. Cells were then washed with PBS and incubated for 1 h at room temperature with Goat Anti-Rabbit IgG H&L (Alexa Fluor® 488). All samples were counterstained with 1 μM TO-PRO-3 (Invitrogen) in PBS for 15 min at room temperature and mounted with Prolong Gold Antifade Reagent (Invitrogen). Negative controls were obtained by omitting the primary antibody and incubating with 1% normal goat serum/PBS. Samples were imaged by confocal microscopy (Zeiss LSM510).

4.5.6 *In Vivo* Osteochondral Defect Model and Treated with Microfracture Treatment

12 white male New Zealand rabbits (mean weight 2500 ± 400 g, age 12 weeks) were used for in vivo experiments. All procedures on animals were approved by the Gulhane Military Medical Academy (GATA) Animal Ethics Committee. Animals were anesthetized by intramuscular injection of 30–40 mg/kg ketamine and 5–7 mg/kg xylazine prior to surgery. A lateral parapatellar longitudinal incision was made to expose the knee joint, the synovial capsule was incised, and the trochlear groove was exposed after the medial luxation of the patella. When the knee was maximally flexed, a defect (1.5 mm in diameter, and 1.5 mm in depth and diameter) was created in the center of the groove using a drill. All debris, including articular cartilage, was removed with a micro curette. Microfracture treatment was performed by creating three holes within each defect to mobilize bone marrow blood. After observing blood flow from holes, defects were filled with physiological saline (saline-treated), 100 μL of Glc-PA/E-PA or a clinically approved formulation of

hyaluronic acid (Hyalgan ®). The wound was closed by suturing of the knee joint capsule and the overlaying skin layer-by-layer. Intra muscular antibiotics were given to each rabbit for 3 days following the operation, no animals were observed to be infected throughout the experimental period. Rabbits were provided with individual cages and observed for 12 weeks prior to sacrifice.

Only one defect was created for each trochlea, and two different treatments were tested for each rabbit. A total of 8 trochleae were used for each treatment; however, two were later excluded due to improper handling.

4.5.7 Histological and Immunohistochemical Stainings of Tissue Sections

Samples were fixed in 4% paraformaldeyde for 48 h at 4 °C and decalcified in 5% formic acid. 5% formic acid solution was changed every 2-3 days. The completion of decalcification was periodically tested with ammonium oxalate test. Decalcified samples were dehydrated in a graded series of ethanol and cleared in two changes of xylene. Samples were embedded in paraffin blocks and sectioned at 5 μm thickness by microtome. For histological and immunohistochemical evaluations, sections were deparaffinized and rehydrated through a series of graded alcohol solutions. For glycosaminoglycan imaging, sections were stained with Safranin-O for 5 min and Fast Green for 5 min, and then dehydrated in graded ethanol solutions and cleared in xylene. Slides were mounted by Histomount® mounting medium and imaged by light microscopy (Zeiss, Axio Scope). For immunohistochemical stainings, slides were treated with an antigen retriever (Sigma) to uncover epitopes for 15 min at 37 °C after rehydration steps. After blocking for 2 h at room temperature, sections were incubated with primary Collagen II antibody (Pierce Antibodies) at 4 °C overnight. Sections were then washed extensively with TBS w/Triton-X (0.01%

vol/vol) and treated with Goat anti-Mouse IgG-HRP at a dilution of 1:500 for 1 h at room temperature to detect bound primary antibodies. Secondary antibody binding was visualized with diaminobenzidine (DAB) and nuclei were stained with hematoxylin (Sigma-Aldrich). Negative controls were obtained by omitting primary antibody and incubating with 1% normal goat serum/TBS. Slides were mounted with Histomount ® mounting medium.

4.5.8 Statistical Analysis

All data were presented as means ± standard error of means (s.e.m). Either one way ANOVA or two way-ANOVA was performed to test the significance of observed differences between the study groups. A value of $p<0.05$ was considered to be statistically significant, except where noted.

CHAPTER 5

5 CONCLUSION and FUTURE PERSPECTIVES

The successful regeneration of cartilage can only be achieved if a sufficient number of cells can be induced to initiate the regeneration process through suitable biochemical and mechanical signals. One of the major limitations of cartilage tissue is the low number of active cells synthesizing ECM and the lack of bioactive molecules coming through blood circulation, which often leads to the production of fibrocartilage tissue instead of hyaline cartilage. A better understanding of the molecular processes that occur during regeneration and the establishment of systems that successfully mimic microenvironments inductive for new tissue formation would greatly improve the prospects of rapid and effective cartilage regeneration. The present dissertation has demonstrated the inductive role of glycosaminoglycan-mimetic environments for the chondrogenic differentiation of progenitor cells in *vitro* and for neo-cartilage tissue formation *in vivo.* Most of the regulatory signaling between chondrocytes and their environment takes place in the pericellular matrix. Because the PCM completely surrounds each chondrocyte, any signal perceived by these cells must be expressed through PCM components. The all-important regulatory role of PCM components is encouraging for the development of ECM-inspired biomaterials that direct cellular behaviors by emulating similar interactions with chondrocytes.

In this thesis, first the chondrogenic differentiation potential of chondroprogenitor cells on various glycosaminoglycan-mimetic environments were examined. Progenitor cells rather than stem cells were chosen for the ease with which their differentiation can be tracked. We found that progenitor cells commit chondrogenic

differentiation on scaffolds that bear sulfonate, carboxylate and hydroxyl functional groups at a specific ratio that results in an overall negative charge. Our observation that a negatively-charged environment is supportive of chondrogenic differentiation is especially noteworthy in this context. Using our understanding the influence of negatively charged functional groups, we have also designed a series of experiments (detailed in Chapter 3) to determine the effect of negatively charged functional groups and their density on MSC chondrogenesis. We observed that MSCs under this treatment are similar in morphology to ATDC5 cells, which is indicative of chondrogenic differentiation. Gene expression analyses also supported the idea that these MSCs preferentially commit to the chondrogenic lineage; indeed, it was found that a specific density of the functional epitope was necessary for the optimal expression of chondrogenic markers.

Hyaluronic acid is the most abundant glycosaminoglycan of cartilage tissue and has several regulatory roles in developing and mature cartilage. The last study presented in this thesis was an investigation of the effect of hyaluronic acid-mimetic molecules on MSC chondrogenesis and cartilage regeneration in a rabbit defect model. The results indicated that cells undergoing chondrogenic differentiation interacted with the hyaluronic acid-mimicking scaffold through their CD44 receptors and that subsequent signaling was dependent on this interaction. This study has significant implications for the design of bioactive scaffolds, as it demonstrates that a biofunctional material can interact with cells through their native signaling pathways and instruct them to behave in a specific way. The inductive properties of hyaluronic acid-mimetic peptide nanofibers were also tested in an osteochondral defect model, and the early and complete regeneration of groups treated with the HA-mimetic hydrogel supported what was observed in our *in vitro* study.

For future studies, it is essential to develop multifactorial strategies to improve current treatment options for cartilage regeneration. Cartilage is a tissue that is constantly exposed to mechanical stimuli and its maintenance and development are dependent on strong mechanical forces. For this reason, it is hard to obtain highly organized, layered and differentiated constructs in static two-dimensional culture environments. Mechanical cues can be integrated into design of bioactive nanofibers, however this poses some requirements that needs to be met for functional tissue generation as such; flatness of surface and three dimensional architecture of defect site can affect the degree of mechanical loading experienced by cells and this lead to mixed and irreproducible results among samples.

BIBLIOGRAPHY

(1) Sophia Fox, A. J.; Bedi, A.; Rodeo, S. A. The basic science of articular cartilage: structure, composition, and function. *Sports Health* **2009**, *1* (6), 461–468 DOI: 10.1177/1941738109350438.

(2) Mackie, E. J.; Ahmed, Y. a; Tatarczuch, L.; Chen, K.-S.; Mirams, M. Endochondral ossification: how cartilage is converted into bone in the developing skeleton. *Int. J. Biochem. Cell Biol.* **2008**, *40* (1), 46–62 DOI: 10.1016/j.biocel.2007.06.009.

(3) Hall, B. K.; Miyake, T. Divide, accumulate, differentiate: cell condensation in skeletal development revisited. *Int. J. Dev. Biol.* **1995**, *39* (6), 881–893.

(4) *Handbook of Histology Methods for Bone and Cartilage*; An, Y. H., Martin, K. L., Eds.; Humana Press: Totowa, NJ, 2003.

(5) Venn, M.; Maroudas, A. Chemical composition and swelling of normal and osteoarthrotic femoral head cartilage. I. Chemical composition. *Ann. Rheum. Dis.* **1977**, *36* (2), 121–129 DOI: 10.1136/ard.36.2.121.

(6) Poole, C. A.; Flint, M. H.; Beaumont, B. W. Chondrons in cartilage: ultrastructural analysis of the pericellular microenvironment in adult human articular cartilages. *J. Orthop. Res.* **1987**, *5* (4), 509–522 DOI: 10.1002/jor.1100050406.

(7) Hunziker, E. B.; Michel, M.; Studer, D. Ultrastructure of adult human articular cartilage matrix after cryotechnical processing. *Microsc. Res. Tech.* **1997**, *37* (4), 271–284 DOI: 10.1002/(SICI)1097-0029(19970515)37:4<271::AID-JEMT3>3.0.CO;2-O.

(8) Wilusz, R. E.; Sanchez-Adams, J.; Guilak, F. The structure and function of the pericellular matrix of articular cartilage. *Matrix Biol.* **2014**, *39*, 25–32 DOI: 10.1016/j.matbio.2014.08.009.

(9) Deshmukh, K.; Nimni, M. E. Isolation and characterization of cyanogen bromide peptides from the collagen of bovine articular cartilage. *Biochem. J.* **1973**, *133* (4), 615–622.

(10) Clark, J. M. The organisation of collagen fibrils in the superficial zones of articular cartilage. *J. Anat.* **1990**, *171*, 117–130.

(11) Watanabe, H.; Yamada, Y.; Kimata, K. Roles of Aggrecan, a Large Chondroitin Sulfate Proteoglycan, in Cartilage Structure and Function. *J. Biochem.* **1998**, *124* (4), 687–693 DOI: 10.1093/oxfordjournals.jbchem.a022166.

(12) Roughley, P. J.; Lee, E. R. Cartilage proteoglycans: structure and potential functions. *Microsc. Res. Tech.* **1994**, *28* (5), 385–397 DOI: 10.1002/jemt.1070280505.

(13) Gattazzo, F.; Urciuolo, A.; Bonaldo, P. ECM: A dynamic microenvironment for stem cell niche. *Biochim. Biophys. Acta* **2014**, *1840* (8), 2506–2519 DOI: 10.1016/j.bbagen.2014.01.010.

(14) Frantz, C.; Stewart, K. M.; Weaver, V. M. The ECM at a glance. *J. Cell Sci.* **2010**, *123* (Pt 24), 4195–4200 DOI: 10.1242/jcs.023820.

(15) Hynes, R. O. The ECM: not just pretty fibrils. *Science* **2009**, *326* (5957), 1216–1219 DOI: 10.1126/science.1176009.

(16) Woods, V. L.; Schreck, P. J.; Gesink, D. S.; Pacheco, H. O.; Amiel, D.; Akeson, W. H.; Lotz, M. Integrin expression by human articular chondrocytes. *Arthritis Rheum.* **1994**, *37* (4), 537–544 DOI: 10.1002/art.1780370414.

(17) Chow, G.; Knudson, C. B.; Homandberg, G.; Knudson, W. Increased expression of CD44 in bovine articular chondrocytes by catabolic cellular mediators. *J. Biol. Chem.* **1995**, *270* (46), 27734–27741.

(18) Knudson, W.; Aguiar, D. J.; Hua, Q.; Knudson, C. B. CD44-anchored hyaluronan-rich pericellular matrices: an ultrastructural and biochemical analysis. *Exp. Cell Res.* **1996**, *228* (2), 216–228 DOI: 10.1006/excr.1996.0320.

(19) Underhill, C. CD44: the hyaluronan receptor. *J. Cell Sci.* **1992**, *103 (Pt 2*, 293–298.

(20) Knudson, C. B.; Knudson, W. Hyaluronan-binding proteins in development, tissue homeostasis, and disease. *FASEB J.* **1993**, *7* (13), 1233–1241.

(21) Lee, G. M.; Johnstone, B.; Jacobson, K.; Caterson, B. The dynamic structure of the pericellular matrix on living cells. *J. Cell Biol.* **1993**, *123* (6 Pt 2), 1899–1907.

(22) Jiang, H.; Peterson, R. S.; Wang, W.; Bartnik, E.; Knudson, C. B.; Knudson, W. A requirement for the CD44 cytoplasmic domain for hyaluronan binding, pericellular matrix assembly, and receptor-mediated endocytosis in COS-7 cells. *J. Biol. Chem.* **2002**, *277* (12), 10531–10538 DOI: 10.1074/jbc.M108654200.

(23) Knudson, W.; Knudson, C. B. Assembly of a chondrocyte-like pericellular matrix on non-chondrogenic cells. Role of the cell surface hyaluronan receptors in the assembly of a pericellular matrix. *J. Cell Sci.* **1991**, *99 (Pt 2)*, 227–235.

(24) Loeser, R. F. Integrin-mediated attachment of articular chondrocytes to ECM proteins. *Arthritis Rheum.* **1993**, *36* (8), 1103–1110.

(25) Shakibaei, M. Inhibition of chondrogenesis by integrin antibody in vitro. *Exp. Cell Res.* **1998**, *240* (1), 95–106 DOI: 10.1006/excr.1998.3933.

(26) Yasuda, T.; Shimizu, K.; Nakagawa, Y.; Ishikawa, H.; Nishihara, H.; Nakamura, T. Possible involvement of RGD (Arg-Gly-Asp)-containing ECM proteins in rat growth plate chondrocyte differentiation in culture. *J. Bone Miner. Res.* **1996**, *11* (10), 1430–1437 DOI: 10.1002/jbmr.5650111009.

(27) Lawrence, R. C.; Felson, D. T.; Helmick, C. G.; Arnold, L. M.; Choi, H.; Deyo, R. A.; Gabriel, S.; Hirsch, R.; Hochberg, M. C.; Hunder, G. G.; et al. Estimates of the prevalence of arthritis and other rheumatic conditions in the United States. Part II. *Arthritis Rheum.* **2008**, *58* (1), 26–35 DOI: 10.1002/art.23176.

(28) Hunziker, E. B. Articular cartilage repair: basic science and clinical progress. A review of the current status and prospects. *Cartilage* **2002**, *10* (6), 432–463 DOI: 10.1053/joca.2002.0801.

(29) Shannon, F.; Devitt, a.; Poynton, a.; Fitzpatrick, P.; Walsh, M. Short-term benefit of arthroscopic washout in degenerative arthritis of the knee. *Int. Orthop.* **2001**, *25* (4), 242–245 DOI: 10.1007/s002640000212.

(30) Lewis, P. B.; McCarty, L. P.; Kang, R. W.; Cole, B. J. Basic science and treatment options for articular cartilage injuries. *J. Orthop. Sports Phys. Ther.* **2006**, *36* (10), 717–727 DOI: 10.2519/jospt.2006.2175.

(31) Bhosale, A. M.; Richardson, J. B. Articular cartilage : structure , injuries and review of management. **2008**, 77–95 DOI: 10.1093/bmb/ldn025.

(32) Gobbi, A.; Karnatzikos, G.; Kumar, A. Long-term results after microfracture treatment for full-thickness knee chondral lesions in athletes. *Knee Surg. Sports Traumatol. Arthrosc.* **2014**, *22* (9), 1986–1996 DOI: 10.1007/s00167-013-2676-8.

(33) Görtz, S.; Bugbee, W. D. Allografts in articular cartilage repair. *Instr. Course Lect.* **2007**, *56*, 469–480.

(34) Boscainos, P. J.; Gross, A. E.; Kellett, C. F. articular defects of the knee. *4* (416), 1–13.

(35) Brittberg, M.; Lindahl, A.; Nilsson, A.; Ohlsson, C.; Isaksson, O.; Peterson, L. Treatment of Deep Cartilage Defects in the Knee with Autologous Chondrocyte Transplantation. *N. Engl. J. Med.* **1994**, *331* (14), 889–895 DOI: 10.1056/NEJM199410063311401.

(36) Dehne, T.; Karlsson, C.; Ringe, J.; Sittinger, M.; Lindahl, A. Chondrogenic differentiation potential of osteoarthritic chondrocytes and their possible use in matrix-associated autologous chondrocyte transplantation. *Arthritis Res. Ther.* **2009**, *11* (5), R133 DOI: 10.1186/ar2800.

(37) Tuan, R. S. A second-generation autologous chondrocyte implantation approach to the treatment of focal articular cartilage defects. *Arthritis Res. Ther.* **2007**, *9* (5), 109 DOI: 10.1186/ar2310.

(38) Vavken, P.; Samartzis, D. Effectiveness of autologous chondrocyte implantation in cartilage repair of the knee: a systematic review of controlled trials. *Cartilage* **2010**, *18* (6), 857–863 DOI: 10.1016/j.joca.2010.03.005.

(39) Bartlett, W. Autologous chondrocyte implantation at the knee using a bilayer collagen membrane with bone graft: A PRELIMINARY REPORT. *J. Bone Jt. Surg. - Br. Vol.* **2005**, *87-B* (3), 330–332 DOI: 10.1302/0301-620X.87B3.15552.

(40) Kon, E.; Filardo, G.; Matteo, B. Di; Perdisa, F.; Marcacci, M. Matrix assisted autologous chondrocyte transplantation for cartilage treatment A SYSTEMATIC REVIEW. **2013**, *2* (2), 18–25.

(41) Kon, E.; Filardo, G.; Condello, V.; Collarile, M.; Di Martino, A.; Zorzi, C.; Marcacci, M. Second-generation autologous chondrocyte implantation: results in patients older than 40 years. *Am. J. Sports Med.* **2011**, *39* (8), 1668–1675 DOI: 10.1177/0363546511404675.

(42) Iwasa, J.; Engebretsen, L.; Shima, Y.; Ochi, M. Clinical application of scaffolds for cartilage tissue engineering. *Knee Surgery, Sport. Traumatol. Arthrosc.* **2008**, *17* (6), 561–577 DOI: 10.1007/s00167-008-0663-2.

(43) Gigante, A.; Bevilacqua, C.; Ricevuto, A.; Mattioli-Belmonte, M.; Greco, F. Membrane-seeded autologous chondrocytes: cell viability and characterization at surgery. *Knee Surg. Sports Traumatol. Arthrosc.* **2007**, *15* (1), 88–92 DOI: 10.1007/s00167-006-0115-9.

(44) Memon, a R.; Quinlan, J. F. Surgical treatment of articular cartilage defects in the knee: are we winning? *Adv. Orthop.* **2012**, *2012*, 528423 DOI: 10.1155/2012/528423.

(45) Bartlett, W.; Skinner, J. a; Gooding, C. R.; Carrington, R. W. J.; Flanagan, a M.; Briggs, T. W. R.; Bentley, G. Autologous chondrocyte implantation versus matrix-induced autologous chondrocyte implantation for osteochondral defects of the knee: a prospective, randomised study. *J. Bone Joint Surg. Br.* **2005**, *87* (5), 640–645 DOI: 10.1302/0301-620X.87B5.15905.

(46) Schulze-Tanzil, G. Activation and dedifferentiation of chondrocytes: Implications in cartilage injury and repair. *Ann. Anat. - Anat. Anzeiger* **2009**, *191* (4), 325–338 DOI: 10.1016/j.aanat.2009.05.003.

(47) Ma, Z.; Ph, D.; Kotaki, M.; Inai, R. Potential of Nanofiber Matrix as Tissue-Engineering Scaffolds. **2005**, *11* (1).

(48) Kim, S. H.; Park, D. Y.; Min, B.-H. A new era of cartilage repair using cell therapy and tissue engineering: turning current clinical limitations into new ideas. *Tissue Eng. Regen. Med.* **2012**, *9* (5), 240–248 DOI: 10.1007/s13770-012-0370-4.

(49) Chung, C.; Burdick, J. A. Engineering cartilage tissue. *Adv. Drug Deliv. Rev.* **2008**, *60* (2), 243–262 DOI: 10.1016/j.addr.2007.08.027.

(50) Makris, E. a; Gomoll, A. H.; Malizos, K. N.; Hu, J. C.; Athanasiou, K. a. Repair and tissue engineering techniques for articular cartilage. *Nat. Rev. Rheumatol.* **2014** DOI: 10.1038/nrrheum.2014.157.

(51) Zhao, W.; Jin, X.; Cong, Y.; Liu, Y.; Fu, J. Degradable natural polymer hydrogels for articular cartilage tissue engineering. *J. Chem. Technol. Biotechnol.* **2013**, *88* (3), 327–339 DOI: 10.1002/jctb.3970.

(52) Mauck, R. L.; Soltz, M. A.; Wang, C. C. B.; Wong, D. D.; Chao, P. G.; Ateshian, G. A. Functional Tissue Engineering of Articular Cartilage Through Dynamic Loading of. **2015**, *122* (June 2000).

(53) Chahine, N. O.; Albro, M. B.; Lima, E. G.; Wei, V. I.; Dubois, C. R.; Hung, C. T.; Ateshian, G. a. Effect of dynamic loading on the transport of solutes into agarose hydrogels. *Biophys. J.* **2009**, *97* (4), 968–975 DOI: 10.1016/j.bpj.2009.05.047.

(54) Grogan, S. P.; Ph, D.; Sovani, S.; Pauli, C.; Chen, J.; Hartmann, A.; Colwell, C. W.; Lotz, M. K.; Lima, D. D. D. Effects of Perfusion and Dynamic Loading on Human Neocartilage Formation in Alginate Hydrogels. **2012**, *18*, 1784–1792 DOI: 10.1089/ten.tea.2011.0506.

(55) Henrionnet, C.; Wang, Y.; Roeder, E.; Gambier, N.; Galois, L.; Mainard, D.; Bensoussan, D.; Gillet, P.; Pinzano, A. Effect of dynamic loading on MSCs chondrogenic differentiation in 3-D alginate culture. *Biomed. Mater. Eng.* **2012**, *22* (4), 209–218 DOI: 10.3233/BME-2012-0710.

(56) Kuo, C. K.; Ma, P. X. Ionically crosslinked alginate hydrogels as sca ! olds for tissue engineering : Part 1 . Structure , gelation rate and mechanical properties. **2001**, *22*, 511–521.

(57) Jeon, O.; Bouhadir, K. H.; Mansour, J. M.; Alsberg, E. Photocrosslinked alginate hydrogels with tunable biodegradation rates and mechanical properties. *Biomaterials* **2009**, *30* (14), 2724–2734 DOI: 10.1016/j.biomaterials.2009.01.034.

(58) Parenteau-Bareil, R.; Gauvin, R.; Berthod, F. Collagen-Based Biomaterials for Tissue Engineering Applications. *Materials (Basel).* **2010**, *3* (3), 1863–1887 DOI: 10.3390/ma3031863.

(59) Alder, D. Polymer Chemistry cartilage tissue engineering formed by integrating. **2014**, 1082–1090 DOI: 10.1039/c3py00869j.

(60) Grigolo, B.; Lisignoli, G.; Piacentini, A.; Fiorini, M.; Gobbi, P.; Mazzotti, G.; Duca, M.; Pavesio, A.; Facchini, A. Evidence for redifferentiation of human chondrocytes grown on a hyaluronan-based biomaterial (HYAFF s 11): molecular , immunohistochemical and ultrastructural analysis. **2002**, *23*, 1187–1195.

(61) Jayakumar, R.; Prabaharan, M.; Nair, S. V; Tamura, H. Novel chitin and chitosan nanofibers in biomedical applications. *Biotechnol. Adv.* **2010**, *28* (1), 142–150 DOI: 10.1016/j.biotechadv.2009.11.001.

(62) Gunatillake, P. A.; Adhikari, R. Biodegradable synthetic polymers for tissue engineering. **2003**, *5*, 1–16.

(63) Kim, B.-S.; Mooney, D. J. Development of biocompatible synthetic extracellular matrices for tissue engineering. *Trends Biotechnol.* **1998**, *16* (5), 224–230 DOI: 10.1016/S0167-7799(98)01191-3.

(64) Middleton, J. C.; Tipton, A. J. Synthetic biodegradable polymers as orthopedic devices. **2000**, *21*.

(65) Maher, S. A.; Ph, D.; Lowman, A. M. Hydrogels for the Repair of Articular Cartilage Defects. **2011**, *17* (4) DOI: 10.1089/ten.teb.2011.0077.

(66) Ameer, G. A.; Mahmood, T. A.; Langer, R. A biodegradable composite scaffold for cell transplantation. **2002**, *20*, 16–19.

(67) Yoo, H. S.; Lee, E. A.; Yoon, J. J.; Park, T. G. Hyaluronic acid modified biodegradable scaffolds for cartilage tissue engineering. *Biomaterials* **2005**, *26* (14), 1925–1933 DOI: 10.1016/j.biomaterials.2004.06.021.

(68) Blunk, T.; Sieminski, A. Differential effects of growth factors on tissue-engineered cartilage. *Tissue …* **2002**, *8* (1).

(69) Van der Kraan, P.; Vitters, E.; van den Berg, W. Differential effect of transforming growth factor beta on freshly isolated and cultured articular chondrocytes. *J. Rheumatol.* **1992**, *19* (1), 140–145.

(70) Shen, H.; Hu, X.; Bei, J.; Wang, S. The immobilization of basic fibroblast growth factor on plasma-treated poly(lactide-co-glycolide). *Biomaterials* **2008**, *29* (15), 2388–2399 DOI: 10.1016/j.biomaterials.2008.02.008.

(71) Cabanas-dan, J. Chemical strategies for the presentation and. **2014**, 2381–2394 DOI: 10.1039/c3tb20853b.

(72) Lee, K.; Silva, E. A.; Mooney, D. J. Growth factor delivery-based tissue engineering : general approaches and a review of recent developments. **2011**, No. August 2010, 153–170.

(73) Hartgerink, J. D.; Beniash, E.; Stupp, S. I. Self-assembly and mineralization of peptide-amphiphile nanofibers. *Science* **2001**, *294* (5547), 1684–1688 DOI: 10.1126/science.1063187.

(74) Shah, R. N.; Shah, N. A.; Del, M. M.; Lim, R.; Hsieh, C.; Nuber, G.; Stupp, S. I. Supramolecular design of self-assembling nanofibers for cartilage regeneration. **2009** DOI: 10.1073/pnas.0906501107.

(75) Bian, L.; Guvendiren, M.; Mauck, R. L.; Burdick, J. a. Hydrogels that mimic developmentally relevant matrix and N-cadherin interactions enhance MSC chondrogenesis. *Proc. Natl. Acad. Sci. U. S. A.* **2013**, *110* (25), 10117–10122 DOI: 10.1073/pnas.1214100110.

(76) Dunkelman, N. S.; Zimber, M. P.; Lebaron, R. G.; Pavelec, R.; Kwan, M.; Purchio, A. F. Cartilage production by rabbit articular chondrocytes on polyglycolic acid scaffolds in a closed bioreactor system. *Biotechnol. Bioeng.* **1995**, *46* (4), 299–305 DOI: 10.1002/bit.260460402.

(77) Vunjak-Novakovic, G.; Martin, I.; Obradovic, B.; Treppo, S.; Grodzinsky, A. J.; Langer, R.; Freed, L. E. Bioreactor cultivation conditions modulate the composition and mechanical properties of tissue-engineered cartilage. *J. Orthop. Res.* **1999**, *17* (1), 130–138 DOI: 10.1002/jor.1100170119.

(78) Mabvuure, N.; Hindocha, S.; Khan, W. S. The role of bioreactors in cartilage tissue engineering. *Curr. Stem Cell Res. Ther.* **2012**, *7* (4), 287–292.

(79) Mauck, R. L.; Nicoll, S. B.; Seyhan, S. L.; Ateshian, G. A.; Hung, C. T. Synergistic action of growth factors and dynamic loading for articular cartilage tissue engineering. *Tissue Eng.* **2003**, *9* (4), 597–611 DOI: 10.1089/107632703768247304.

(80) Athanasiou, K. A.; Darling, E. M.; Hu, J. C.; DuRaine, G. D.; Reddi, A. H. *Articular Cartilage*; CRC Press, 2013.

(81) Elder, B. D.; Athanasiou, K. A. Hydrostatic pressure in articular cartilage tissue engineering: from chondrocytes to tissue regeneration. *Tissue Eng. Part B. Rev.* **2009**, *15* (1), 43–53 DOI: 10.1089/ten.teb.2008.0435.

(82) Hunziker, E. B. Articular cartilage repair: basic science and clinical progress. A review of the current status and prospects. *Cartilage* **2002**, *10* (6), 432–463 DOI: 10.1053/joca.2002.0801.

(83) Athanasiou, K. a. *Articular Cartilage Tissue Engineering*.

(84) Knudson, C. B.; Knudson, W. Cartilage proteoglycans. *Semin. Cell Dev. Biol.* **2001**, *12* (2), 69–78 DOI: 10.1006/scdb.2000.0243.

(85) Hileman, R. E.; Fromm, J. R.; Weiler, J. M.; Linhardt, R. J. interactions : definition of consensus sites in glycosaminoglycan binding proteins. **1998**, 156–167.

(86) Kuschert, G. S.; Coulin, F.; Power, C. a; Proudfoot, a E.; Hubbard, R. E.; Hoogewerf, a J.; Wells, T. N. Glycosaminoglycans interact selectively with chemokines and modulate receptor binding and cellular responses. *Biochemistry* **1999**, *38* (39), 12959–12968.

(87) Jiao, X.; Billings, P. C.; O'Connell, M. P.; Kaplan, F. S.; Shore, E. M.; Glaser, D. L. Heparan sulfate proteoglycans (HSPGs) modulate BMP2 osteogenic bioactivity in C2C12 cells. *J. Biol. Chem.* **2007**, *282* (2), 1080–1086 DOI: 10.1074/jbc.M513414200.

(88) Rodgers, K. D.; San Antonio, J. D.; Jacenko, O. Heparan sulfate proteoglycans: a GAGgle of skeletal-hematopoietic regulators. *Dev. Dyn.* **2008**, *237* (10), 2622–2642 DOI: 10.1002/dvdy.21593.

(89) Kirn-Safran, C. B.; Gomes, R. R.; Brown, A. J.; Carson, D. D. Heparan sulfate proteoglycans: coordinators of multiple signaling pathways during chondrogenesis. *Birth Defects Res. C. Embryo Today* **2004**, *72* (1), 69–88 DOI: 10.1002/bdrc.20005.

(90) Fisher, M. C.; Li, Y.; Seghatoleslami, M. R.; Dealy, C. N.; Kosher, R. a. Heparan sulfate proteoglycans including syndecan-3 modulate BMP activity during limb cartilage differentiation. *Matrix Biol.* **2006**, *25* (1), 27–39 DOI: 10.1016/j.matbio.2005.07.008.

(91) French, M. M.; Smith, S. E.; Akanbi, K.; Sanford, T.; Hecht, J.; Farach-Carson, M. C.; Carson, D. D. Expression of the heparan sulfate proteoglycan, perlecan, during mouse embryogenesis and perlecan chondrogenic activity in vitro. *J. Cell Biol.* **1999**, *145* (5), 1103–1115.

(92) Roughley, P. J. The structure and function of cartilage proteoglycans. *Eur. Cell. Mater.* **2006**, *12*, 92–101.

(93) Iozzo, R. V; Cohen, I. R.; Grässel, S.; Murdoch, a D. The biology of perlecan: the multifaceted heparan sulphate proteoglycan of basement membranes and pericellular matrices. *Biochem. J.* **1994**, *302 (Pt 3*, 625–639.

(94) Yang, W. D.; Gomes, R. R.; Alicknavitch, M.; Farach-Carson, M. C.; Carson, D. D. Perlecan domain I promotes fibroblast growth factor 2 delivery in collagen I fibril scaffolds. *Tissue Eng.* **2005**, *11* (1-2), 76–89 DOI: 10.1089/ten.2005.11.76.

(95) Costell, M.; Gustafsson, E.; Aszódi, a; Mörgelin, M.; Bloch, W.; Hunziker, E.; Addicks, K.; Timpl, R.; Fässler, R. Perlecan maintains the integrity of cartilage and some basement membranes. *J. Cell Biol.* **1999**, *147* (5), 1109–1122.

(96) French, M. M.; Gomes, R. R.; Timpl, R.; Höök, M.; Czymmek, K.; Farach-Carson, M. C.; Carson, D. D. Chondrogenic activity of the heparan sulfate proteoglycan perlecan maps to the N-terminal domain I. *Journal of bone and mineral research : the official journal of the American Society for Bone and Mineral Research*. January 2002, pp 48–55.

(97) Hassell, J.; Yamada, Y.; Arikawa-Hirasawa, E. Role of perlecan in skeletal development and diseases. *Glycoconj. J.* **2003**, *19* (4-5), 263–267 DOI: 10.1023/A:1025340215261.

(98) Melrose, J.; Hayes, A. J.; Whitelock, J. M.; Little, C. B. Perlecan, the "jack of all trades" proteoglycan of cartilaginous weight-bearing connective tissues. *Bioessays* **2008**, *30* (5), 457–469 DOI: 10.1002/bies.20748.

(99) Maroudas, A.; Muir, H.; Wingham, J. The correlation of fixed negative charge with glycosaminoglycan content of human articular cartilage. *Biochim. Biophys. Acta* **1969**, *177* (3), 492–500.

(100) Ghosh, S.; Laha, M.; Mondal, S.; Sengupta, S.; Kaplan, D. L. In vitro model of mesenchymal condensation during chondrogenic development. *Biomaterials* **2009**, *30* (33), 6530–6540 DOI: 10.1016/j.biomaterials.2009.08.019.

(101) Varghese, S.; Hwang, N. S.; Canver, A. C.; Theprungsirikul, P.; Lin, D. W.; Elisseeff, J. Chondroitin sulfate based niches for chondrogenic differentiation of mesenchymal stem cells. *Matrix Biol.* **2008**, *27* (1), 12–21 DOI: 10.1016/j.matbio.2007.07.002.

(102) Ghone, N. V; Grayson, W. L. Recapitulation of mesenchymal condensation enhances in vitro chondrogenesis of human mesenchymal stem cells. *J. Cell. Physiol.* **2012**, No. February, 1–29 DOI: 10.1002/jcp.24078.

(103) Niece, K. L.; Hartgerink, J. D.; Donners, J. J. J. M.; Stupp, S. I. Self-assembly combining two bioactive peptide-amphiphile molecules into nanofibers by electrostatic attraction. *J. Am. Chem. Soc.* **2003**, *125* (24), 7146–7147 DOI: 10.1021/ja028215r.

(104) Mammadov, R.; Tekinay, A. B.; Dana, A.; Guler, M. O. Microscopic characterization of peptide nanostructures. *Micron* **2012**, *43* (2-3), 69–84 DOI: 10.1016/j.micron.2011.07.006.

(105) Holmes, T. C.; de Lacalle, S.; Su, X.; Liu, G.; Rich, a; Zhang, S. Extensive neurite outgrowth and active synapse formation on self-assembling peptide scaffolds. *Proc. Natl. Acad. Sci. U. S. A.* **2000**, *97* (12), 6728–6733.

(106) Silva, G. a; Czeisler, C.; Niece, K. L.; Beniash, E.; Harrington, D. a; Kessler, J. a; Stupp, S. I. Selective differentiation of neural progenitor cells by high-epitope density nanofibers. *Science* **2004**, *303* (5662), 1352–1355 DOI: 10.1126/science.1093783.

(107) Ceylan, H.; Tekinay, A. B.; Guler, M. O. Selective adhesion and growth of vascular endothelial cells on bioactive peptide nanofiber functionalized stainless steel surface. *Biomaterials* **2011**, *32* (34), 8797–8805 DOI: 10.1016/j.biomaterials.2011.08.018.

(108) Storrie, H.; Guler, M. O.; Abu-Amara, S. N.; Volberg, T.; Rao, M.; Geiger, B.; Stupp, S. I. Supramolecular crafting of cell adhesion. *Biomaterials* **2007**, *28* (31), 4608–4618 DOI: 10.1016/j.biomaterials.2007.06.026.

(109) Shukunami, C.; Shigeno, C.; Atsumi, T.; Ishizeki, K.; Suzuki, F.; Hiraki, Y. Chondrogenic differentiation of clonal mouse embryonic cell line ATDC5 in vitro: differentiation-dependent gene expression of parathyroid hormone (PTH)/PTH-related peptide receptor. *J. Cell Biol.* **1996**, *133* (2), 457–468.

(110) Hall, B. K.; Miyake, T. All for one and one for all: condensations and the initiation of skeletal development. *Bioessays* **2000**, *22* (2), 138–147 DOI: 10.1002/(SICI)1521-1878(200002)22:2<138::AID-BIES5>3.0.CO;2-4.

(111) Goldring, M. B.; Tsuchimochi, K.; Ijiri, K. The control of chondrogenesis. *J. Cell. Biochem.* **2006**, *97* (1), 33–44 DOI: 10.1002/jcb.20652.

(112) Mammadov, R.; Mammadov, B.; Toksoz, S.; Aydin, B.; Yagci, R.; Tekinay, A. B.; Guler, M. O. Heparin mimetic peptide nanofibers promote angiogenesis. *Biomacromolecules* **2011**, *12* (10), 3508–3519 DOI: 10.1021/bm200957s.

(113) Mammadov, B.; Mammadov, R.; Guler, M. O.; Tekinay, A. B. Cooperative effect of heparan sulfate and laminin mimetic peptide nanofibers on the promotion of neurite outgrowth. *Acta Biomater.* **2012**, *8* (6), 2077–2086 DOI: 10.1016/j.actbio.2012.02.006.

(114) Mammadov, R.; Mammadov, B.; Guler, M. O.; Tekinay, A. B. Growth factor binding on heparin mimetic peptide nanofibers. *Biomacromolecules* **2012** DOI: 10.1021/bm3010897.

(115) Atsumi, T.; Miwa, Y.; Kimata, K.; Ikawa, Y. A chondrogenic cell line derived from a differentiating culture of AT805 teratocarcinoma cells. *Cell Differ. Dev. Off. J. Int. Soc. Dev. Biol.* **1990**, *30* (2), 109–116.

(116) Barna, M.; Niswander, L. Visualization of cartilage formation: insight into cellular properties of skeletal progenitors and chondrodysplasia syndromes. *Dev. Cell* **2007**, *12* (6), 931–941 DOI: 10.1016/j.devcel.2007.04.016.

(117) DeLise, a M.; Fischer, L.; Tuan, R. S. Cellular interactions and signaling in cartilage development. *Cartilage* **2000**, *8* (5), 309–334 DOI: 10.1053/joca.1999.0306.

(118) Barry, F. P. Biology and clinical applications of mesenchymal stem cells. *Birth Defects Res. C. Embryo Today* **2003**, *69* (3), 250–256 DOI: 10.1002/bdrc.10021.

(119) Barry, F. P.; Murphy, J. M. Mesenchymal stem cells: clinical applications and biological characterization. *Int. J. Biochem. Cell Biol.* **2004**, *36* (4), 568–584 DOI: 10.1016/j.biocel.2003.11.001.

(120) Diao, H.; Wang, J.; Shen, C.; Xia, S.; Guo, T.; Dong, L.; Zhang, C.; Chen, J.; Zhao, J.; Zhang, J. Improved cartilage regeneration utilizing mesenchymal stem cells in TGF-beta1 gene-activated scaffolds. *Tissue Eng. Part A* **2009**, *15* (9), 2687–2698 DOI: 10.1089/ten.TEA.2008.0621.

(121) Manning, C. N.; Schwartz, A. G.; Liu, W.; Xie, J.; Havlioglu, N.; Sakiyama-Elbert, S. E.; Silva, M. J.; Xia, Y.; Gelberman, R. H.; Thomopoulos, S. Controlled delivery of mesenchymal stem cells and growth factors using a nanofiber scaffold for tendon repair. *Acta Biomater.* **2013**, *9* (6), 6905–6914 DOI: 10.1016/j.actbio.2013.02.008.

(122) Mohan, N.; Nair, P. D.; Tabata, Y. Growth factor-mediated effects on chondrogenic differentiation of mesenchymal stem cells in 3D semi-IPN poly(vinyl alcohol)-poly(caprolactone) scaffolds. *J. Biomed. Mater. Res. A* **2010**, *94* (1), 146–159 DOI: 10.1002/jbm.a.32680.

(123) Sundelacruz, S.; Kaplan, D. L. Stem cell- and scaffold-based tissue engineering approaches to osteochondral regenerative medicine. *Semin. Cell Dev. Biol.* **2009**, *20* (6), 646–655 DOI: 10.1016/j.semcdb.2009.03.017.

(124) Danišovič, L.; Varga, I.; Polák, S. Growth factors and chondrogenic differentiation of mesenchymal stem cells. *Tissue Cell* **2012**, *44* (2), 69–73 DOI: 10.1016/j.tice.2011.11.005.

(125) Alberti, K.; Davey, R. E.; Onishi, K.; George, S.; Salchert, K.; Seib, F. P.; Bornhäuser, M.; Pompe, T.; Nagy, A.; Werner, C.; et al. Functional immobilization of signaling proteins enables control of stem cell fate. *Nat. Methods* **2008**, *5* (7), 645–650 DOI: 10.1038/nmeth.1222.

(126) Mann, B. K.; Schmedlen, R. H.; West, J. L. Tethered-TGF-beta increases extracellular matrix production of vascular smooth muscle cells. *Biomaterials* **2001**, *22* (5), 439–444.

(127) Richardson, T. P.; Peters, M. C.; Ennett, A. B.; Mooney, D. J. Polymeric system for dual growth factor delivery. *Nat. Biotechnol.* **2001**, *19* (11), 1029–1034 DOI: 10.1038/nbt1101-1029.

(128) Sohier, J.; Vlugt, T. J. H.; Cabrol, N.; Van Blitterswijk, C.; de Groot, K.; Bezemer, J. M. Dual release of proteins from porous polymeric scaffolds. *J. Control. Release* **2006**, *111* (1-2), 95–106 DOI: 10.1016/j.jconrel.2005.11.016.

(129) Bowen-Pope, D. F.; Malpass, T. W.; Foster, D. M.; Ross, R. Platelet-derived growth factor in vivo: levels, activity, and rate of clearance. *Blood* **1984**, *64* (2), 458–469.

(130) Naldini, L.; Vigna, E.; Narsimhan, R. P.; Gaudino, G.; Zarnegar, R.; Michalopoulos, G. K.; Comoglio, P. M. Hepatocyte growth factor (HGF) stimulates the tyrosine kinase activity of the receptor encoded by the proto-oncogene c-MET. *Oncogene* **1991**, *6* (4), 501–504.

(131) Poynton, A. R.; Lane, J. M. Safety profile for the clinical use of bone morphogenetic proteins in the spine. *Spine (Phila. Pa. 1976).* **2002**, *27* (16 Suppl 1), S40–S48.

(132) Lee, K.; Silva, E. A.; Mooney, D. J. Growth factor delivery-based tissue engineering: general approaches and a review of recent developments. *J. R. Soc. Interface* **2011**, *8* (55), 153–170 DOI: 10.1098/rsif.2010.0223.

(133) Park, H.; Temenoff, J. S.; Holland, T. A.; Tabata, Y.; Mikos, A. G. Delivery of TGF-beta1 and chondrocytes via injectable, biodegradable hydrogels for cartilage tissue engineering applications. *Biomaterials* **2005**, *26* (34), 7095–7103 DOI: 10.1016/j.biomaterials.2005.05.083.

(134) Ayerst, B. I.; Day, A. J.; Nurcombe, V.; Cool, S. M.; Merry, C. L. R. New strategies for cartilage regeneration exploiting selected glycosaminoglycans to enhance cell fate determination. *Biochem. Soc. Trans.* **2014**, *42* (3), 703–709 DOI: 10.1042/BST20140031.

(135) Chen, W.-C.; Yao, C.-L.; Chu, I.-M.; Wei, Y.-H. Compare the effects of chondrogenesis by culture of human mesenchymal stem cells with various

type of the chondroitin sulfate C. *J. Biosci. Bioeng.* **2011**, *111* (2), 226–231 DOI: 10.1016/j.jbiosc.2010.10.002.

(136) Goude, M. C.; McDevitt, T. C.; Temenoff, J. S. Chondroitin sulfate microparticles modulate transforming growth factor-β1-induced chondrogenesis of human mesenchymal stem cell spheroids. *Cells. Tissues. Organs* **2014**, *199* (2-3), 117–130 DOI: 10.1159/000365966.

(137) Guo, Y.; Yuan, T.; Xiao, Z.; Tang, P.; Xiao, Y.; Fan, Y.; Zhang, X. Hydrogels of collagen/chondroitin sulfate/hyaluronan interpenetrating polymer network for cartilage tissue engineering. *J. Mater. Sci. Mater. Med.* **2012**, *23* (9), 2267–2279 DOI: 10.1007/s10856-012-4684-5.

(138) DeAngelis, P. L. Glycosaminoglycan polysaccharide biosynthesis and production: today and tomorrow. *Appl. Microbiol. Biotechnol.* **2012**, *94* (2), 295–305 DOI: 10.1007/s00253-011-3801-6.

(139) Ikeda, Y.; Charef, S.; Ouidja, M.-O.; Barbier-Chassefière, V.; Sineriz, F.; Duchesnay, A.; Narasimprakash, H.; Martelly, I.; Kern, P.; Barritault, D.; et al. Synthesis and biological activities of a library of glycosaminoglycans mimetic oligosaccharides. *Biomaterials* **2011**, *32* (3), 769–776 DOI: 10.1016/j.biomaterials.2010.09.043.

(140) Kwon, H. J.; Yasuda, K. Chondrogenesis on sulfonate-coated hydrogels is regulated by their mechanical properties. *J. Mech. Behav. Biomed. Mater.* **2013**, *17*, 337–346 DOI: 10.1016/j.jmbbm.2012.10.006.

(141) Cui, H.; Webber, M. J.; Stupp, S. I. Self-assembly of peptide amphiphiles: From molecules to nanostructures to biomaterials. *Biopolymers* **2010**, *94* (1), 1–18 DOI: 10.1002/bip.21328.

(142) Paramonov, S. E.; Jun, H.; Hartgerink, J. D. Self-Assembly of Peptide - Amphiphile Nanofibers : The Roles of Hydrogen Bonding and Amphiphilic Packing. **2006**, No. 11, 7291–7298.

(143) Hartgerink, J. D.; Beniash, E.; Stupp, S. I. Self-assembly and mineralization of peptide-amphiphile nanofibers. *Science* **2001**, *294* (5547), 1684–1688 DOI: 10.1126/science.1063187.

(144) Cooper, G. M. Cell Proliferation in Development and Differentiation. Sinauer Associates 2000.

(145) Pevsner-Fischer, M.; Levin, S.; Zipori, D. The origins of mesenchymal stromal cell heterogeneity. *Stem Cell Rev.* **2011**, *7* (3), 560–568 DOI: 10.1007/s12015-011-9229-7.

(146) Chen, W.-C.; Wei, Y.-H.; Chu, I.-M.; Yao, C.-L. Effect of chondroitin sulphate C on the in vitro and in vivo chondrogenesis of mesenchymal stem cells in crosslinked type II collagen scaffolds. *J. Tissue Eng. Regen. Med.* **2013**, *7* (8), 665–672 DOI: 10.1002/term.1463.

(147) Goldring, M. B.; Tsuchimochi, K.; Ijiri, K. The control of chondrogenesis. *J. Cell. Biochem.* **2006**, *97* (1), 33–44 DOI: 10.1002/jcb.20652.

(148) Lee, J. W.; Kim, Y. H.; Kim, S.-H.; Han, S. H.; Hahn, S. B. Chondrogenic differentiation of mesenchymal stem cells and its clinical applications. *Yonsei Med. J.* **2004**, *45 Suppl*, 41–47.

(149) Storrie, H.; Guler, M. O.; Abu-Amara, S. N.; Volberg, T.; Rao, M.; Geiger, B.; Stupp, S. I. Supramolecular crafting of cell adhesion. *Biomaterials* **2007**, *28* (31), 4608–4618 DOI: 10.1016/j.biomaterials.2007.06.026.

(150) Hortensius, R. A.; Harley, B. A. C. The use of bioinspired alterations in the glycosaminoglycan content of collagen-GAG scaffolds to regulate cell activity. *Biomaterials* **2013**, *34* (31), 7645–7652 DOI: 10.1016/j.biomaterials.2013.06.056.

(151) Lim, J. J.; Hammoudi, T. M.; Bratt-Leal, A. M.; Hamilton, S. K.; Kepple, K. L.; Bloodworth, N. C.; McDevitt, T. C.; Temenoff, J. S. Development of nano- and microscale chondroitin sulfate particles for controlled growth factor delivery. *Acta Biomater.* **2011**, *7* (3), 986–995 DOI: 10.1016/j.actbio.2010.10.009.

(152) Benoit, D. S. W.; Anseth, K. S. Heparin functionalized PEG gels that modulate protein adsorption for hMSC adhesion and differentiation. *Acta Biomater.* **2005**, *1* (4), 461–470 DOI: 10.1016/j.actbio.2005.03.002.

(153) Benoit, D. S. W.; Durney, A. R.; Anseth, K. S. The effect of heparin-functionalized PEG hydrogels on three-dimensional human mesenchymal stem cell osteogenic differentiation. *Biomaterials* **2007**, *28* (1), 66–77 DOI: 10.1016/j.biomaterials.2006.08.033.

(154) Kocabey, S.; Ceylan, H.; Tekinay, A. B.; Guler, M. O. Glycosaminoglycan mimetic peptide nanofibers promote mineralization by osteogenic cells. *Acta Biomater.* **2013**, *9* (11), 9075–9085 DOI: 10.1016/j.actbio.2013.07.007.

(155) Ustun, S.; Tombuloglu, A.; Kilinc, M.; Guler, M. O.; Tekinay, A. B. Growth and differentiation of prechondrogenic cells on bioactive self-assembled peptide nanofibers. *Biomacromolecules* **2013**, *14* (1), 17–26 DOI: 10.1021/bm301538k.

(156) Bhosale, A. M.; Richardson, J. B. Articular cartilage: structure, injuries and review of management. *Br. Med. Bull.* **2008**, *87*, 77–95 DOI: 10.1093/bmb/ldn025.

(157) Mithoefer, K.; Williams, R. J.; Warren, R. F.; Potter, H. G.; Spock, C. R.; Jones, E. C.; Wickiewicz, T. L.; Marx, R. G. The microfracture technique for the treatment of articular cartilage lesions in the knee. A prospective cohort study. *J. Bone Joint Surg. Am.* **2005**, *87* (9), 1911–1920 DOI: 10.2106/JBJS.D.02846.

(158) Mithoefer, K.; McAdams, T.; Williams, R. J.; Kreuz, P. C.; Mandelbaum, B. R. Clinical efficacy of the microfracture technique for articular cartilage repair in the knee: an evidence-based systematic analysis. *Am. J. Sports Med.* **2009**, *37* (10), 2053–2063 DOI: 10.1177/0363546508328414.

(159) Toh, W. S.; Lim, T. C.; Kurisawa, M.; Spector, M. Modulation of mesenchymal stem cell chondrogenesis in a tunable hyaluronic acid hydrogel microenvironment. *Biomaterials* **2012**, *33* (15), 3835–3845 DOI: 10.1016/j.biomaterials.2012.01.065.

(160) Kim, I. L.; Mauck, R. L.; Burdick, J. a. Hydrogel design for cartilage tissue engineering: A case study with hyaluronic acid. *Biomaterials* **2011**, *32* (34), 8771–8782 DOI: 10.1016/j.biomaterials.2011.08.073.

(161) Knudson, C. B. Hyaluronan and CD44: strategic players for cell-matrix interactions during chondrogenesis and matrix assembly. *Birth Defects Res. C. Embryo Today* **2003**, *69* (2), 174–196 DOI: 10.1002/bdrc.10013.

(162) Wu, S.-C.; Chen, C.-H.; Chang, J.-K.; Fu, Y.-C.; Wang, C.-K.; Eswaramoorthy, R.; Lin, Y.-S.; Wang, Y.-H.; Lin, S.-Y.; Wang, G.-J.; et al. Hyaluronan initiates chondrogenesis mainly via CD44 in human adipose-derived stem cells. *J. Appl. Physiol.* **2013**, *114* (11), 1610–1618 DOI: 10.1152/japplphysiol.01132.2012.

(163) Drury, J. L.; Mooney, D. J. Hydrogels for tissue engineering: scaffold design variables and applications. *Biomaterials* **2003**, *24* (24), 4337–4351 DOI: 10.1016/S0142-9612(03)00340-5.

(164) Lee, K. Y.; Mooney, D. J. Hydrogels for Tissue Engineering. *Chem. Rev.* **2001**, *101* (7), 1869–1880 DOI: 10.1021/cr000108x.

(165) Lutolf, M. P.; Hubbell, J. a. Synthetic biomaterials as instructive extracellular microenvironments for morphogenesis in tissue engineering. *Nat. Biotechnol.* **2005**, *23* (1), 47–55 DOI: 10.1038/nbt1055.

(166) Fakhari, a; Berkland, C. Applications and emerging trends of hyaluronic acid in tissue engineering, as a dermal filler and in treatment. *Acta Biomater.* **2013**, *9* (7), 7081–7092 DOI: 10.1016/j.actbio.2013.03.005.

(167) Weyers, A.; Linhardt, R. J. Neoproteoglycans in tissue engineering. *FEBS J.* **2013**, *280* (10), 2511–2522 DOI: 10.1111/febs.12187.

(168) Xu, X.-D.; Liang, L.; Cheng, H.; Wang, X.-H.; Jiang, F.-G.; Zhuo, R.-X.; Zhang, X.-Z. Construction of therapeutic glycopeptide hydrogel as a new substitute for antiproliferative drugs to inhibit postoperative scarring formation. *J. Mater. Chem.* **2012**, *22* (35), 18164 DOI: 10.1039/c2jm32519e.

(169) Zhao, F.; Heesters, B. A.; Chiu, I.; Gao, Y.; Shi, J.; Zhou, N.; Carroll, M. C.; Xu, B. L-Rhamnose-containing supramolecular nanofibrils as potential immunosuppressive materials. *Org. Biomol. Chem.* **2014**, *12* (35), 6816–6819 DOI: 10.1039/c4ob01362j.

(170) Zhao, F.; Weitzel, C. S.; Gao, Y.; Browdy, H. M.; Shi, J.; Lin, H.-C.; Lovett, S. T.; Xu, B. β-Galactosidase-instructed formation of molecular nanofibers and a hydrogel. *Nanoscale* **2011**, *3* (7), 2859–2861 DOI: 10.1039/c1nr10333d.

(171) Roytman, R.; Adler-Abramovich, L.; Kumar, K. S. A.; Kuan, T.-C.; Lin, C.-C.; Gazit, E.; Brik, A. Exploring the self-assembly of glycopeptides using a diphenylalanine scaffold. *Org. Biomol. Chem.* **2011**, *9* (16), 5755–5761 DOI: 10.1039/c1ob05071k.

(172) Ren, K.; He, C.; Xiao, C.; Li, G.; Chen, X. Injectable glycopolypeptide hydrogels as biomimetic scaffolds for cartilage tissue engineering. *Biomaterials* **2015**, *51*, 238–249 DOI: 10.1016/j.biomaterials.2015.02.026.

(173) Nicoll, S. B.; Barak, O.; Csóka, A. B.; Bhatnagar, R. S.; Stern, R. Hyaluronidases and CD44 undergo differential modulation during chondrogenesis. *Biochem. Biophys. Res. Commun.* **2002**, *292* (4), 819–825 DOI: 10.1006/bbrc.2002.6697.

(174) Harada, H.; Takahashi, M. CD44-dependent intracellular and extracellular catabolism of hyaluronic acid by hyaluronidase-1 and -2. *J. Biol. Chem.* **2007**, *282* (8), 5597–5607 DOI: 10.1074/jbc.M608358200.

(175) Johnstone, B.; Hering, T. M.; Caplan, A. I.; Goldberg, V. M.; Yoo, J. U. In Vitro Chondrogenesis of Bone Marrow-Derived Mesenchymal Progenitor Cells. **1998**, *272* (238), 265–272.

(176) O'Driscoll, S. W.; Keeley, F. W.; Salter, R. B. The chondrogenic potential of free autogenous periosteal grafts for biological resurfacing of major full-thickness defects in joint surfaces under the influence of continuous passive motion. An experimental investigation in the rabbit. *J. Bone Joint Surg. Am.* **1986**, *68* (7), 1017–1035.

(177) Athanasiou, K. A.; Darling, E. M.; Hu, J. C. Articular Cartilage Tissue Engineering. *Synth. Lect. Tissue Eng.* **2009**, *1* (1), 1–182 DOI: 10.2200/S00212ED1V01Y200910TIS003.

(178) Ishida, O.; Tanaka, Y.; Morimoto, I.; Takigawa, M.; Eto, S. Chondrocytes are regulated by cellular adhesion through CD44 and hyaluronic acid pathway. *J. Bone Miner. Res.* **1997**, *12* (10), 1657–1663 DOI: 10.1359/jbmr.1997.12.10.1657.

(179) García-Carvajal ZY, Garciadiego-Cázares D, Parra-Cid C, Aguilar-Gaytán R, Velasquillo C, Ibarra C, Castro Carmona JS. Cartilage tissue engineering: the role of extracellular matrix (ECM) and novel strategies. In: Andrades JA, editor. Regenerative Medicine and Tissue Engineering. Rijeka: InTech; **2013**. p. 365-397. doi:10.5772/55917

(180) Chen, F. H.; Rousche, K. T.; Tuan, R. S. Technology Insight: adult stem cells in cartilage regeneration and tissue engineering. *Nat. Clin. Pract. Rheumatol.* **2006**, *2* (7), 373–382 DOI: 10.1038/ncprheum0216.

APPENDIX

Copyright Clearance Agreements†

Reference Number	License Supplier	License Number
180	Nature Publishing Group	3691511348164
50	Nature Publishing Group	3691511351207
155	American Chemical Society	Permisson not required

† All license agreements between Seher Yaylacı and the License Suppliers are made by means of Copyright Clearance Center (CCC).